GLOBAL AND LOCAL CIRCULATIONS ASSOCIATED WITH SOUTH AMERICAN SUMMER PRECIPITATION

by

Lee Andrew Byerle

A thesis submitted to the faculty of
The University of Utah
in partial fulfillment of the requirements for the degree of

Master of Science

Department of Meteorology

The University of Utah

June 1998

REPORT DOCUMENTATION PAGE	Form Approved OMB No. 0704-0188

1. AGENCY USE ONLY *(Leave blank)*	2. REPORT DATE	3. REPORT TYPE AND DATES COVERED
	2 October 1998	

4. TITLE AND SUBTITLE
GLOBAL AND LOCAL CIRCULATIONS ASSOCIATED WITH SOUTH AMERICAN SUMMER PRECIPITATION

5. FUNDING NUMBERS

6. AUTHOR(S)
LEE ANDREW BYERLE

7. PERFORMING ORGANIZATION NAME(S) AND ADDRESS(ES)
THE UNIVERSITY OF UTAH

8. PERFORMING ORGANIZATION REPORT NUMBER
98-070

9. SPONSORING/MONITORING AGENCY NAME(S) AND ADDRESS(ES)
THE DEPARTMENT OF THE AIR FORCE
AFIT/CIA, BLDG 125
2950 P STREET
WPAFB OH 45433

10. SPONSORING/MONITORING AGENCY REPORT NUMBER

11. SUPPLEMENTARY NOTES

12a. DISTRIBUTION AVAILABILITY STATEMENT
Unlimited Distribution
In Accordance With 35-205/AFIT Sup 1

12b. DISTRIBUTION CODE

13. ABSTRACT *(Maximum 200 words)*

14. SUBJECT TERMS

15. NUMBER OF PAGES
163

16. PRICE CODE

17. SECURITY CLASSIFICATION OF REPORT	18. SECURITY CLASSIFICATION OF THIS PAGE	19. SECURITY CLASSIFICATION OF ABSTRACT	20. LIMITATION OF ABSTRACT

CONTENTS

ABSTRACT

Precipitation regimes over South America involving variations of one to two weeks are documented using 15 years of gridded data, 20 years of outgoing longwave radiation (OLR) measurements obtained from satellites and 6 years of cloud data from the International Satellite Cloud Climatology Project (ISCCP). The gridded data were produced by an assimilation system from the European Center for Medium-range Weather Forecasts (ECMWF). Comparisons of assimilated OLR fields with those obtained from satellite observations show model skill in reproducing tropical patterns of convection.

The 6-month atmospheric evolution of the austral summer is discussed, based on the ECMWF reanalysis, with a focus on circulations over South America. The South Atlantic Convergence Zone (SACZ) is a typical feature of summer convection over South America, and it appears well-described by the gridded data. Fourteen-year averages are used to define the seasonal evolution every 2 weeks, and averages are removed from individual times to define anomalies. Previous research has shown the existence of a meridional "seesaw" of alternating wet and dry events over tropical and subtropical South America. This investigation focuses on 2-week modulations of the SACZ with the goal of ascertaining the dependence of precipitation regimes over South America on convection over the Central Pacific Ocean.

This is accomplished using empirical orthogonal function analyses of filtered OLR anomalies confined to two regions: one includes the South Pacific Convergence Zone (SPCZ), extending from the dateline eastward to 20 E; the other extends from 100 W to 0 W, including South America and the SACZ. Four convective patterns are identified: those with an enhanced/suppressed SACZ with a well-defined SPCZ (referred to as "with SPCZ"), and those with an enhanced/suppressed SACZ without a clear composite

signature in the SPCZ ("SACZ only"). These patterns occur with about the same frequency. The "with SPCZ" events are linked to biweekly modulations of the tropical circulation. They exhibit shorter waves over midlatitudes than do "SACZ only" cases, suggesting more synoptic variability links to the Pacific. In contrast, the "SACZ only" events are associated with larger precipitation anomalies over the Western Hemisphere and slower amplification rates. For the 15-year period considered, "with SPCZ" cases are twice as likely to occur during warm El Niño Southern Oscillation events than are "SACZ only" cases.

Moisture flux convergence is the major moisture source for these events. Enhanced subtropical precipitation events over South America are linked to situations of strong northerly flow at low levels and a westward displacement of the Atlantic subtropical high. Moisture from the Amazon basin and the Western Atlantic is transported southward, enhancing rainfall over the subtropical plains and the neighboring western basin of the Atlantic Ocean.

ACKNOWLEDGMENTS

I would first like to express my heartfelt appreciation to my committee advisor, Professor Julia Nogués-Paegle. Her direction, patience and inspiration made completion of this thesis possible. Without her countless hours of guidance, this project would still be in its planning stages. Thanks to Dr. Kingtse Mo for her many helpful suggestions and for providing several analyses. I also appreciate Dr. Jan Paegle for his encouragement and helpful comments throughout this research. I would like to thank Professors John Horel, Steve Krueger, Jan Paegle and Jim Steenburgh for influencing my academic development. I appreciate the administrative support provided by Kathy Roberts, Leslie Allaire and Melea Adams, and the computer administration support of Lloyd Staley. Thanks to all the friends in the Meteorology Department for their support and great memories. I appreciate my parents for always emphasizing the importance of a good education. Finally, I thank my wife, Amy, for her unending patience and encouragement that kept me going throughout this endeavor.

I would like to recognize the use of the Grid Analysis and Display System (GrADS), helpful in producing many datasets and figures for this manuscript. Funding for this research was supported by NSF Grant ATM 9523536. I appreciate the Air Force for funding my salary and tuition through the Air Force Institue of Technology, Wright-Patterson AFB, Ohio.

CHAPTER 1

INTRODUCTION

Cloudiness and precipitation patterns during the South American summer have vital agricultural and economic ramifications, as well as important roles in local and large-scale atmospheric circulations. Remote and local influences of precipitation anomalies over this region may be influenced by a variety of timescales. For interannual periods, El Nino Southern Oscillation (ENSO) signals affect large-scale shifts in convection. Relationships of precipitation over South America to ENSO are documented by Ropelewski and Halpert (1996) for northeastern and southeastern South America. These regions flank the South Atlantic Convergence Zone (SACZ), a band of convection extending, periodically, from South America into the Southwest Atlantic Ocean. The SACZ plays a large role in the distribution of rainfall in the vicinity of South America (e.g., Nogués-Paegle and Mo 1997; hereafter referred to as NPM97). Horel et al. (1989) studied the annual cycle of convection over the tropical Americas, showing the impact of the onset and decay of the wet season associated with features such as the upper-level Bolivian high, situated over the Bolivian plateau. This region serves as an elevated source of sensible and latent heat. Idealized modelling studies have also simulated seasonal circulations over South America, showing, for example, the importance of orographic effects associated with the sharp terrain of the Andes Mountains (Gandu and Geisler 1991, Kleeman 1989) and active diurnal cycles (Figueroa et al. 1995) and their effects on activity in the SACZ.

On shorter timescales, summer circulations over South America have been linked to large-scale, east-to-west moving tropical disturbances known as intraseasonal or 30- to 60-day oscillations, first identified by Madden and Julian (1971). Kousky and Casarin (1986)

associated rainfall anomalies over the Atlantic with suppressed convection over Southern Brazil using half-monthly means of outgoing longwave radiation (OLR) anomalies and 200 mb winds. Kalnay et al. (1986) identified intraseasonal variations in the SACZ, noting its increased activity during January 1979, followed by suppressed convection the following month. Links between convection over South America and neighboring regions to the large-scale circulation have also been found for shorter time scales. Grimm and Silva Dias (1995) noted a "chain of connections" using influence functions from a linear barotropic vorticity equation model, including a link between the SACZ and the South Pacific Convergence Zone (SPCZ). Vincent (1994) also associated modulations in the SPCZ with intraseasonal oscillations. Lenters and Cook (1995) analyzed the summertime climatology over South America through an analysis of the atmospheric water vapor budget, in relation to large-scale connections. Other links to the large-scale have been suggested by Buchmann et al. (1995). Using the National Center for Atmospheric Research (NCAR) community climate model, they generated rainfall deficits over North and South America through tropical Atlantic heating anomalies. Nogués-Paegle et al. (1998) used forecasts from the NCEP Medium Range Forecast Model to examine links between forecast errors in midlatitudes and those in the tropics.

Relative to intraseasonal variations, NPM97 described a meridional seesaw pattern in the SACZ. Using rotated empirical orthogonal function analyses (REOF) of satellite-derived outgoing longwave radiation, filtered to retain variations longer than 10 days, they found alternating wet and dry conditions during summer over tropical and subtropical South America. An intensified SACZ is associated with negative rainfall anomalies over the subtropical plains (Fig. 1.1). These are classified as negative events. Fig. 1.1 a and c shows composites (from 1979 to 1993) of two types of negative events with differing convective regimes over the Pacific. They have been identified from two types of OLR eigenmodes (NPM97 and Mo 1997, personal communication). The first focuses on South America, extending from 40°S to 10°N and from 100°W to the Greenwich Meridian

Figure 1.1 OLR composite anomalies (1979-1993) contoured every 5 W/m^2 for negative cases (1979 to 1993) for a) "with SPCZ" observed, b) ECMWF "with SPCZ," c) "SACZ only" observed, and d) ECMWF "SACZ only." Observed OLR (a and c) values are from calculated satellite measurements (Liebmann and Smith 1996). The colorbars show shaded OLR intervals. REOF analysis areas are outlined in (a) and (b) from 180°W to 20°E and from 40°S to 40°N; and in (c) and (d) from 100°W to the Greenwich Meridian and 40°S to 10°N.

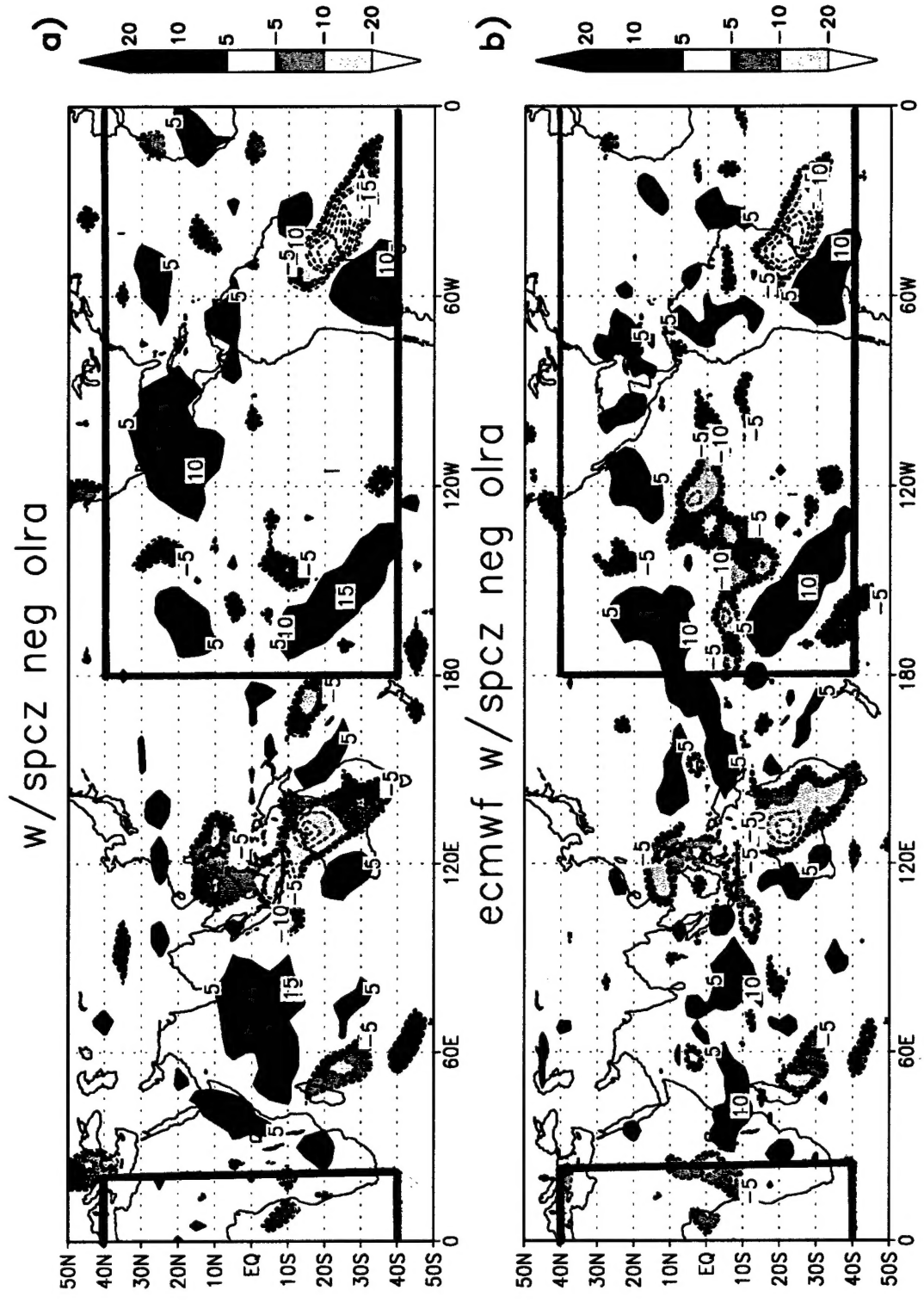
a)
20
10
5
-5
-10
-20
w/spcz neg olra
50N
40N
30N
20N
10N
EQ
10S
20S
30S
40S
50S
0
60E
120E
180
120W
60W
0
b)
ecmwf w/spcz neg olra

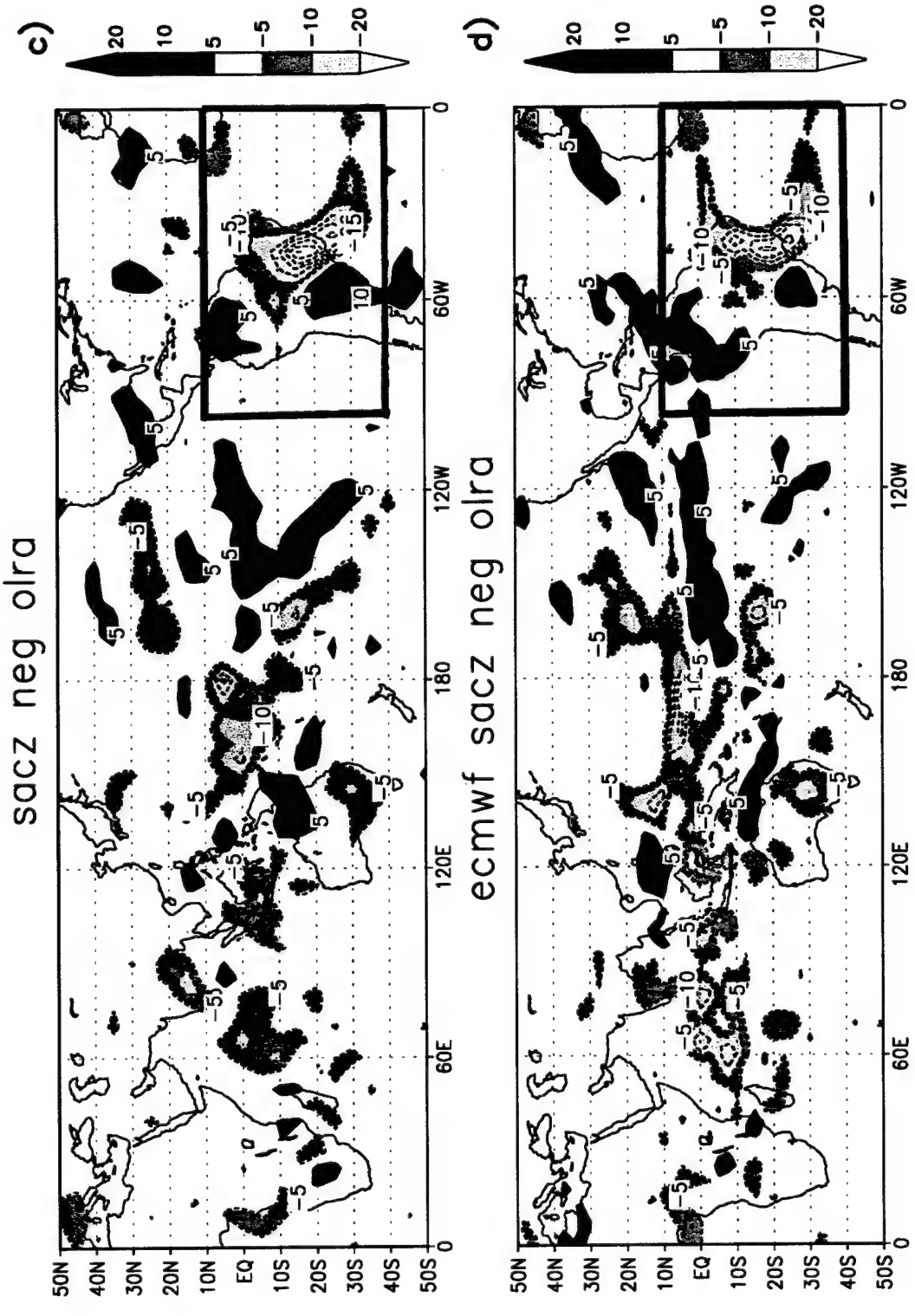

Figure 1.1 Continued

(denoted as REOF A). The second is applied to a sector from 180°W to 20°E and from 40° S to 40°N (denoted as REOF B). The two REOF areas are outlined in Figs. 1.1 and 1.2. Filtered data are projected onto these EOFs to obtain time series of principal components (PCs). An event is chosen when the magnitude of the PC is greater than 1.2 of its own standard deviation and lasts for 5 or more days. Events selected by REOF A and B are used to study SACZ cases with possible connections to atmospheric processes over the Pacific Ocean. These are referred to as "SACZ with SPCZ" (abbreviated "with SPCZ"), shown in Fig. 1.1 a and b. Events chosen with REOF A but not with REOF B are referred to as "SACZ only (as in Fig. 1.1 c and d)."

The study includes global-scale diagnostics that require gridded data sets for extended time periods. It uses reanalyses produced by the European Center for Medium-Range Weather Forecasts (ECMWF), available from 1979 through 1993. These analyses constitute a retrospective interpolation of available data into regular grids. Several variables are archived; some of them are directly influenced by observations (such as temperature, winds and heights of isobaric surfaces) and others are derived by the assimilation models. The outgoing long- wave radiation is among the latter, and it gives an integrated view of radiation and cloud processes simulated by the assimilation model. The corresponding OLR composites obtained from the ECMWF reanalyses are shown in Fig. 1.1 b and d. It is clear that the model-derived field agrees well with those obtained from satellite measurements, lending credibility to the accuracy of the derived products.

When the SACZ weakens, precipitation over the subtropical plains of South America is enhanced (Fig. 1.2). These periods are defined as positive events. Two types of positive events, based on "with SPCZ" and "SACZ only" REOF analyses, are shown in Fig. 1.2 a and c, respectively. The REOF areas for "with SPCZ" and "SACZ only" events are also outlined in Fig. 1.2. The results of rainfall surpluses and deficits over South America (NPM97) agree with those of Kousky and Casarin (1986). Moisture influx during positive cases is enhanced by a low-level jet east of the Andes. NPM97 found

Figure 1.2 OLR composite anomalies (1979-1993) contoured every 5 W/m^2 for positive cases (1979 to 1993) for a) "with SPCZ" observed, b) ECMWF "with SPCZ," c) "SACZ only" observed, and d) ECMWF "SACZ only." Observed OLR (a and c) values are from calculated satellite measurements (Liebmann and Smith 1996). The colorbars show shaded OLR intervals. REOF analysis areas are outlined in (a) and (b) from 180°W to 20°E and from 40°S to 40°N; and in (c) and (d) from 100°W to the Greenwich Meridian and 40°S to 10°N.

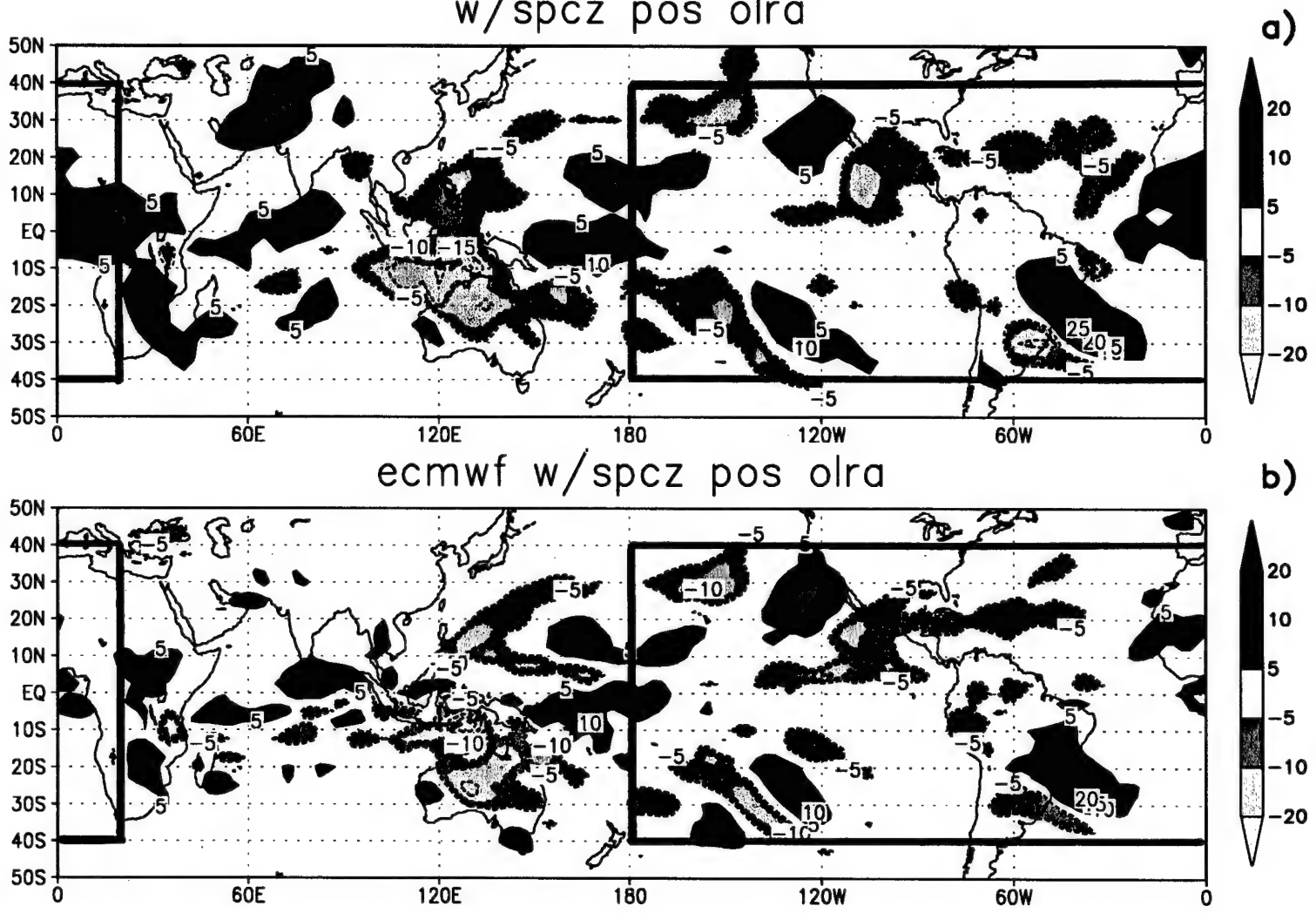
w/spcz pos olra
a)
ecmwf w/spcz pos olra
b)
50N
40N
30N
20N
10N
EQ
10S
20S
30S
40S
50S
0
60E
120E
180
120W
60W
20
10
5
-5
-10
-20

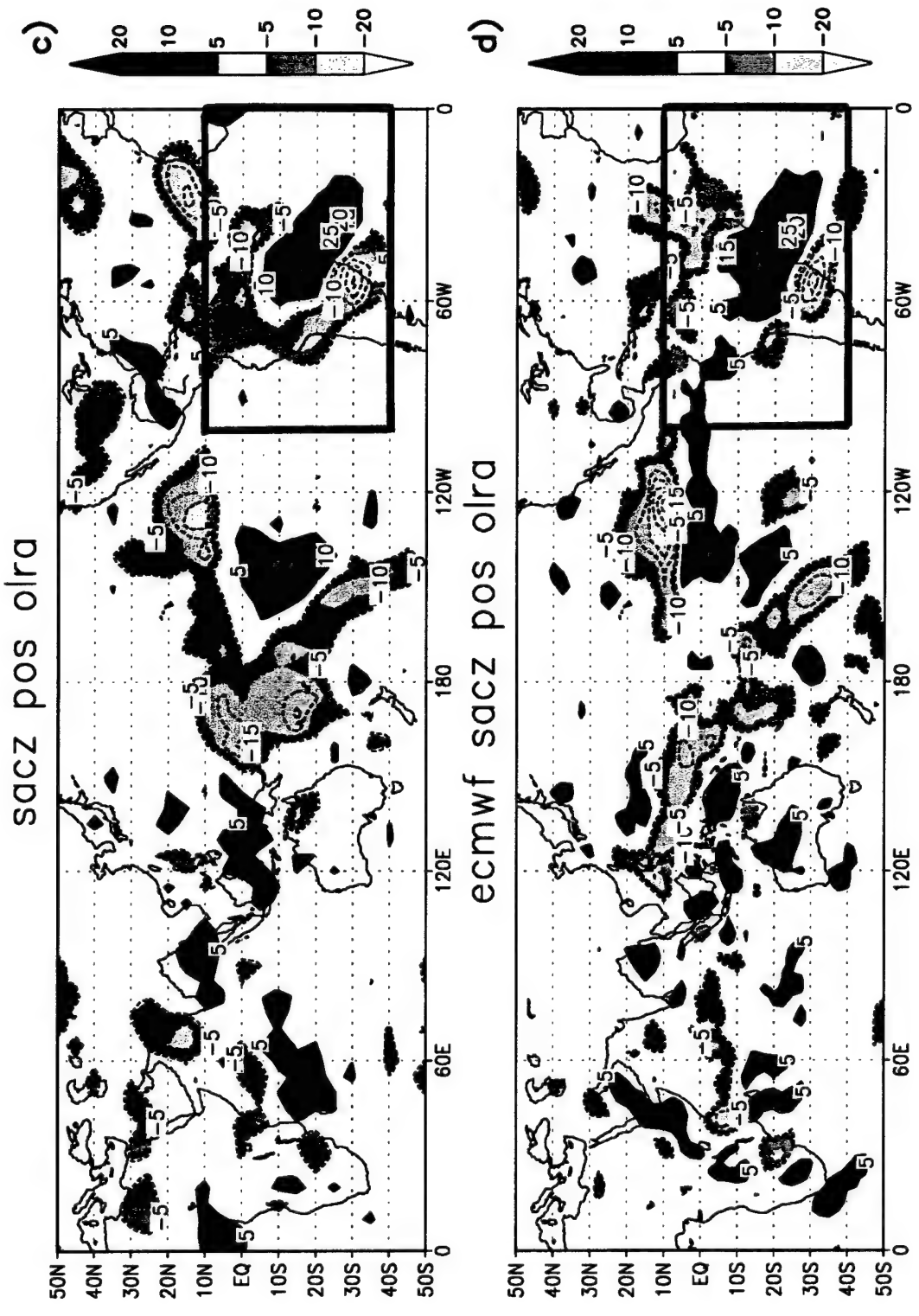

Figure 1.2 Continued

negative events to be three times more likely to occur during ENSO periods for the years 1973 to 1993, indicating that ENSO modulates not only shifts in average patterns, but it also influences some aspects of intraseasonal variability.

In addition to "with SPCZ" and "SACZ only" events, a third type of composite was also produced using REOF analysis (Mo 1997, personal communication). It consists of events in the list for REOF B but not in the list for REOF A. These are denoted as "SPCZ only" cases. This composite shows the development of the SACZ associated with an active SPCZ but without evidence of a "seesaw" in the precipitation over the SACZ (seen for "with SPCZ" cases). The significance of the "SPCZ only" cases will be further illustrated in Chapters 4 and 5.

The low-level jet during wet episodes over the subtropical plains of South America is important for drawing moisture out of the Amazon Basin. In particular, the study of Eltahir and Bras (1994) indicated that moisture flux out of the Amazon basin accounts for about 68% of the flux into the basin. Thus, the atmosphere over the Amazon basin is not a closed system. It may highly contribute to the hydrological cycle in the surrounding regions. Because of the morphology of the terrain surrounding the Amazon basin, most of the flux out of the basin is expected to take place towards the south. Moisture flux diagnostics are presented in this study to ascertain whether and when the Amazon region most strongly modulates precipitation regimes over South American subtropical latitudes.

The main goals of this study are: 1) to document the origin and evolution of these two types of intraseasonal positive (Fig. 1.2) and negative (Fig. 1.1) rainfall events over South America and their likely moisture sources; 2) to analyze the remote and local influences associated with these events and atmospheric circulations; and 3) to assess the validity of the ECMWF Reanalysis in portraying the events. Chapters 4 and 5 examine the negative and positive events, respectively, through analyses of precipitation and OLR, midlatitude circulations, transients, moisture sources and comparisons with observations. An overview of the data sources and methodology is given in Chapter 2, including comparisons with

other assimilated and observed analyses. Chapter 3 provides a description of the atmospheric seasonal cycle over the Southern Hemisphere from November through April. This will help determine the veracity of the ECMWF reanalysis, will describe the seasonal cycle, and will outline the seasonally evolving mean climatology used to define anomalies. Finally, Chapter 6 summarizes the findings and conclusions.

CHAPTER 2

DATA AND METHODOLOGY

This chapter discusses the data sets and diagnostics used in this investigation. The primary data are the ECMWF Reanalysis and a portion of the ISCCP dataset for analysis validation. Various outgoing longwave radiation (OLR) and precipitation datasets are also used to determine whether differences between data sets do not exceed the intraseasonal signals relevant to the present study.

2.1 The ECMWF Reanalysis

The European Center for Medium-range Weather Forecasts' (ECMWF) archives of analyses and forecasts have been used extensively by the scientific community. In 1996, the Center completed a 15-year (1979-1993) reanalysis of data using a spectral version (T106 resolution, with 31 vertical hybrid levels or 17 pressure levels) of its operational data assimilation system and model. The motivation for the project was research applications in areas such as modelling, general circulation diagnostics and observing system performance. The principal components of the reanalysis are one-dimensional variational analysis of the cloud cleared radiances, optimal interpolation analysis and a global atmospheric model (Gibson et al. 1997). Sources of observational data for the reanalysis are data acquired in real time from the World Meteorological Organization's Global Telecommunications System (GTS); an archive of First GARP Global Experiment (FGGE) level II-b data; radiance data from TOVS [Television and Infrared Operational Satellite (TIROS) Operational Vertical Sounder]; cloud track wind data, generated for the FGGE level II-b dataset; ship and buoy observations from the Comprehensive Ocean Atmosphere Data Set (COADS); level II-b data from the Alpine Experiment; and portions

of national archives from Japan and Australia. The Japanese archive provides additional data over the Northern Pacific and radiosonde data from around Japan. The National Meteorological Center at Melbourne provides surface pressures from pseudo observations called "PAOBS."

For this research, the ECMWF reanalysis data set was extracted from the archives at the National Center for Atmospheric Research (NCAR), Scientific Computing Division. Variables were obtained twice a day (00 Z and 12 Z), with 11 levels chosen for the upper-air fields, and a single level for supplementary fields on a 2.5 degree X 2.5 degree grid. The upper-air meteorological fields are geopotential (gz), temperature (K), zonal wind component (u), meridional wind component (v) and specific humidity (q) at levels (from bottom to top) 1000, 925, 850, 775, 700, 600, 500, 300, 250, 200 and 100 mb. Supplementary fields have also been obtained. They are large-scale precipitation, convective precipitation, surface flux of latent heat (to obtain evaporation) and top of atmosphere thermal radiation (to examine OLR). The upper-air fields consist of a 144 X 49 grid array (covering the latitudes 60°S to 60°N), with each parameter available at each level. The supplementary fields are on a 144 X 73 grid array.

2.2 ISCCP Data

Cloud data from 1985 to 1991 from the International Satellite Cloud Climatology Project (ISCCP) are used for comparison and analysis in Chapters 4 and 5. Established as part of the World Climate Research Program, ISCCP is a cloud climatology that uses data from polar-orbiting and geostationary satellites. Two common types of data are used: high resolution images and sounder measurements. The high resolution images utilize the solar (VIS) and infrared (IR) spectra to observe changes in clouds and to measure surface properties. Sounder measurements use the thermal infrared and microwaves to measure temperature structure and humidity distribution. The data used for this research are pentad averages prepared by Johnson (1996) from the 3-h or C1 data set distributed by the Langley Distributed Active Archive Center (DAAC).

The ISCCP cloud analysis (Rossow et al. 1991) is divided into three steps. (1) Cloud detection using VIS and IR radiances to make estimates of VIS and IR clear-sky background radiances. The degree of cloudiness at each place and time is determined by comparing the data to estimated clear-sky backgrounds. (2) Radiation analysis compares the data to a radiative transfer model to derive cloud optical depth (for the VIS spectrum) and cloud top temperature (VIS and IR spectrums). Cloud top temperatures are compared to TOVS profile data to estimate cloud top heights. (3) Through statistical analysis, monthly summaries of cloud-coverage, optical-depth and cloud-top-pressure are derived at 3-hourly intervals at a resolution of approximately 250 km. This reduces the volume of the data set. At this level in the processing, the 3-h ISCCP/C1 dataset becomes complete.

2.3 Model Comparisons

A data assimilation system interpolates the vast array of information from conventional and remote platforms to produce a grid of atmospheric values at regular intervals in space and time. This is done with a numerical model to produce a first guess and interpolation of available data that falls within a certain range of the first guess. Observations of evaporation, precipitation and radiation fluxes are not assimilated, but the gridded fields are modelled results obtained in the process of assimilating basic atmospheric variables. Therefore, their veracity might be doubted. This chapter offers comparisons with observations and variables obtained from other assimilating systems for calibration purposes.

Fig. 2.1 compares average January (1985 to 1993) outgoing longwave radiation (OLR) values with those obtained from satellite estimates (Liebmann and Smith 1996). The ECMWF produces higher values of OLR than observed in several regions: over the Pacific Intertropical Convergence Zones (ITCZ), in the region of the South Pacific Convergence Zone (SPCZ), over the South Pacific, off the West Coast of South America, and from the Atlantic ITCZ to Africa. Over the South American tropics at about 15°S, the monthly bias in Fig. 2.1 a shows a maximum (50 W/m^2) in the difference between model and observed

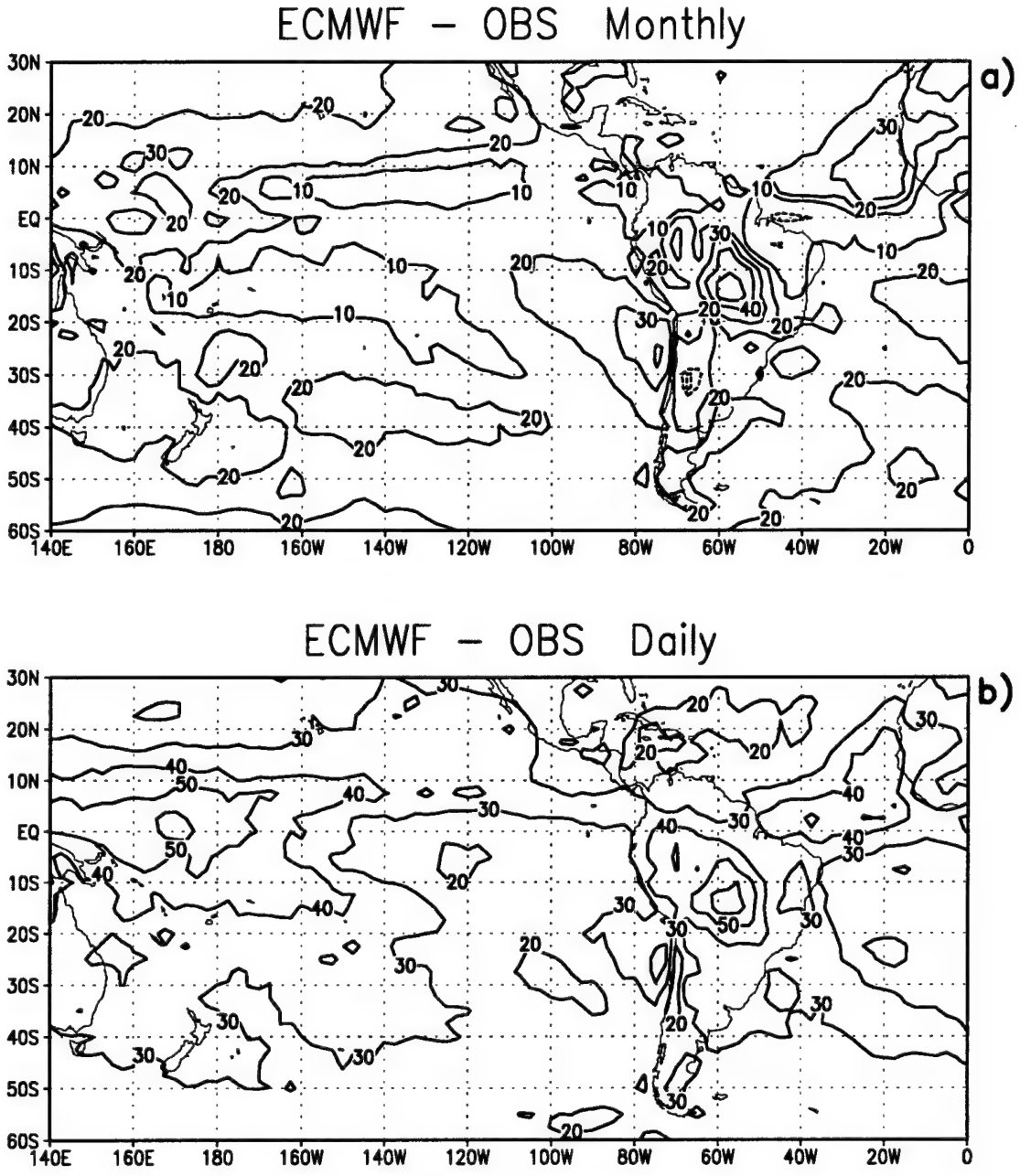

Figure 2.1 The average root-mean-squared diefference between ECMWF and satellite-derived OLR values (Liebmann and Smith 1996) for January from 1985 to 1993 for (a) monthly values, and (b) daily values, contoured every 10 W/m^2.

OLR, similar to the maximum root-mean-squared daily variations (60 W/m^2) in Fig. 2.1 b over the same region. The similarities between the monthly bias and the daily variations suggest the monthly bias is the main contributor to differences between modelled and observed OLR. These differences may be attributed to inadequate representation of cloud tops or to the radiative transfer model. Such biases are removed in the calculation of anomalies, defined as differences from 14-year biweekly averages.

To examine the ECMWF precipitation representation, several comparisons have been made for the month of January (1988 to 1992) using various assimilated and observed precipitation datasets (Figs. 2.2-2.5). Convective and large-scale (dynamical) are the two precipitation types generated by the ECMWF model. Convection is tied to a simple cloud model (Gibson et al. 1997) for deep, shallow and mid-level convection. Large-scale models utilize bulk properties of clouds (Tiedtke 1993) and prognostic equations for cloud water/ice. Thus, precipitation and deep clouds are co-located in the analyses. Fig. 2.2 compares average ECMWF January precipitation for the years 1988 to 1992 to that produced by the Xie-Arkin (Xie and Arkin 1996) precipitation analysis. The Xie-Arkin analysis is derived in a two-stage process from monthly gauge observations and satellite estimates. The difference between the two (Fig. 2.2 c) shows the ECMWF producing considerably larger amounts of precipitation over the Andes corridor and over the Pacific ITCZs. Increased orographic convection in the ECMWF model can be attributed to the more realistic topographic representation given with the T106 spectral resolution, though the ECMWF erroneously places a large maximum in precipitation at around 32°S, 74°W. The Xie-Arkin analysis appears to show a better representation of precipitation over the Andes than does the ECMWF. This is illustrated by comparing it to results of other global precipitation observation projects such as those in Fig. 2.3.

Fig. 2.3 a shows the 1988 to 1992 January precipitation average for the Global Precipitation Climatology Project (GPCP), which uses a satellite gauge model technique (Huffman et al. 1995). It combines precipitation estimates from microwave satellite data

Figure 2.2 Total rainfall averages for January (1988 to 1992) for (a) the ECMWF reanalysis, and (b) the Xie-Arkin precipitation analysis (Xie and Arkin 1996). ECMWF minus Xie-Arkin is shown in (c). Values are contoured every 2 mm/day.

ECMWF

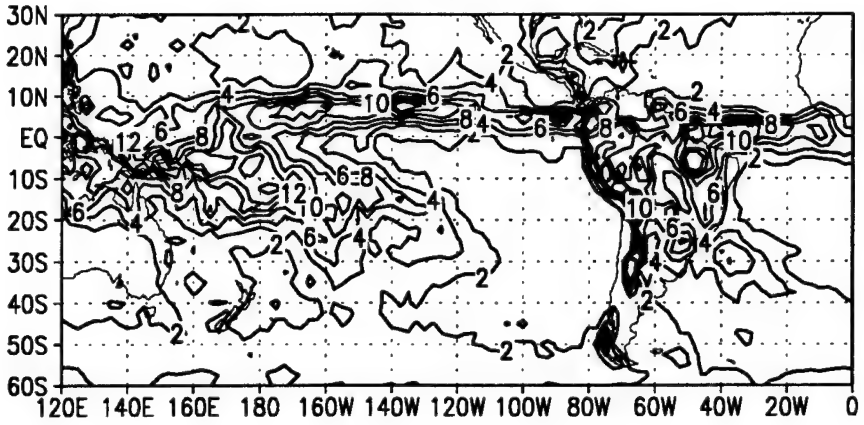

a)

XIAR

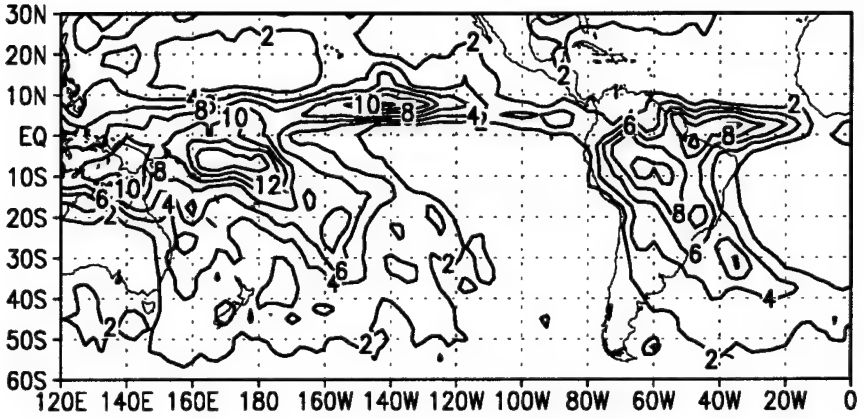

b)

ECMWF – XIAR

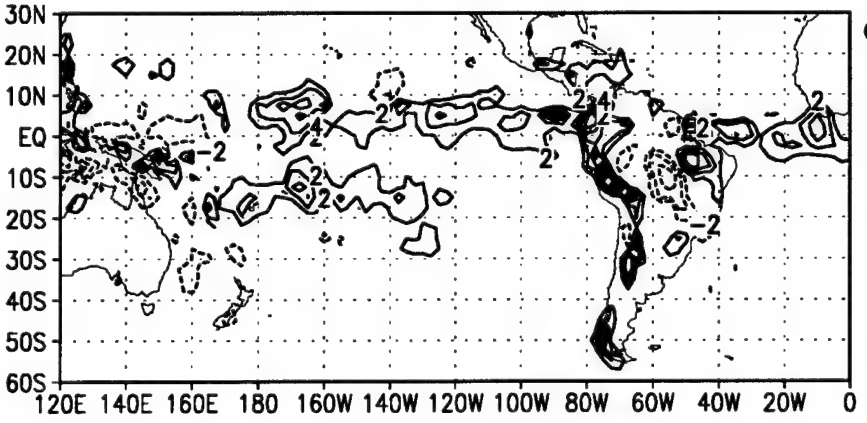

c)

Figure 2.3 Total rainfall averages for January (1988 to 1992) for (a) the Global Precipitation Climatology Project dataset (GPCP) (Huffman et al. 1995), and (b) the Merged Precipitation dataset (MRGD) (Schemm et al. 1992). GPCP minus MRGD is shown in (c). Values are contoured every 2 mm/day.

GPCP

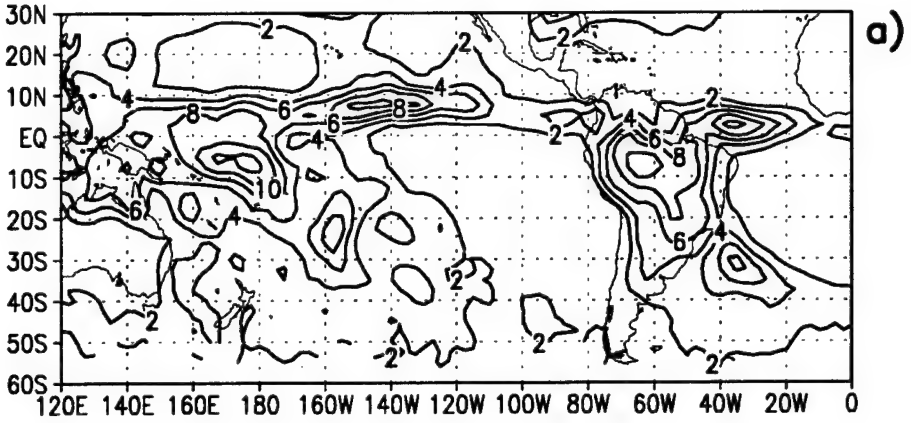

MRGD

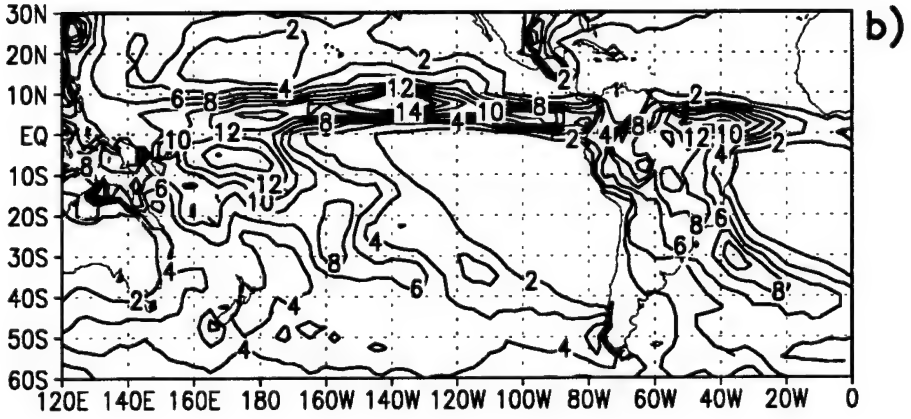

GPCP – MRGD

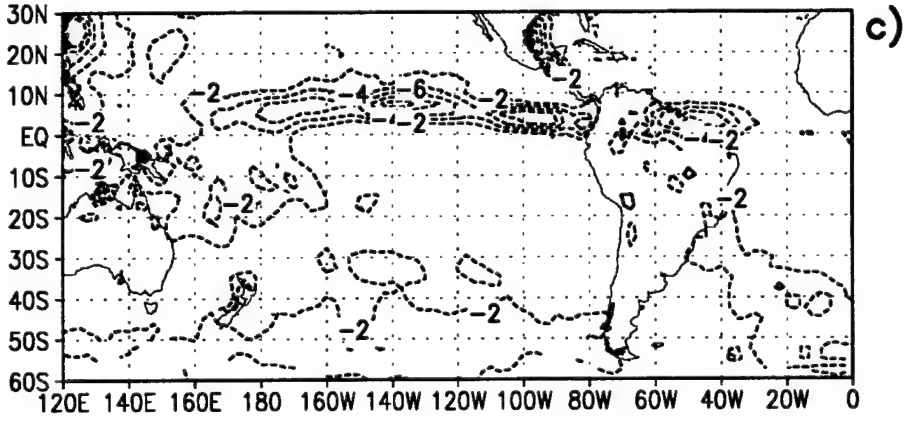

(86 GHz Goddard Scattering Algorithm 2), two infrared (IR) satellite datasets (Geo-IR and the NOAA 10 platform), rain gauges and numerical weather prediction models (the ECMWF operational T106 model). The merged precipitation dataset (MRGD) (Fig. 2.3 b) combines monthly total precipitation data with oceanic Microwave Sounder Unit measurements at three channels (Spencer et al. 1993). Channel 1 is for cloud water and water vapor at 50.3 GHz, and channels 2 (53.74 GHz) and 3 (54.96 GHz) are for airmass temperature. The two data sets show accumulations near the southern tip of South America linked to midlatitude storm tracks. While the ECMWF assimilation shows this feature, the Xie-Arkin assimilation does not (see Fig. 2.2 c). Fig. 2.3 c shows pronounced differences between the observational datasets over the Pacific and Atlantic ITCZs with the MRGD analysis showing higher amounts. The maximum difference in precipitation over the Pacific ITCZ is smaller in the ECMWF versus Xie-Arkin precipitation (Fig. 2.2 c) than it is with the difference between the other observational (satellite-derived) datasets (Fig. 2.3 c). Janowiak et al. 1995 described various methods used to estimate rainfall and a general assessment of various data sets, including some of the significant differences between them. The ECMWF and Xie-Arkin analyses are in closer agreement over the oceans than are the GPCP and MRGD analyses.

Fig. 2.4 shows comparisons between two observational precipitation data sets (exact years used for the climatologies are unknown). The Jaeger data (Jaeger 1976) are from contemporary precipitation atlases over land. Over the ocean, Jaeger uses U.S. Marine Climatic Atlas data. The Legates-Willmott (Legates and Willmott 1990) data set applies bulk corrections to gauge values over land to correct for evaporation and wind catchment problems. The Legates-Willmott analysis shows a strong meridional maxima in precipitation over the Pacific ITCZ. This is in agreement with the findings of Janowiak et al. 1995, who also illustrated the reliability of the Legates-Willmott data set over land masses compared to the oceans, where it didn't have enough input data (such as ship data). The Jaeger analysis is much drier than the Legates-Willmott analysis. Janowiak et al. 1995

Figure 2.4 Total rainfall averages for January for (a) the Jaeger Precipitation climatology Jaeger 1976), and (b) the Legates-Willmott precipitation climatology (Legates and Willmott 1990). Jaeger minus Legates-Willmott is shown in (c). Values are contoured every 2 mm/day.

JAGR

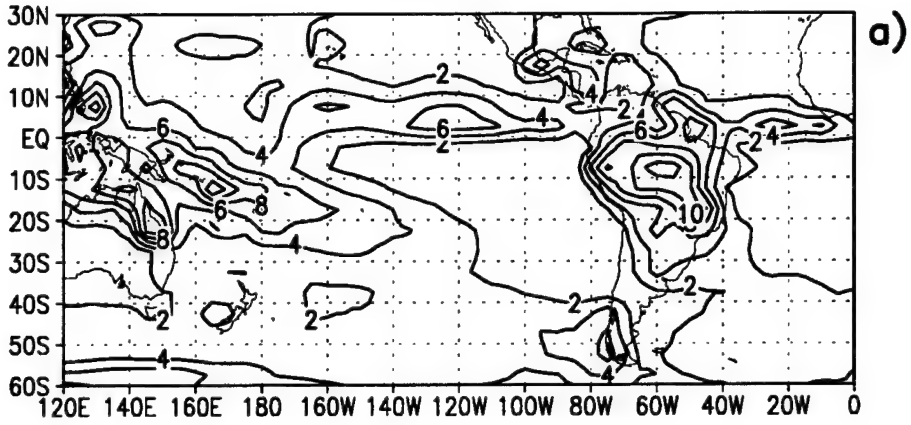

LEWI

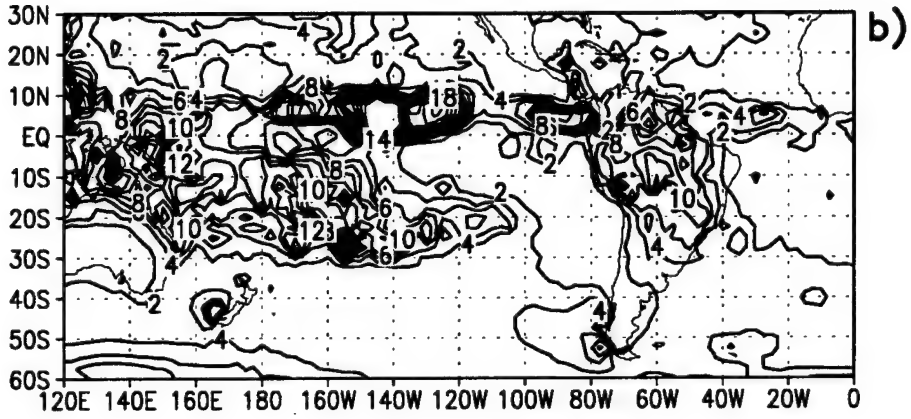

JAGR – LEWI

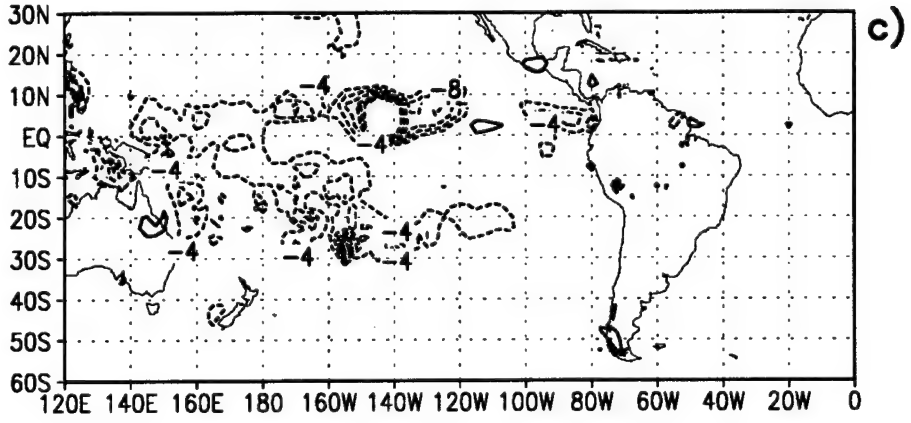

also showed that the Jaeger analysis was much drier than the Legates-Willmott and 6 satellite-derived data sets. Fig. 2.5 shows ECMWF minus GPCP and ECMWF minus Jaeger rainfall differences for January. Although the ECMWF consistently produces too much precipitation over the ITCZs and the SPCZ, the levels of uncertainty match the observational precipitation uncertainties in Fig. 2.3 c. Overall uncertainties in Fig. 2.5 are small in regions such as the SACZ and the subtropical plains of South America, primary areas where precipitation patterns will be examined in this thesis.

Two comparisons are also made of upper-level variables. Fig. 2.6 compares the 200 mb U and V wind components of the ECMWF reanalysis and the NCEP reanalysis. Fig. 2.6 a shows the average ECMWF January and February 200 mb winds for 1993, while Fig. 2.6 b shows the vector difference between ECMWF and NCEP (the root mean square difference is contoured). The most pronounced differences appear over the Eastern Pacific from 120°W to 80°W and from the Equator to 30°S, where the root mean square differences are between 8 to 10 m/s. Variation is also evident over the tropical Atlantic. Differences are small over South America and over midlatitudes. Fig. 2.7 compares ECMWF horizontal divergence to NCEP horizontal divergence at 200 mb. The ECMWF shows stronger divergence over the Pacific and Atlantic ITCZs, in the vicinity of the SPCZ (165°W, 10°S), and near the Equator at about 75°W. The NCEP analysis shows stronger divergence over Northeastern South America (2×10^{-6} s^{-1} more) at 40°W and 5°S.

Fig. 2.7 c and d compares 850 mb winds from the ECMWF and NCEP. Australian PAOBs were wrongly inserted in the NCEP assimilation over the southern oceans, and this explains the differences observed between the two analyses south of 30°S over the oceans. Low level wind differences might result in substantial differences in moisture fluxes. This is an important quantity for this study in clarifying the role of different moisture sources over South America. A comparison is presented in Fig. 2.8 between ECMWF and NCEP analyses for two events of interest. The overall patterns of moisture flux vectors are similar. Substantial differences, though, are shown in precipitating areas, coinciding with

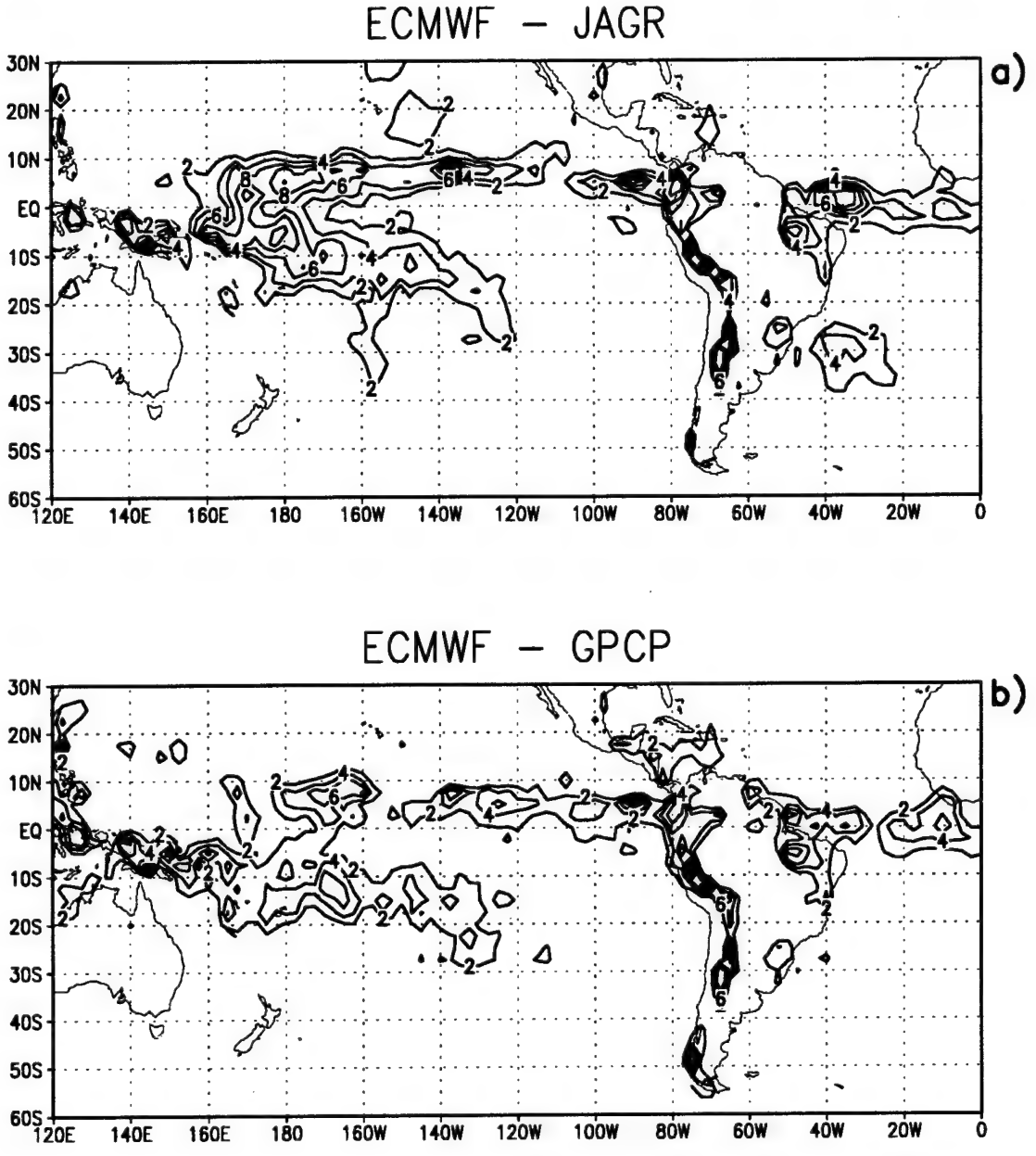

Figure 2.5 Total rainfall averages for January for (a) ECMWF (1988-1992) minus the Jaeger dataset (Jaeger 1976), and (b) ECMWF (1988-1992) minus the GPCP (1988-1992) dataset (Huffman et al. 1995). Values are contoured every 2 mm/day.

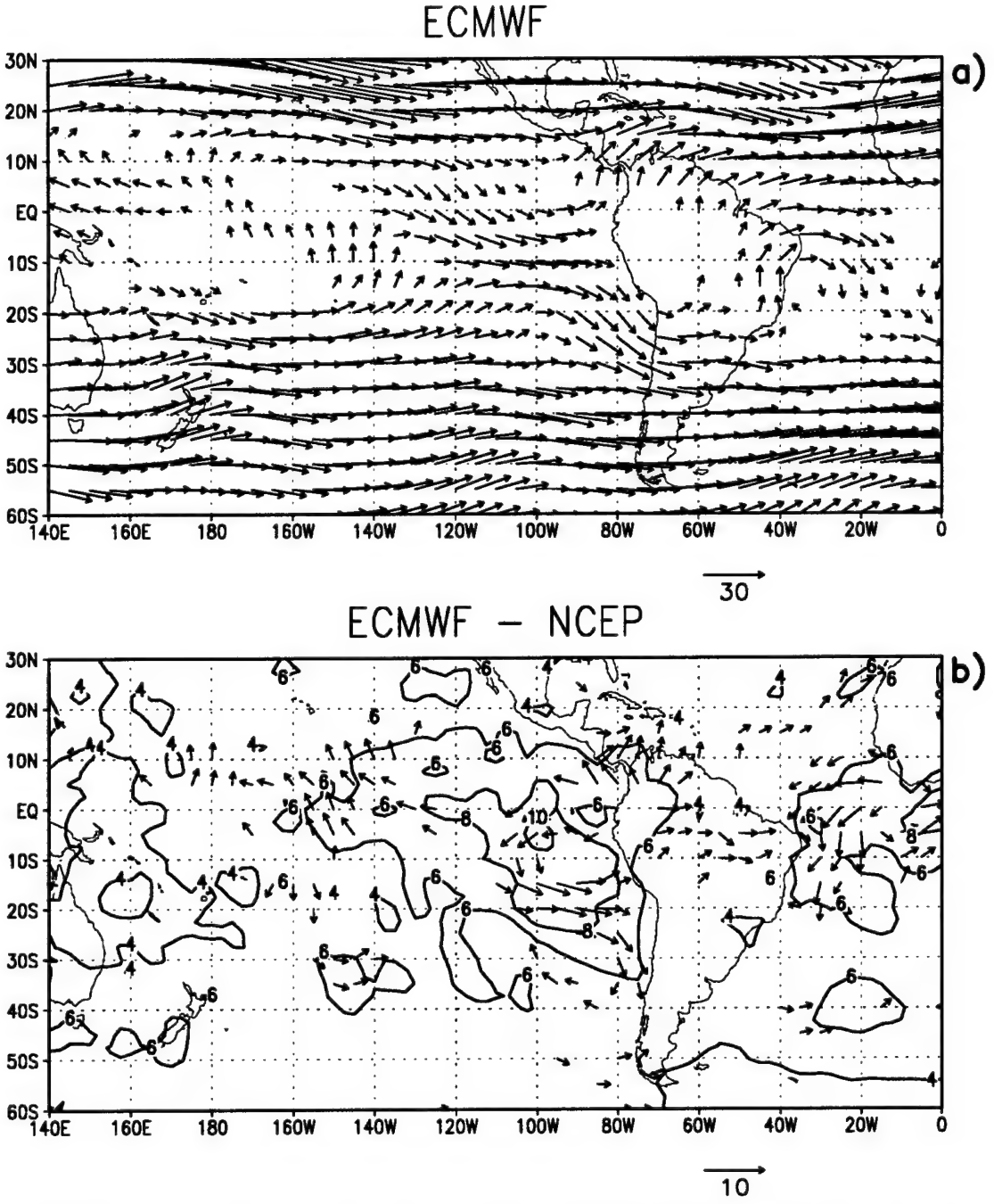

Figure 2.6 Monthly-averaged 200 mb wind vectors (m/s) are shown in (a) for January and February 1993. Values less than 5 m/s are not plotted. ECMWF minus NCEP winds (m/s), for the same period, are shown in (b) with contours of the root mean square differences (every 2 m/s). Values in (b) less than 2 m/s are not plotted.

Figure 2.7 Monthly-averaged 200 mb horizontal divergence is contoured (every 2 X 10^{-6} s^{-1}) in (a) for January and February 1993. ECMWF minus NCEP horizontal divergence for the same period is shown in (b), with shaded root mean square differences (every 2 m/s). Monthly-averaged 850 mb wind vectors (m/s) are shown in (c) for January and February 1993. Values less than 2 m/s are not contoured. ECMWF minus NCEP winds (m/s) for the same period are shown in (d) with contours of the root mean square differences (every 2 m/s). Values in (d) less than 3 m/s are not plotted.

ECMWF

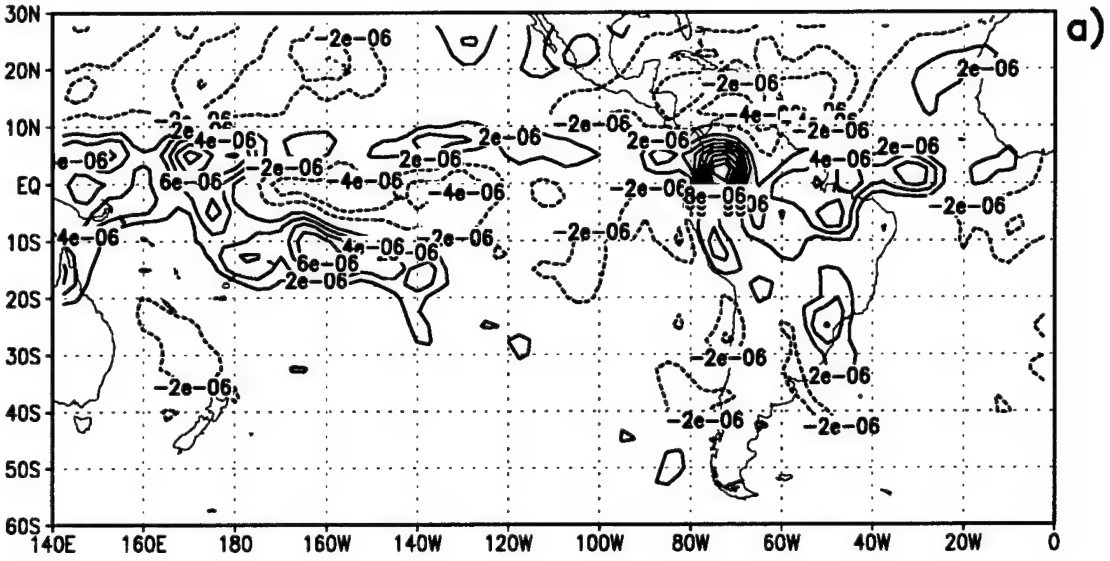

ECMWF – NCEP

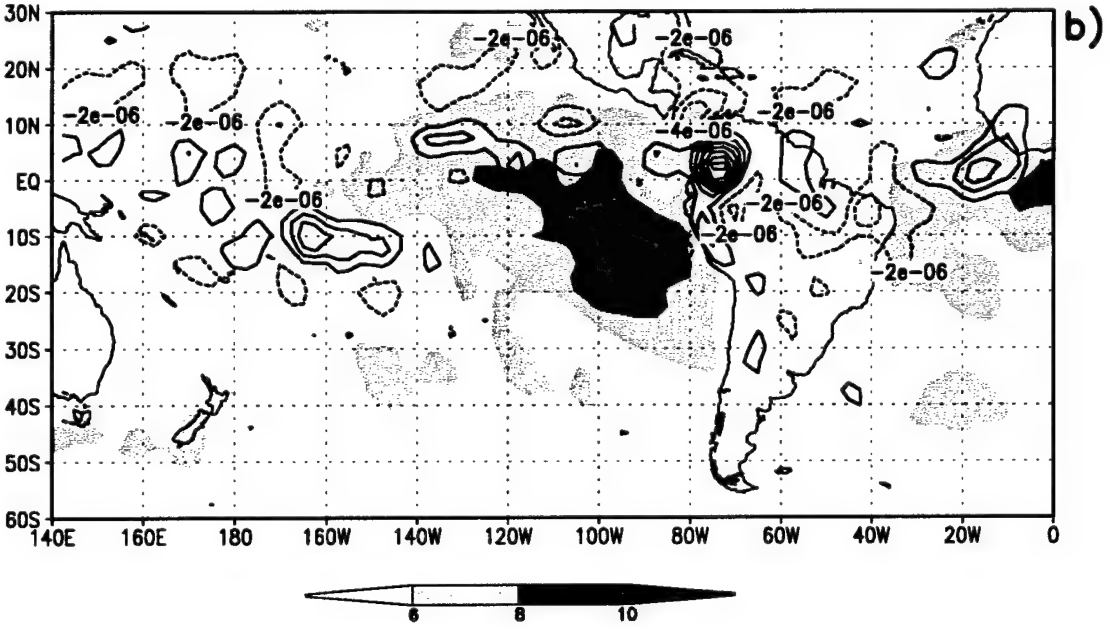

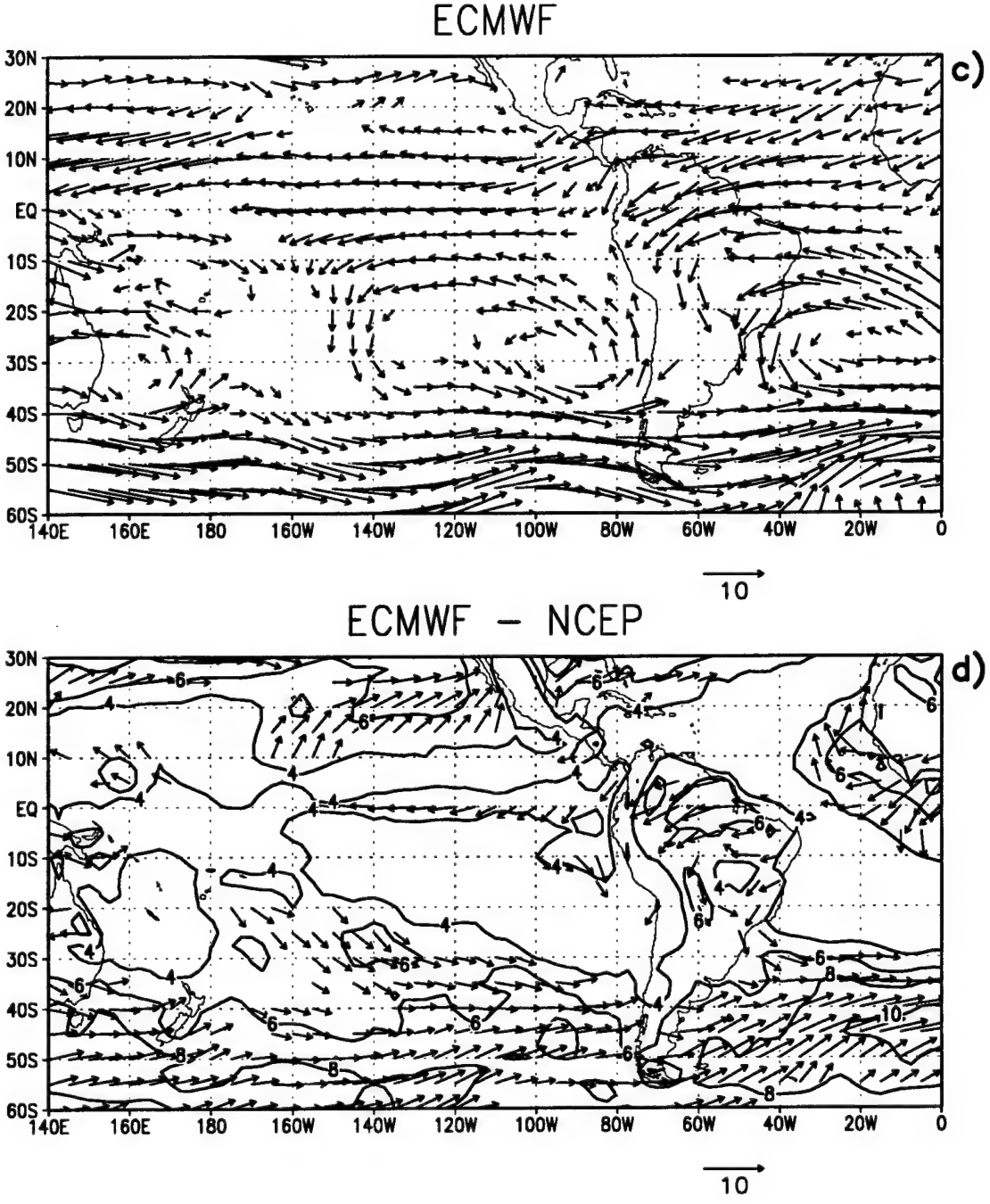

Figure 2.7 Continued

Figure 2.8 Average moisture flux vectors and horizontal convergence of moisture flux (contoured) for 20-25 December 1980 for (a) ECMWF, and (b) NCEP. Vector units are multiplied times 10 g cm^{-1} s^{-1}. Horizontal convergence of moisture flux is contoured every 5 X 10^{-8} s^{-1}. Values less than 75 g cm^{-1} s^{-1} are not contoured. A second case is shown in (c) as in (a), but for 26-31 March 1993, and (d) as in (b), but for 26-31 March 1993.

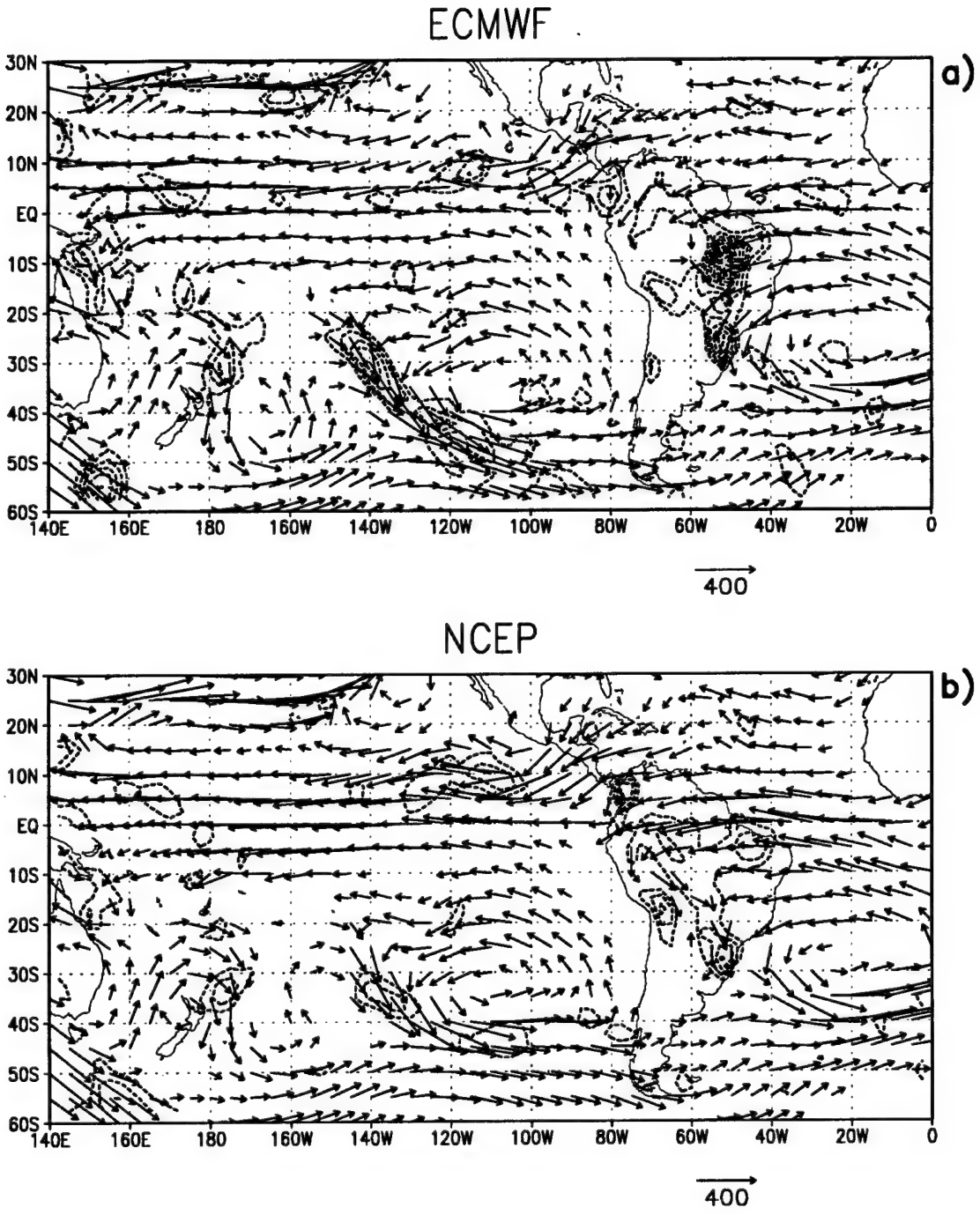
ECMWF
a)
30N
20N
10N
EQ
10S
20S
30S
40S
50S
60S
140E
160E
180
160W
140W
120W
100W
80W
60W
40W
20W
0
400
NCEP
b)
30N
20N
10N
EQ
10S
20S
30S
40S
50S
60S
140E
160E
180
160W
140W
120W
100W
80W
60W
40W
20W
0
400

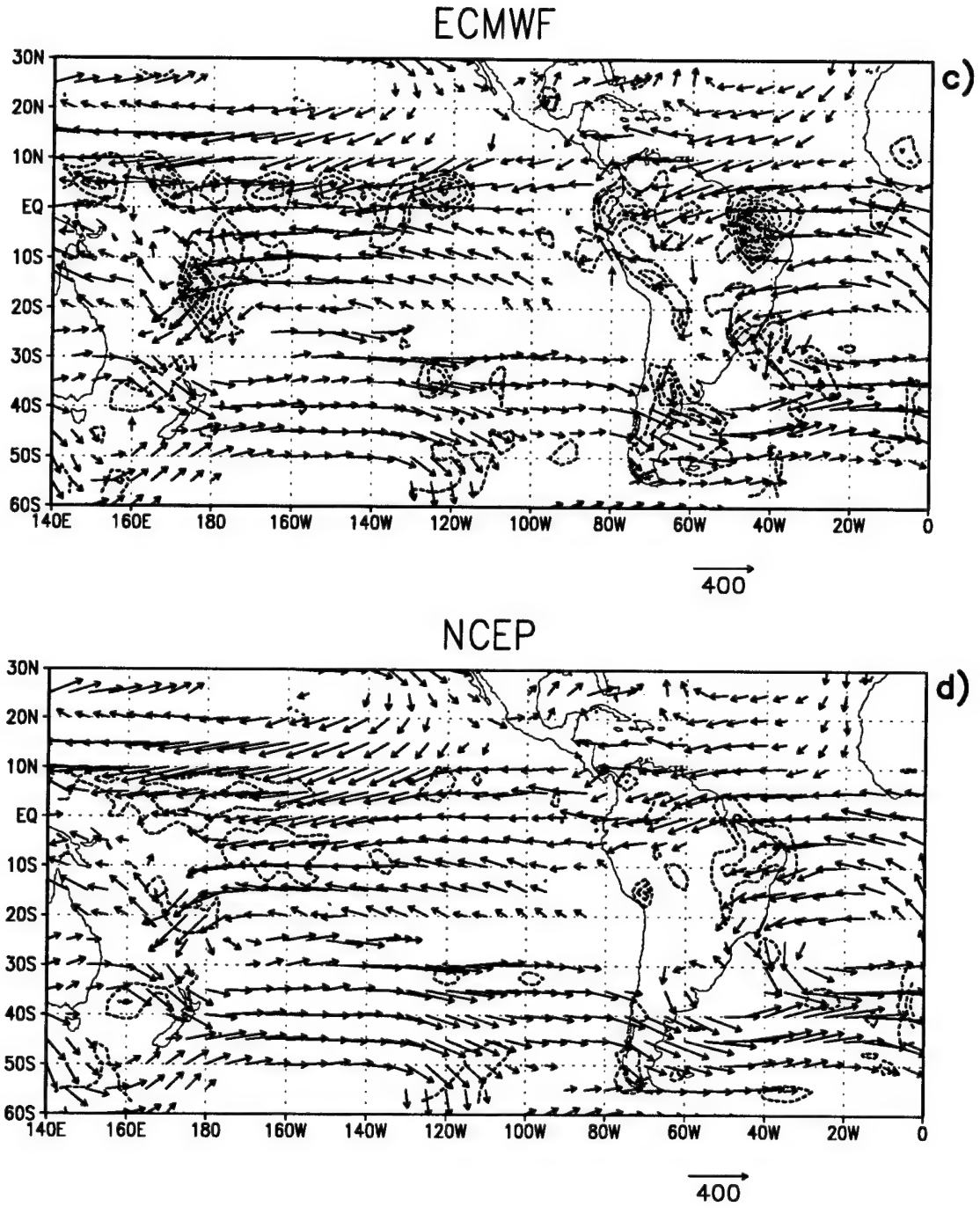

Figure 2.8 Continued

moisture flux convergence (for example, over the SPCZ in Fig. 2.8 a and b). The ECMWF produces stronger moisture flux convergence over South America and in the SPCZ. This indicates that the differences are not only due to low-level wind differences but also are linked to moisture and precipitation analysis differences.

2.4 Methodology

Nogués-Paegle and Mo (NPM97) identified alternating wet and dry events over South America using empirical orthogonal function analysis on OLRA total anomalies during austral summer months from 1974/75 to 1997/95. Intraseasonal (10 to 90 days) filtered OLR anomalies were projected onto REOF 5 and times series principal components (PCs) were obtained. An event was labelled "positive" when the PC was greater than 1.2 of its own standard deviation and lasted for 5 or more days. Fig. 1.2 shows composite OLR anomalies of positive events (1979-1993) using observed (Liebmann and Smith 1996) and ECMWF assimilated data. Positive OLR anomalies, selected based on the specified REOF PCs, are evident over the SACZ region. When the PC was less than 1.2 of its own standard deviation and lasted at least 5 days, it was labelled a "negative" event. Examples of negative events are shown in the composites of OLR anomalies in Fig. 1.2. An increase in convection in the SACZ occurred with negative REOF loadings (small OLR values over the SACZ), and a decrease in convective activity in the SACZ was found in the positive phase (higher OLR values over the SACZ, positive loadings in the REOF analysis). In this category, events were specified "with SPCZ." Figs. 1.1 a,b and 1.2 a,b show "with SPCZ" composites, identified through the REOF analysis. The “with SPCZ” events correspond to a region between 40°S and 40°N, and from the dateline eastward to 20°E (outlined in Figs. 1.1 a ,b and 1.2 a,b). In addition, Mo (personal communication, 1997) projected OLR anomalies onto REOF 5 without including a large portion of the Pacific Ocean (from 100°W to the Greenwich Meridian, as depicted in Figs. 1.1 c,d and 1.2 c,d). The objective was to identify alternating wet and dry periods without regard to activity occurring in the region of the SPCZ. These events were categorized "SACZ only (see

Figs. 1.1 c,d and 1.2 c,d)." For "with SPCZ," 19 positive and 14 negative events were identified from 1974/75 to 1994/95. For "SACZ only," 19 positive and 16 negative events were identified. This study examines the events during the austral summer months from 1979 to 1993, coinciding with the ECMWF reanalysis dataset. For the "with SPCZ" category, there are 15 positive events and 12 negative events during 14 summers. For the "SACZ only" category, there are 12 positive and 13 negative events during 14 summers.

The ECMWF reanalyzed fields from 1 November to 30 April were used to examine the events during the years 1979 to 1993. Daily values consist of an average of the 00 UTC and 12 UTC variables (helping to remove the diurnal cycle) for the upper-air data, while daily values for the supplementary fields are represented as an average of analyses/forecasts available at 00, 06, 12 and 18 Z. A 14-year climatology of the austral summer was produced to represent the seasonal cycle (1979-1992). The climatology is in the form of 12 2-week (approximately 15 days) averages beginning 1 November and lasting to 30 April. Composites of all events occurring between November 1979 and November 1993 were produced. In addition, variables for the days leading up to event start dates were taken into account. For each event, variables at day -8, day -6, day -4, day -2, and day -1 were computed to examine precursors leading to the beginning of the event. To examine the duration and demise of the events, variables were calculated at day 0, day +1, day +2, day +4, day +6, day +8, day +10, and day +12.

The primary datasets for this study have been described in this chapter, including some comparisons to evaluate various model-derived products from the ECMWF Reanalysis. Extensive comparisons were made among precipitation data sets. Discrepancies between ECMWF precipitation and satellite-derived observational precipitation analyses are comparable to the general discrepancies among the observational fields, themselves. The comparisons show the difficulty in estimating precipitation, as well as some biases among different measuring systems. For a future study, evaluation using more than one data set for precipitation estimation may be appropriate. Satellite-

derived systems such as the MRGD and the GPCP appear to be effective analysis tools. In particular, the upcoming Tropical Rainfall Measurement Mission will provide improved estimates of tropical precipitation through a suite of satellite measurements and ground validation. The upcoming chapter further evaluates reanalyzed fields from the ECMWF and describes features of the Southern Hemisphere summer.

CHAPTER 3

CLIMATOLOGY

Features of the atmospheric seasonal cycle as described by the ECMWF analyses from November through April are discussed in this section to 1) assess the veracity of the seasonal cycle in ECMWF analyses and 2) show the characteristics of the seasonally evolving mean climatology that is used to define anomalies.

Belts of high surface pressure in subtropical latitudes with low pressure towards the poles and the equator are well represented in the analyses. Oceanic surface pressure values are known to be lowest during winter and largest in summer, in contrast to what is observed over the continents (Fig. 3.1). The analyzed fields show higher values in the Pacific and Atlantic subtropical highs in November and April rather than in January. Extensive stratus decks over the cold currents of the Eastern Pacific Ocean shield the incoming solar radiation, modifying the resulting surface pressure and temperature. The surface analyses, therefore, may strongly reflect assimilating model physics.

Land areas respond to seasonal changes on the surface energy balance by developing low pressure during summer and monsoonal circulations which transport moisture-laden air from the oceans. Regions with high orography channel this flow, forcing large-scale ascent over the mountains and sustaining there high precipitation values. Fig. 3.1 shows surface wind divergence from the subtropical highs, with largest values over the eastern oceans. Strongest surface winds over the Pacific are found to the west of the South American coast, with a northwestward component which attains its maximum amplitude in boreal spring (Fig. 3.1 c). This occurs at a time when the Pacific equatorial trough in these analyses is displaced toward the American coast.

Figure 3.1 Average ECMWF (1979-1993) 1000 mb height contours (m) and winds (m/s) for (a) November, (b) January, and (c) April.

November a)

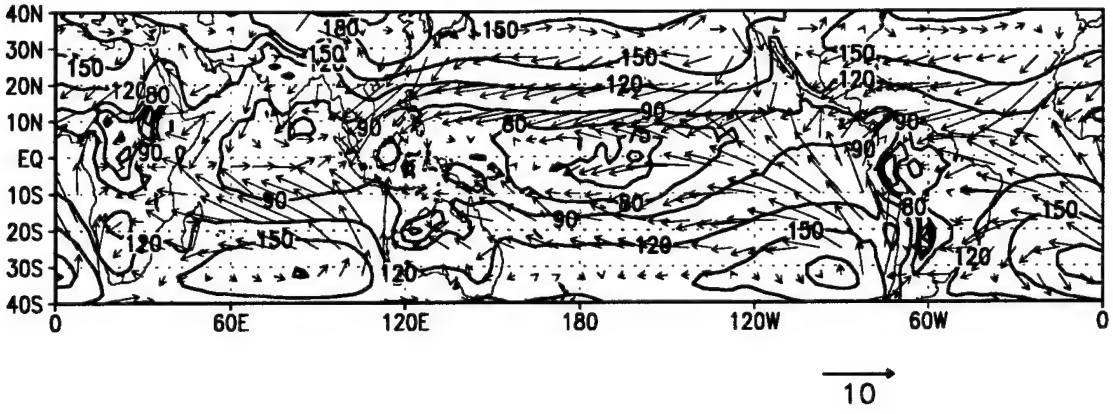

January b)

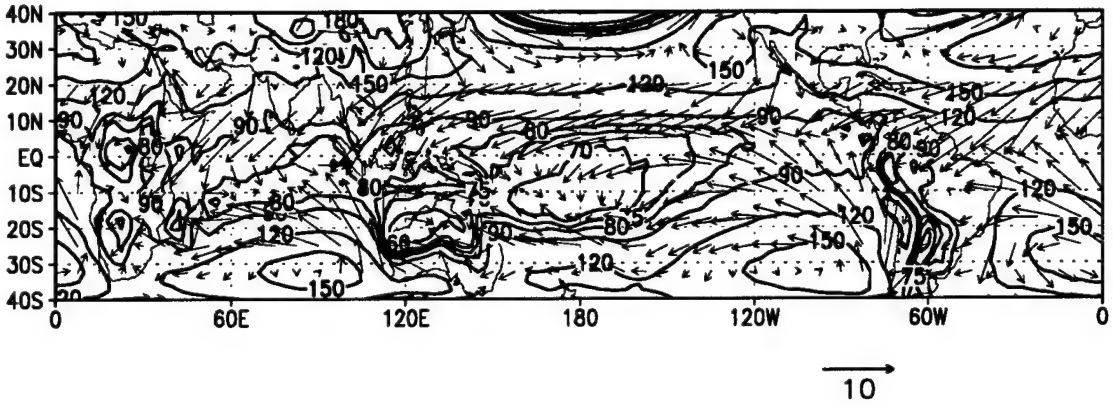

April c)

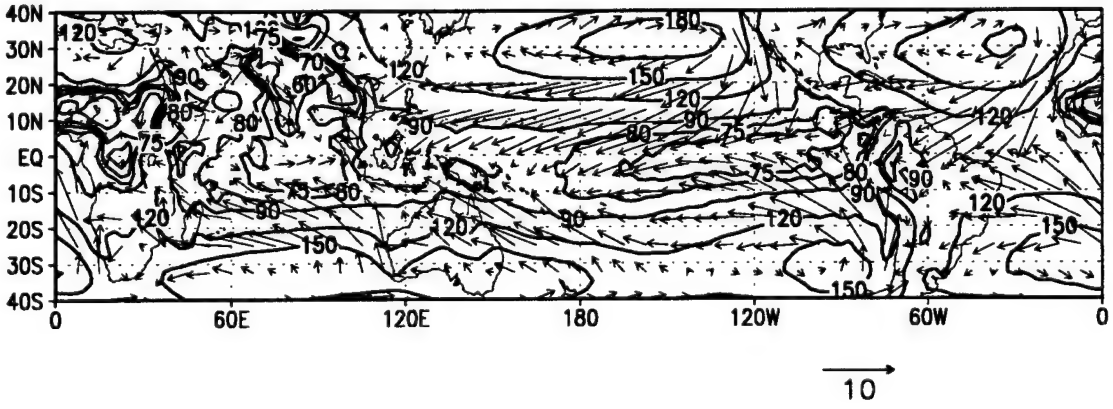

During January (Fig 3.1 b), the center of the Pacific trough is found at the dateline, displaced into the Southern Hemisphere (approximately 10°S). The surface wind at equatorial latitudes responds to the surface pressure gradient and attains a strong zonal component as it converges into the South Pacific Convergence Zone (defined below). The northeasterly flow into the east coast of South America stops at about 10°N during early November, and it moves southward to about 10°S as the season progresses (Fig. 3.1 b and c).

The regions of surface convergence are reflected well in the precipitation fields (Fig. 3.2). These are also co-located with warm sea surface temperatures, with well-defined precipitation bands over the ITCZs, with monsoonal rains over Africa and South America, and with the Western Atlantic. Precipitation over the Western Atlantic is well-defined during the austral summer and exhibits a northwest-to-southeast tilt referred to as the South Pacific convergence zone (SPCZ). During this time of the year, precipitation over tropical South America attains maximum values.

The ECMWF reanalysis (with T106 resolution) is able to capture the double ITCZ symmetric about the equator during March to April (Fig. 3.2 f). The validity of this feature has been confirmed with satellite estimates of rain using the Global Precipitation Climatology Project data set (Huffman et al. 1995). Also, the position of the Pacific trough in April (Fig. 3.1 c) corresponds with this pattern. The ITCZ remains at about 10° N in all panels of Fig. 3.2, with precipitation attaining maximum values early in the season (Fig. 3.2 a) when activity in the SPCZ region is weak. In contrast, as the SPCZ strengthens (Fig. 3.2 c and d), the ITCZ weakens. A similar signature appears in the difference between evaporation and precipitation (shown in Fig. 3.3), with large negative values in the ITCZ early in the season (11/1-11/15) and large SPCZ values later, during mid-summer (Fig. 3.3 c and d). Over the tropical continents, precipitation exceeds evaporation during the 6-month period considered, here. These precipitation patterns are sustained by convergence of vertically integrated moisture flux, diverging from

Figure 3.2 Two-week ECMWF averages of precipitation are shown for (a) November 1-15, (b) December 1-15, (c) December 31-January 14, (d) January 30-February 13, (e) March 1-15, and (f) March 31-April 14. The averages are from November 1 to April 30, 1979-1993. Precipitation is contoured and shaded every 5 mm/day.

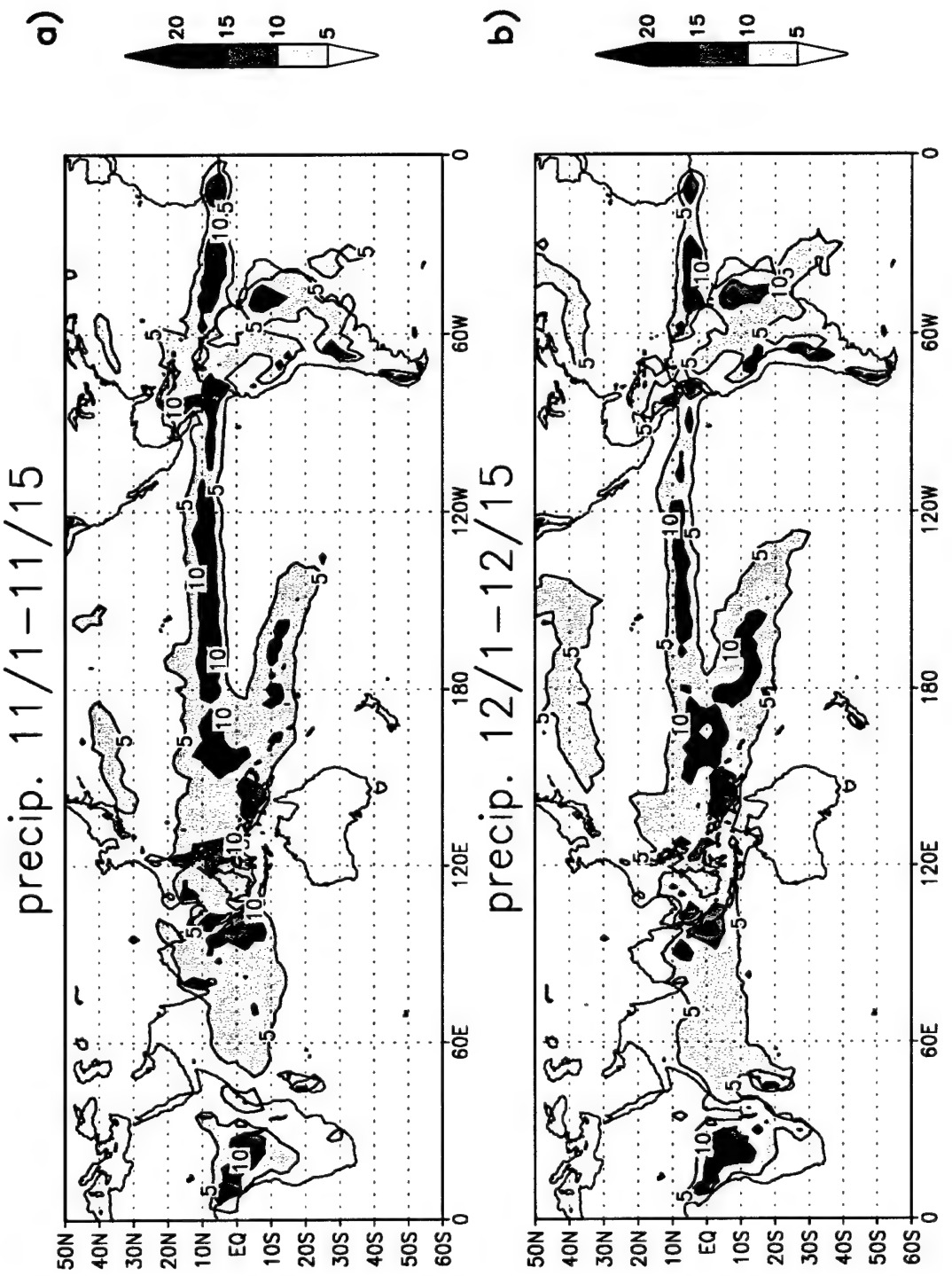
a)
20
15
10
5
precip. 11/1–11/15
50N
40N
30N
20N
10N
EQ
10S
20S
30S
40S
50S
60S
0
60E
120E
180
120W
60W
0
b)
20
15
10
5
precip. 12/1–12/15
50N
40N
30N
20N
10N
EQ
10S
20S
30S
40S
50S
60S
0
60E
120E
180
120W
60W
0

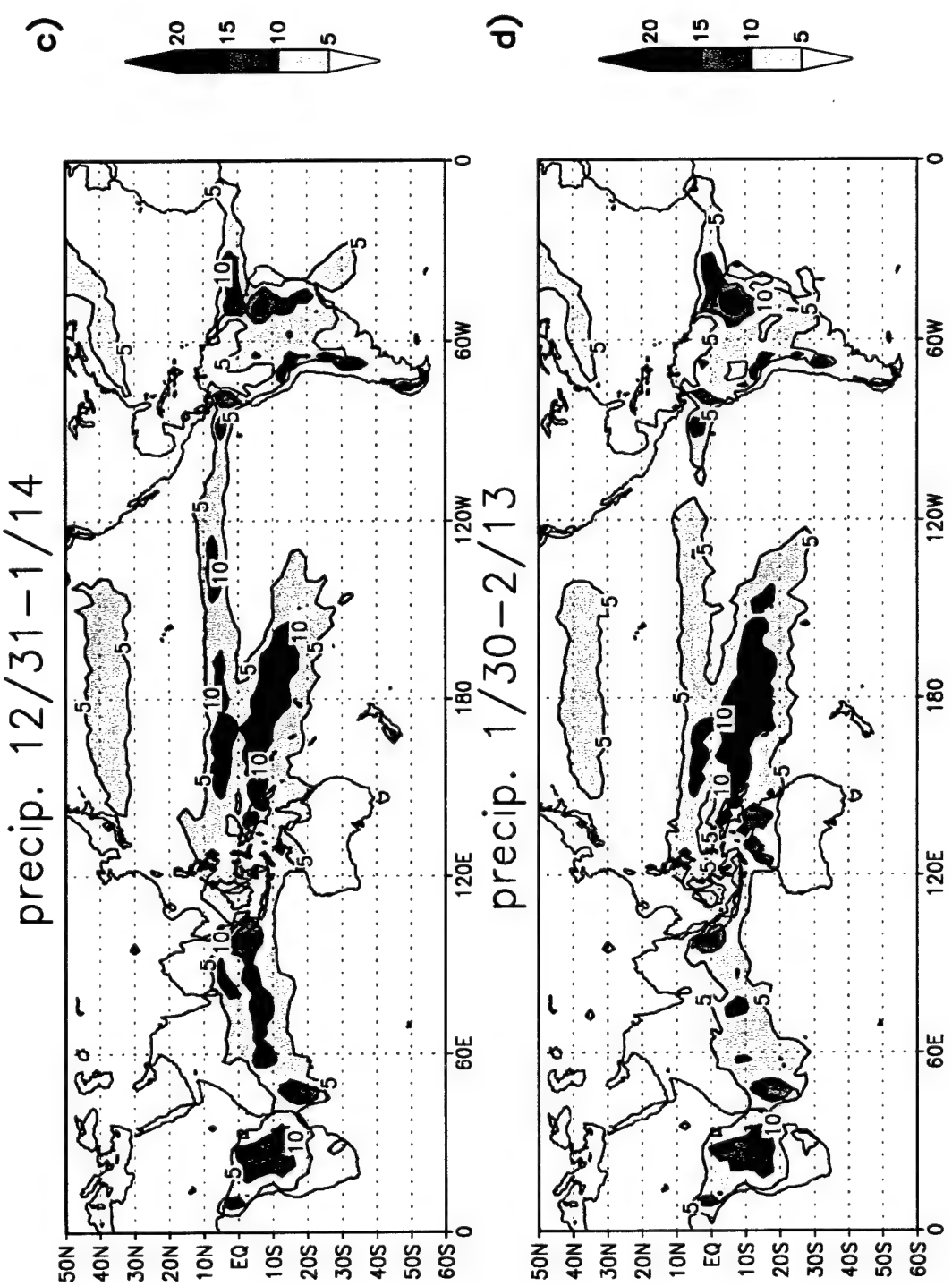

Figure 3.2 Continued

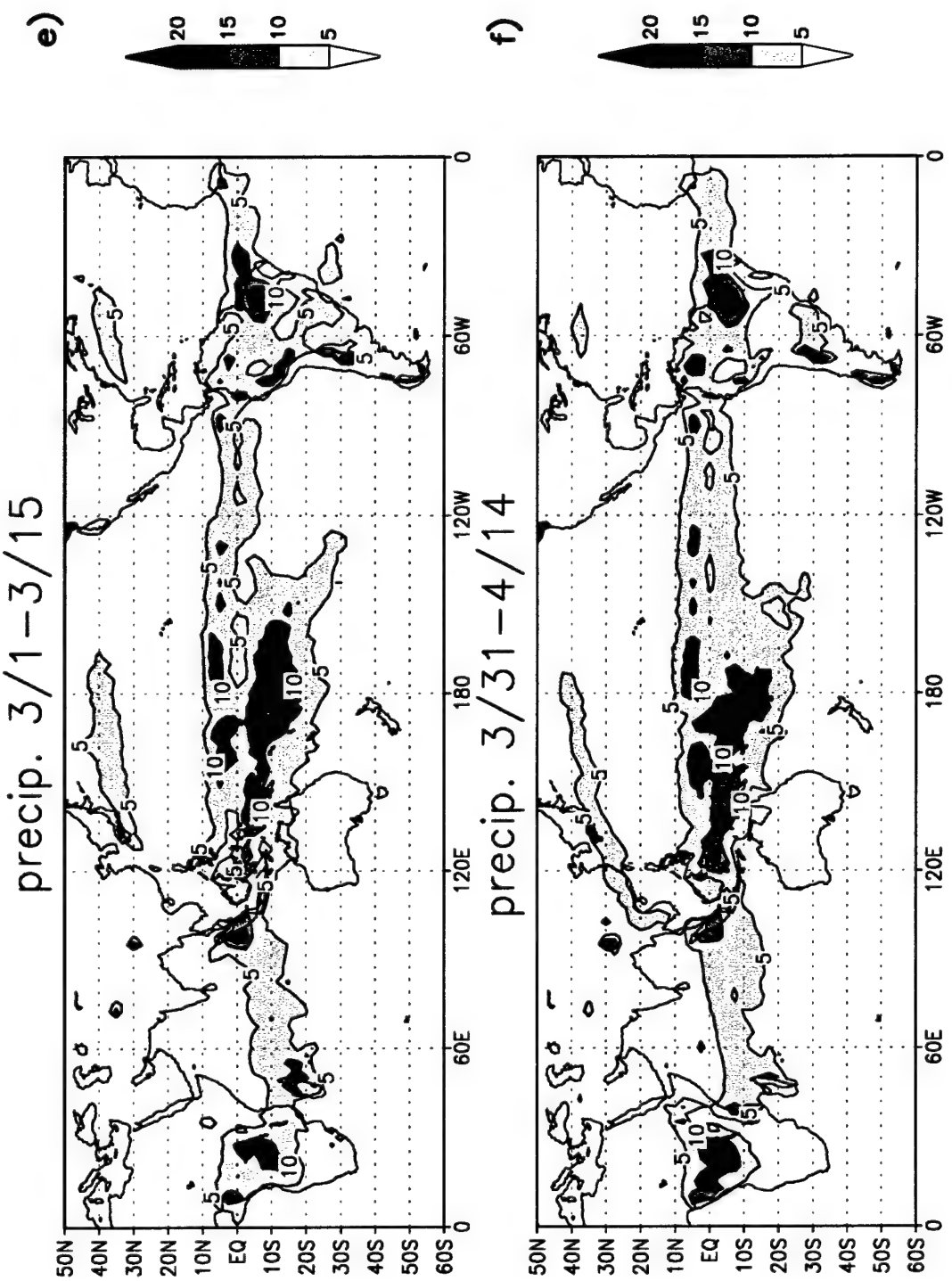

Figure 3.2 Continued

Figure 3.3 Two-week ECMWF averages of evaporation minus precipitation are shown for (a) November 1-15, (b) December 1-15, (c) December 31-January 14, (d) January 30-February 13, (e) March 1-15, and (f) March 31-April 14. The averages are from November 1 to April 30, 1979-1993. Differences are shaded and contoured every 2 mm/day.

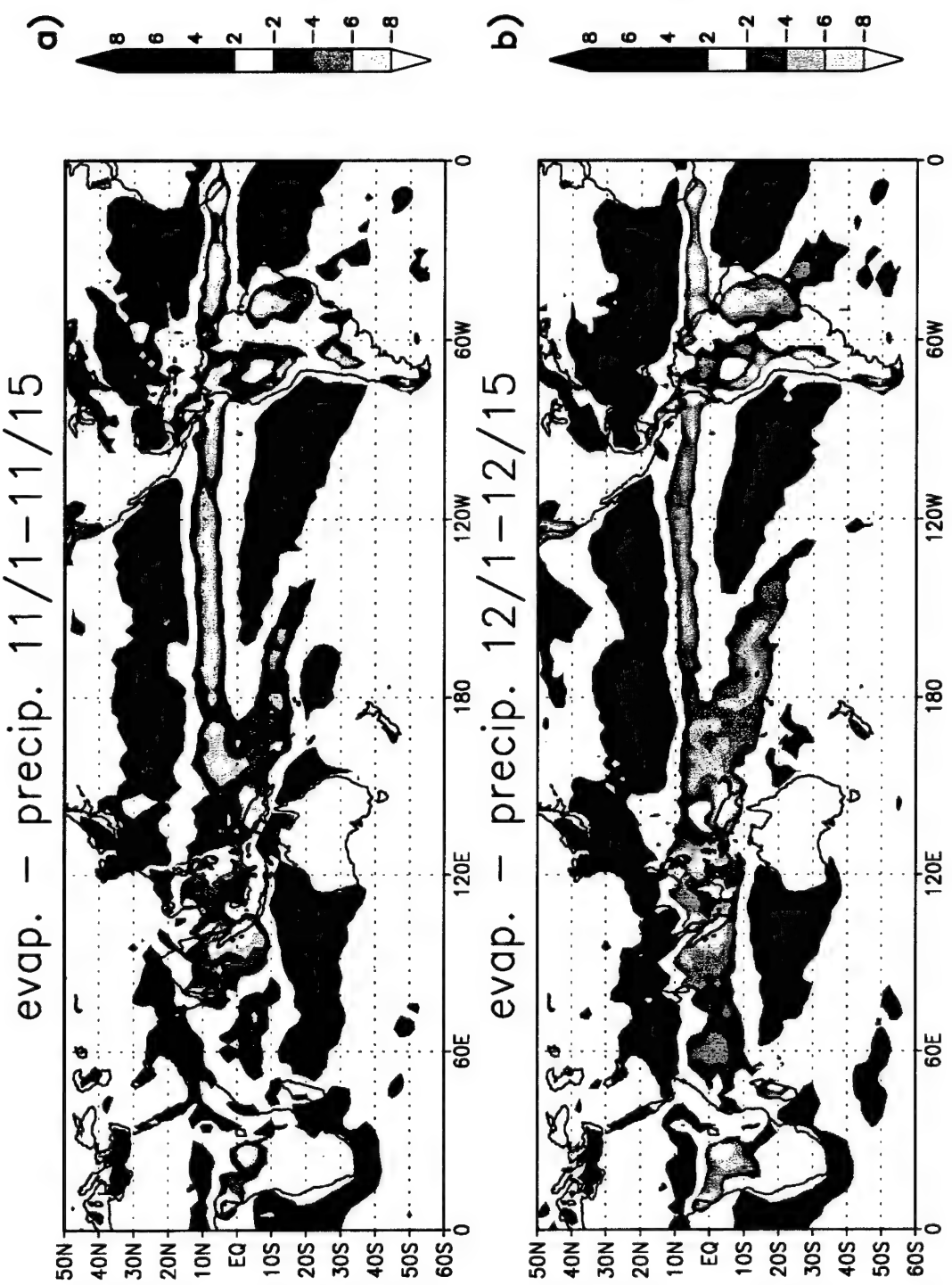
a)
8
6
4
2
−2
−4
−6
−8
evap. − precip. 11/1−11/15
50N
40N
30N
20N
10N
EQ
10S
20S
30S
40S
50S
60S
0
60E
120E
180
120W
60W
0
b)
8
6
4
2
−2
−4
−6
−8
evap. − precip. 12/1−12/15
50N
40N
30N
20N
10N
EQ
10S
20S
30S
40S
50S
60S
0
60E
120E
180
120W
60W
0

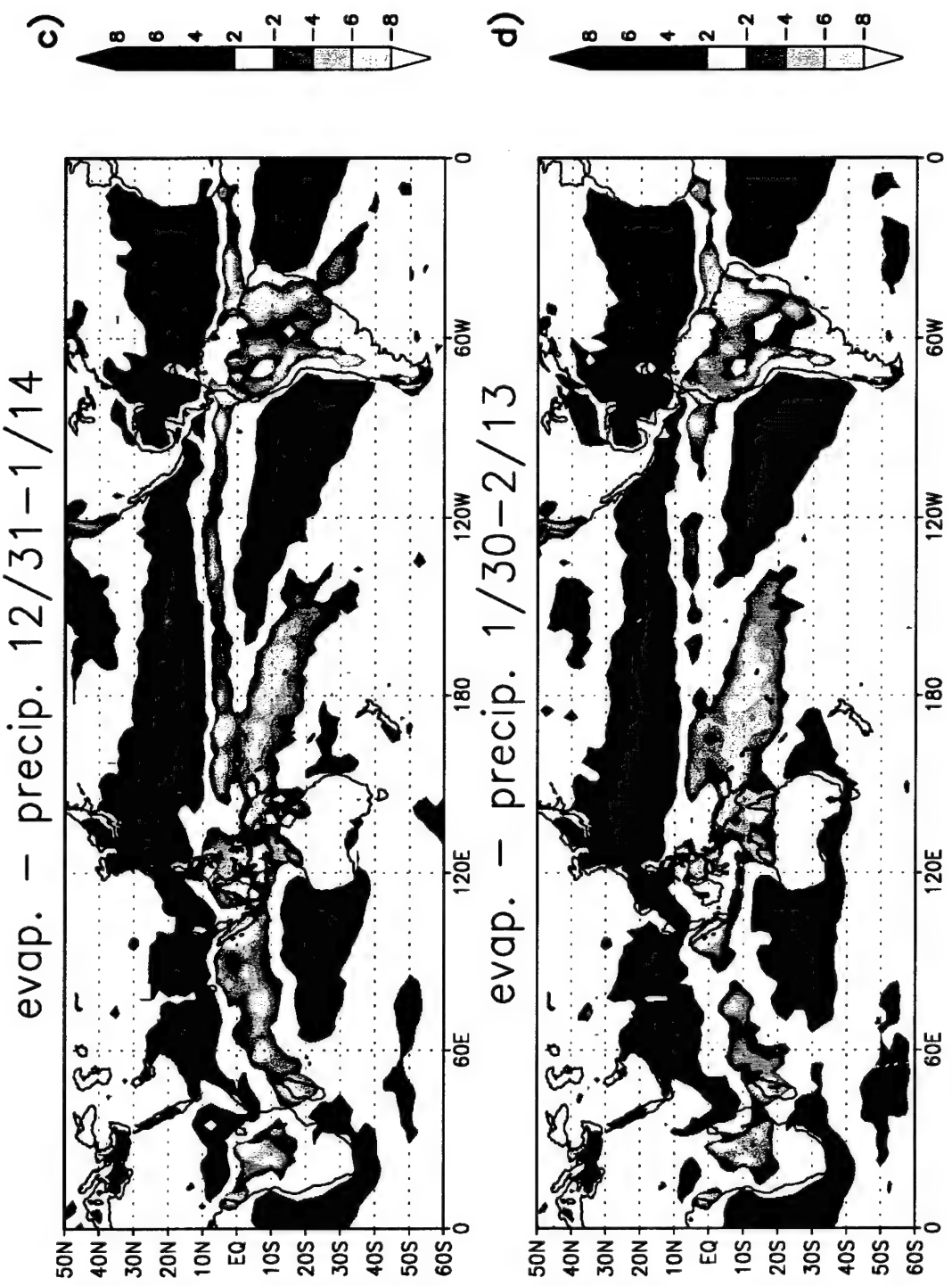

Figure 3.3 Continued

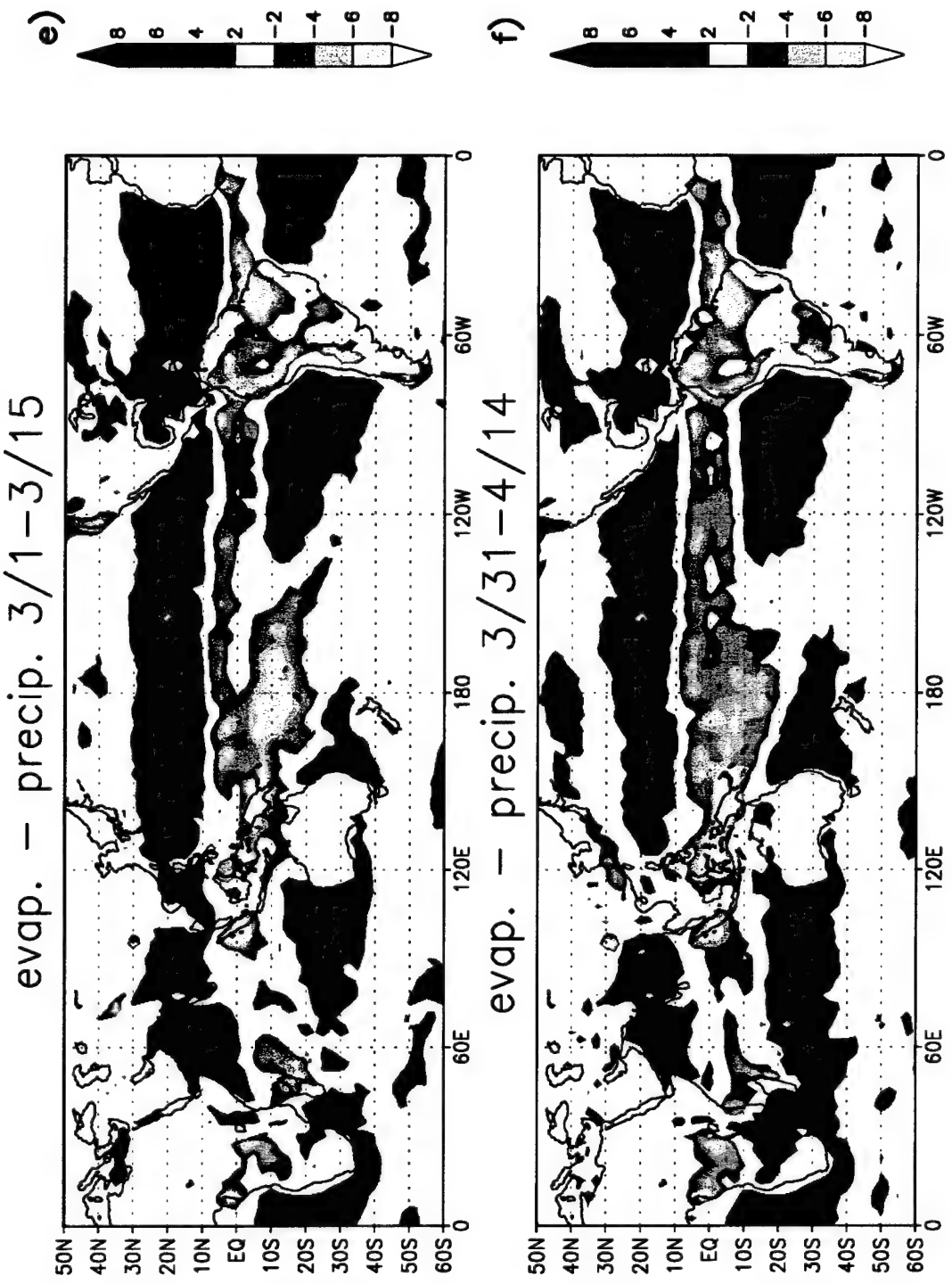

Figure 3.3 Continued

subtropical latitudes where evaporation exceeds precipitation. In Chapter 4, similar oscillations are shown in which evaporation exceeds precipitation. In Chapter 4, we show similar oscillations between the ITCZ and the SPCZ with enhanced precipitation over tropical South America in much shorter time scales.

Over tropical South America, the Amazon basin is the center of maximum convection during December, January and February (DJF), where the central and southern portions receive more than 60% of their annual mean precipitation (Legates and Willmott 1990). Convective activity penetrates farthest south in area and extent during this time and is mostly in the form of convective rain with a strong diurnal pattern (Silva Dias et al. 1987). An area of low-level moisture convergence extending from Central Brazil into the Atlantic (Fig. 3.2) also becomes strongest and most persistent during this time. This area is known as the South Atlantic Convergence Zone (SACZ). Fig. 3.4 shows the seasonal march of mean precipitable water averaged between 40°W and 60°W. The increase is noticeable in the Amazon basin and at subtropical latitudes, and it also depicts the SACZ in January (Fig. 3.4 b). These are realistic features of the ECMWF reanalysis.

Seasonal changes over the Americas are strongly influenced by coastal geometry and orography. Similar to other monsoonal circulations, a well-defined high pressure system is found at upper-levels (Fig. 3.4) while the lower levels are modified by the prevailing orography. These and other features of the seasonal march over the Americas have been discussed by Horel et al. 1989. The biweekly average march of 100 mb wind along 20°S is shown in Fig. 3.5 . The "Periods" along the y-axis in Fig. 3.5 a correspond to two week averages, beginning with the November 1-15 (Period 1) average, and ending with the April 15-30 (Period 12) average. The orientation of the vectors shows the seasonal westward progression of the anticyclone (referred to as the Bolivian High) and its gradual shift eastward late in the summer. A downstream trough is evident over Northeast Brazil, and zonal flow prevails south of 35°S (Fig. 3.4 b). These are dominant features during DJF that are described well by the reanalysis. The seasonal march at 850 mb is shown in

Figure 3.4 Biweekly ECMWF averages of mean precipitable water (mm), averaged from 40°W to 60°W, are shown in (a), beginning 1-15 November (period 1 on the y-axis) and ending 15-30 April (period 12 on the y-axis). Values are contoured every mm. In (b), the 15 January (period 6) biweekly averaged precipitable water is contoured every 5 mm.

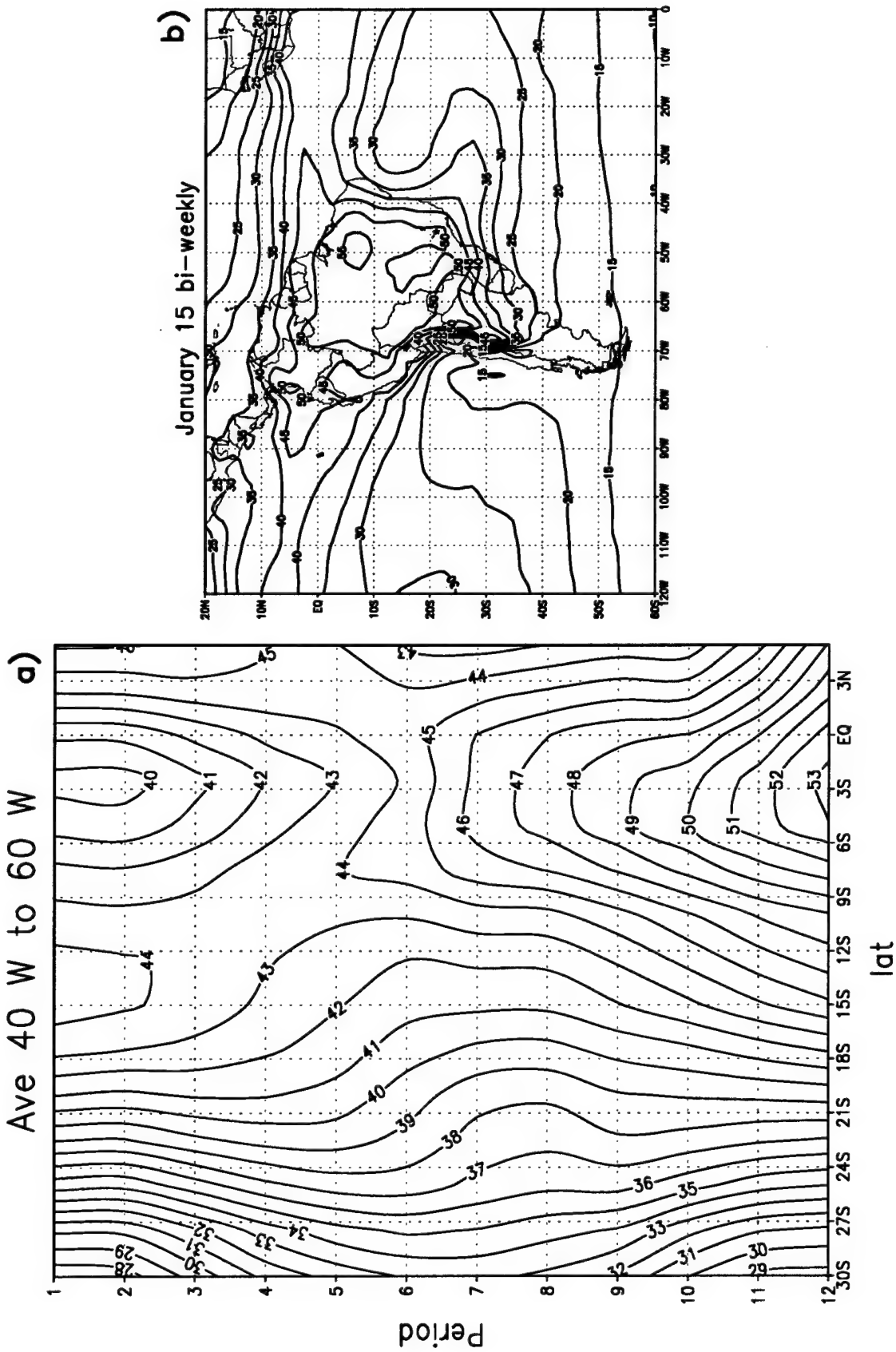
a)
Ave 40 W to 60 W
Period
lat
b)
January 15 bi-weekly

Figure 3.5 A Hovmöller diagram in (a) shows 2-week ECMWF 100 mb wind vector climatology (m/s) from 1979-1992, centered at 20°S, beginning 1-15 November (period 1 on the y-axis) and ending 15-30 April (period 12 on the y-axis). The 2-week 100 mb wind vector average for 15-29 January (period 6) is shown in (b).

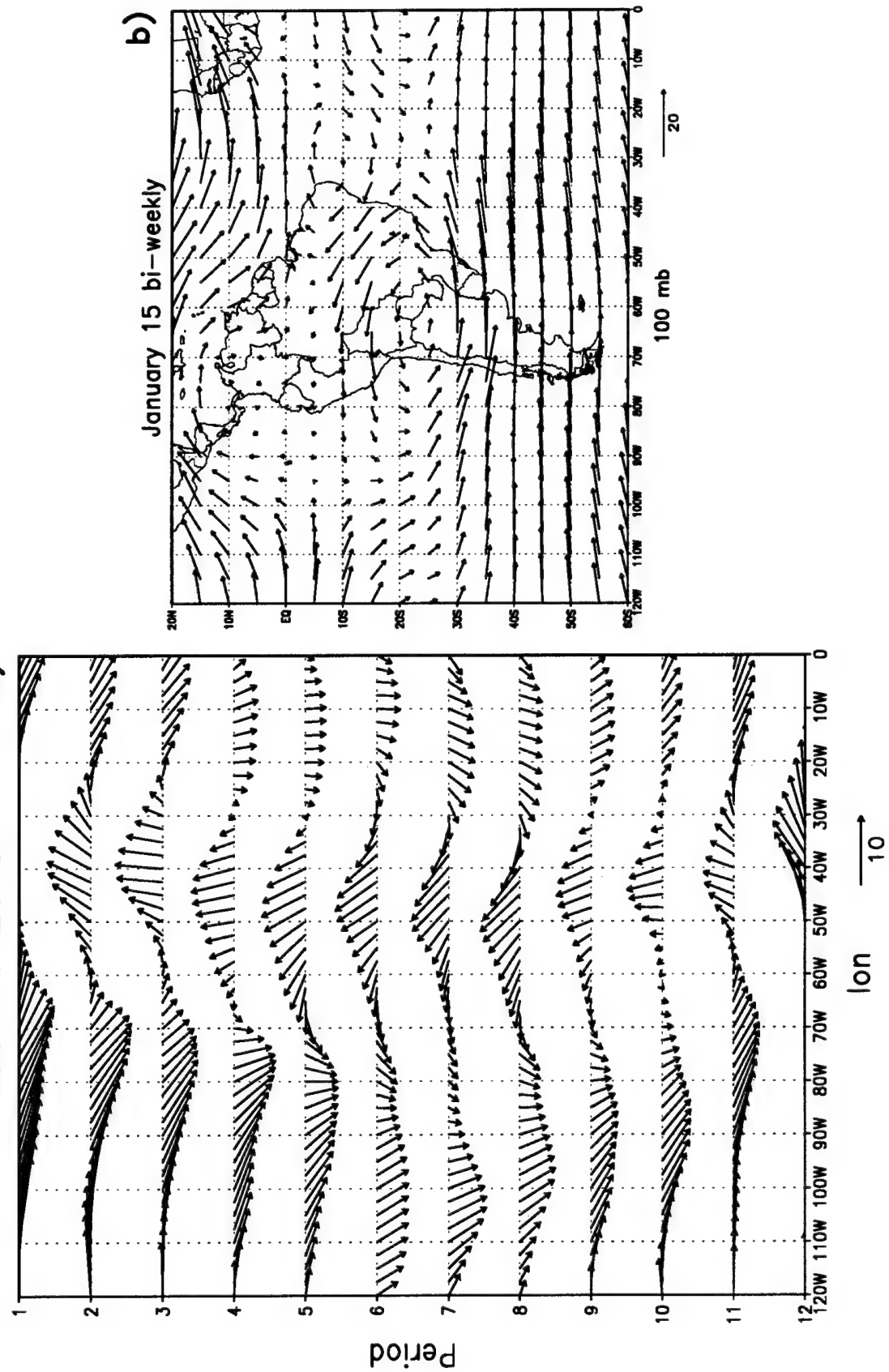
a)
100 mb 20 S
Period
1
2
3
4
5
6
7
8
9
10
11
12
120W 110W 100W 90W 80W 70W 60W 50W 40W 30W 20W 10W 0
lon
10
b)
January 15 bi-weekly
20N
10N
EQ
10S
20S
30S
40S
50S
60S
120W 110W 100W 90W 80W 70W 60W 50W 40W 30W 20W 10W 0
100 mb
20

Figure 3.6 A Hovmöller diagram in (a) shows 2-week ECMWF 850 mb wind vector climatology (m/s) from 1979-1992, centered at 20°S, beginning 1-15 November (period 1 on the y-axis) and ending 15-30 April (period 12 on the y-axis). The 2-week 850 mb wind vector average for 15-29 January (period 6) is shown in (b).

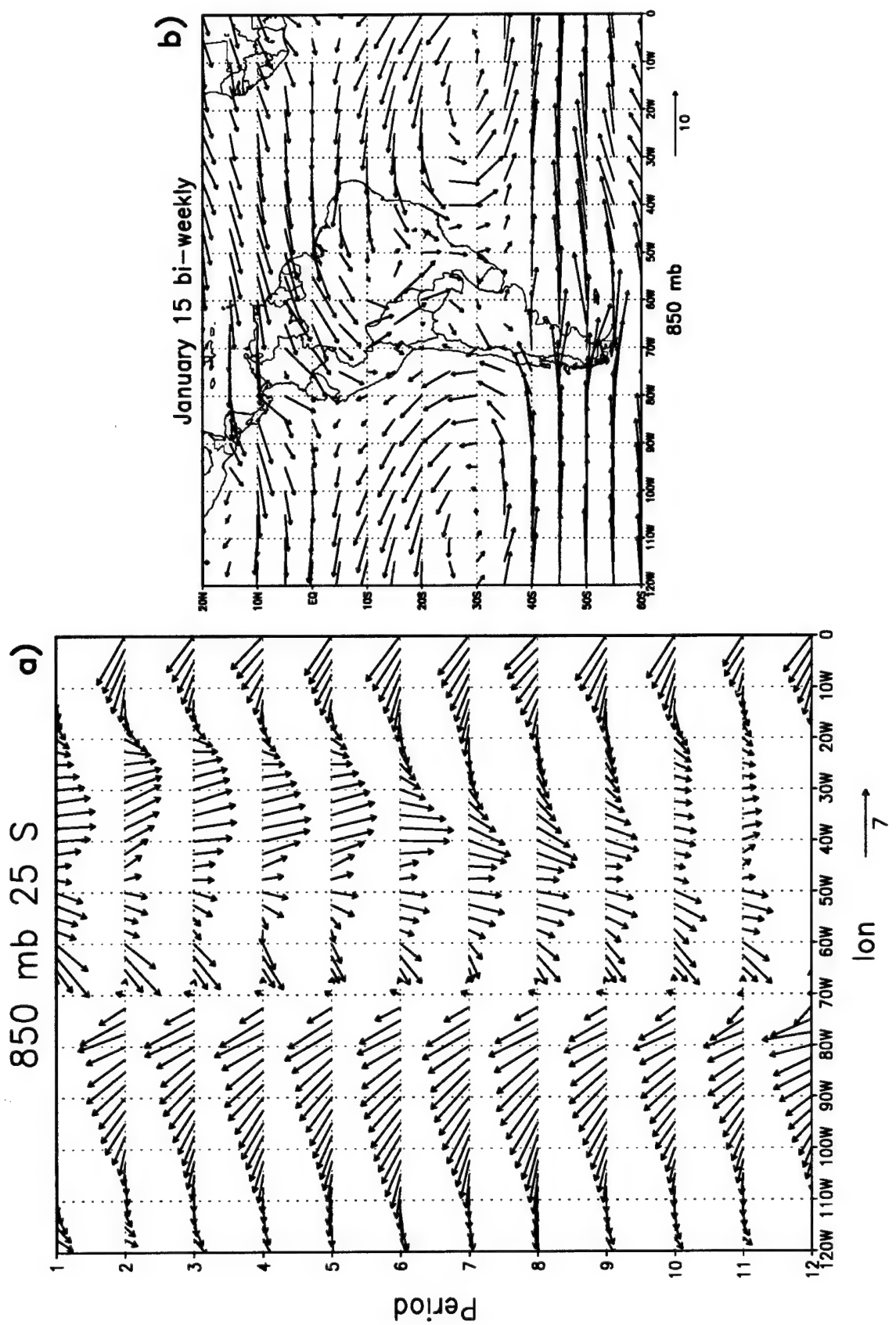
a)
850 mb 25 S
Period
lon
7
120W 110W 100W 90W 80W 70W 60W 50W 40W 30W 20W 10W 0
b)
January 15 bi-weekly
850 mb
10

Figure 3.7 Two-week ECMWF averages of evaporation are shown for (a) November 1-15, (b) December 1-15, (c) December 31-January 14, (d) January 30-February 13, (e) March 1-15, and (f) March 31-April 14. The averages are from November 1 to April 30, 1979-1993. Differences are shaded and contoured every mm/day.

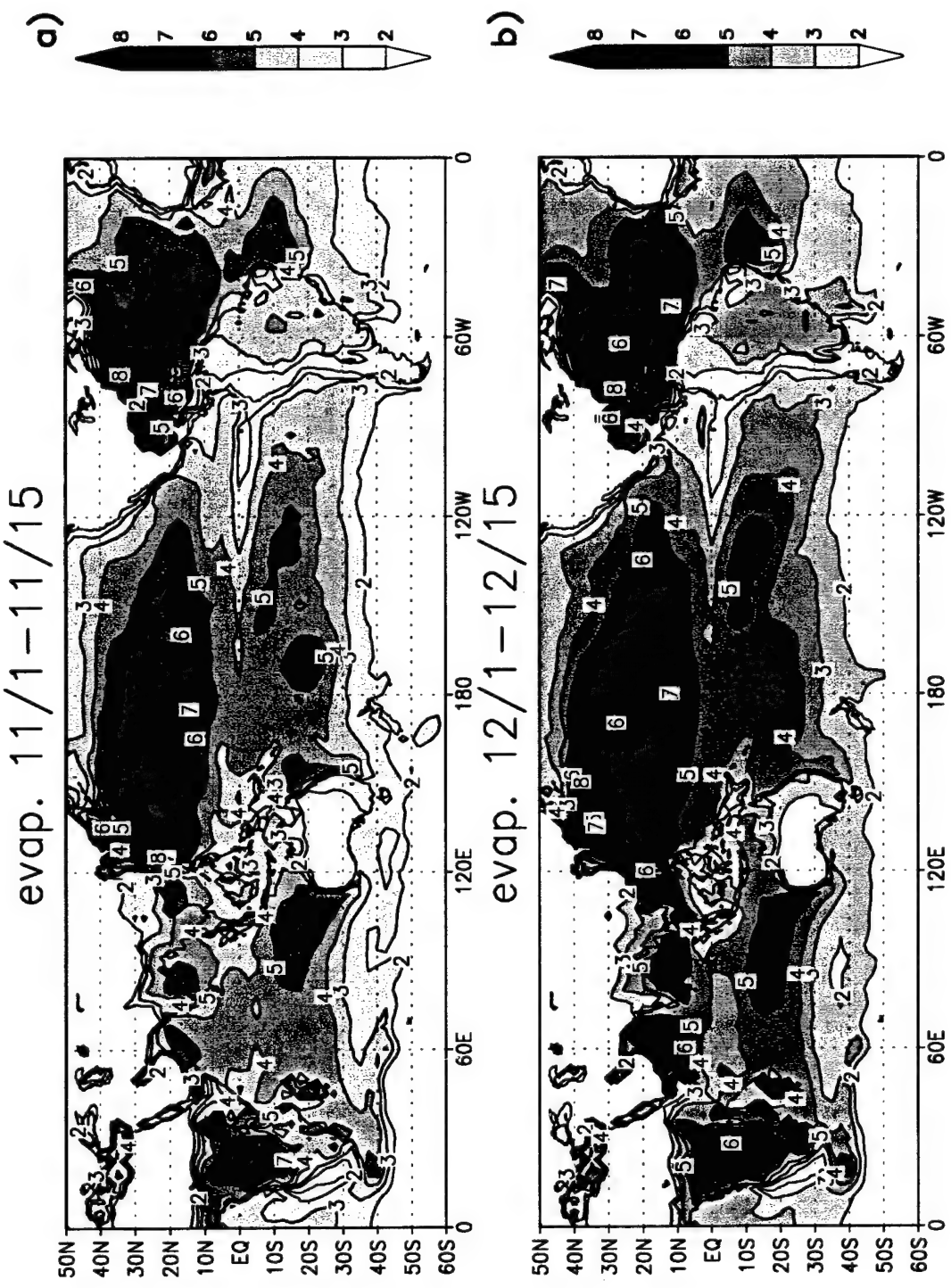
a)
b)
evap. 11/1–11/15
evap. 12/1–12/15
8 7 6 5 4 3 2
50N 40N 30N 20N 10N EQ 10S 20S 30S 40S 50S 60S
0 60E 120E 180 120W 60W 0

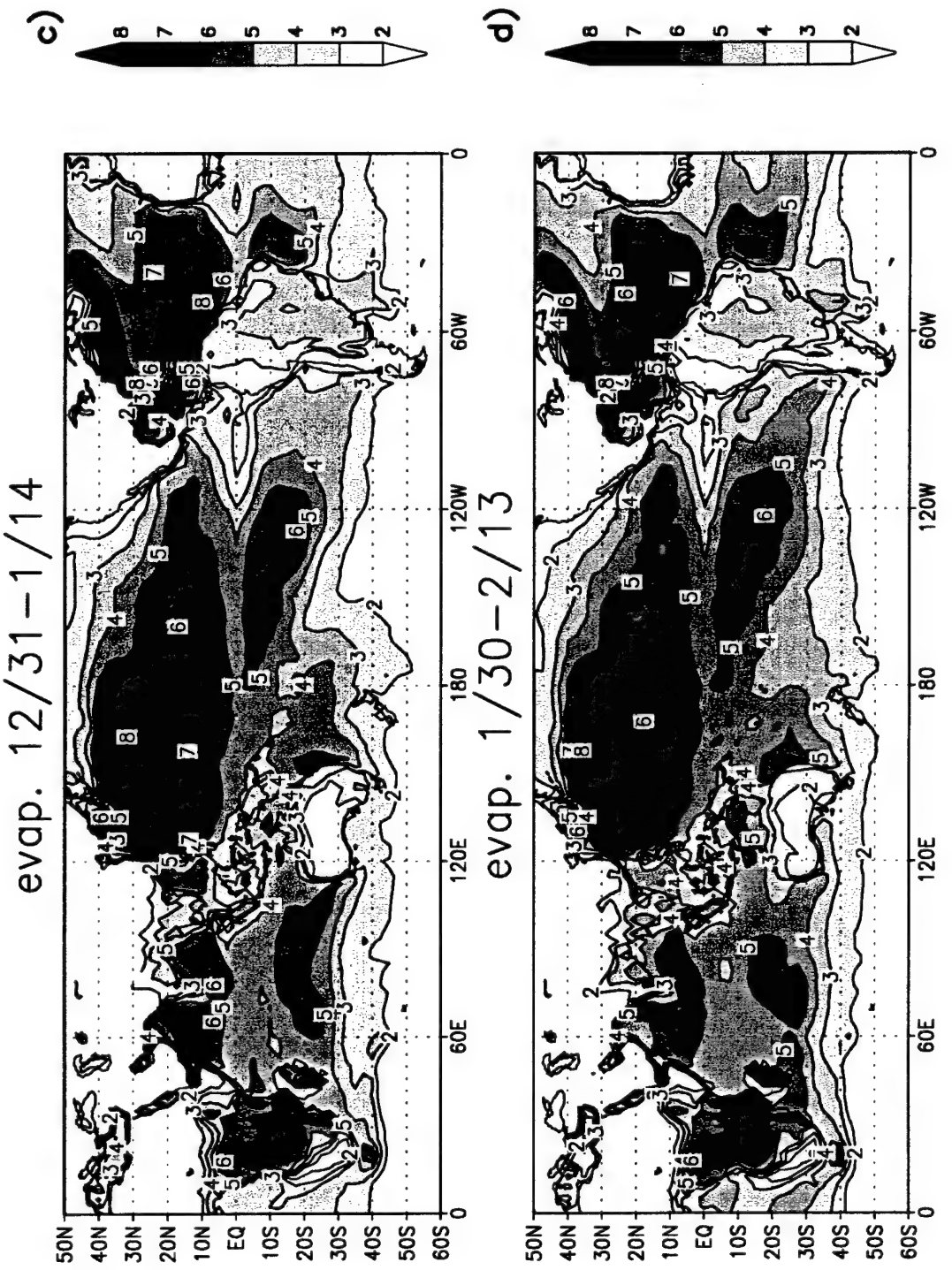

Figure 3.7 Continued

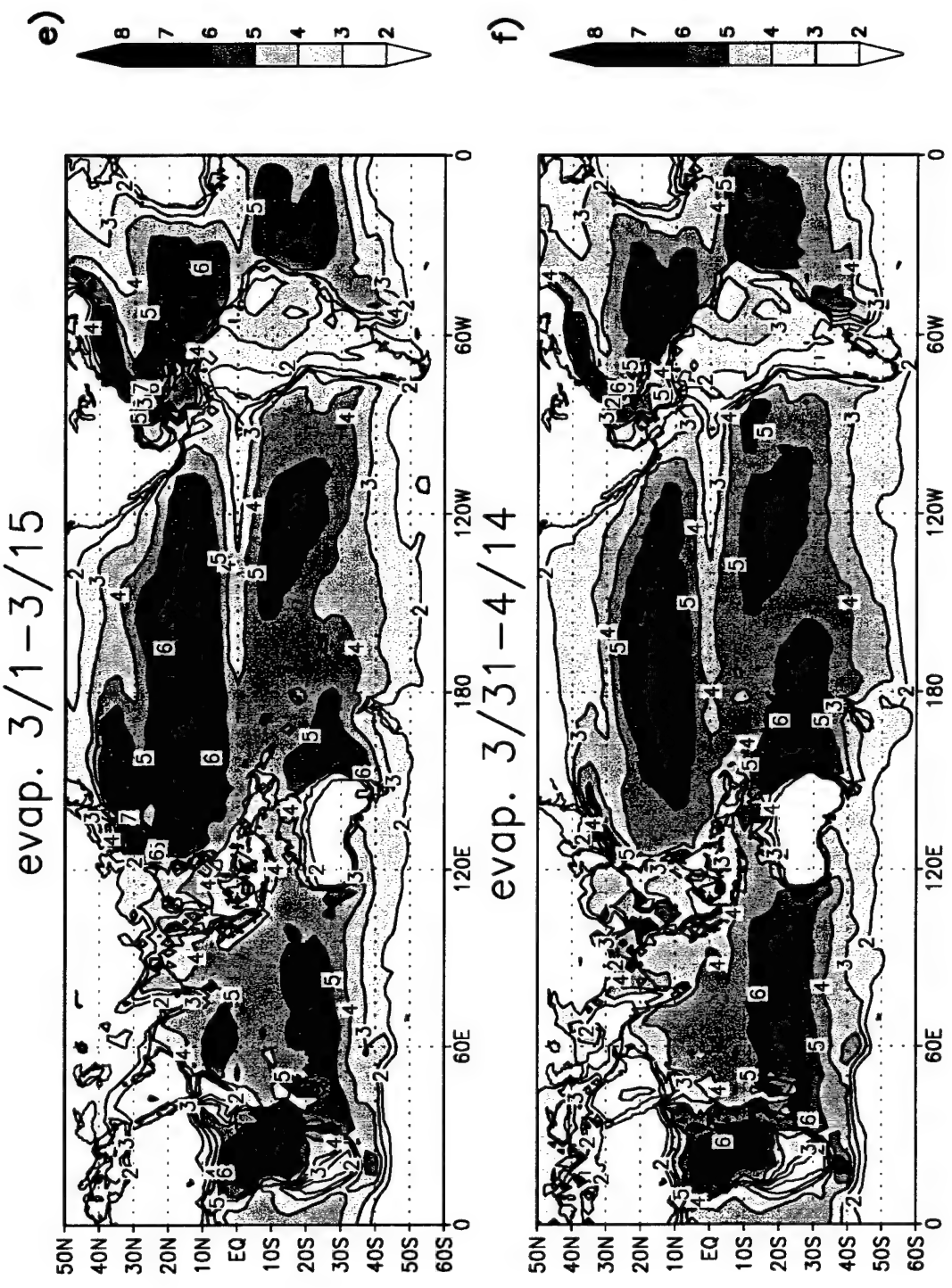

Figure 3.7 Continued

Fig. 3.6. Along 70°W, the Andes act as a node blocking southerly flow to the West. Southeasterly flow west of the Andes appears independent of the seasonal march, suggesting the Pacific subtropical high (Fig. 3.6 b) fluctuates little during the Summer. A broad area of northerly low-level flow throughout the Summer is also evident along the eastern slopes of the Andes. Over northern South America, northeasterly surface winds are predominant (see Fig. 3.1) and strongest in April. At 850 mb, flow with an easterly component protrudes into the Amazon and turns southward as it approaches and is blocked by the Andes. This agrees with the results of Gandu and Geisler (1991), who simulated this blocked flow using a nonlinear, primitive equations model. The southward intrusion of moist oceanic air maximizes in January at about 40°W, resulting from the westward-migrating Atlantic subtropical high. This is also reflected at the 1000 mb level (see Fig. 3.1 b), where diverging surface winds move over the continent. Part of this research is to examine conditions in which moisture is intraseasonally transported to the subtropical plains by a low-level jet (NPM97).

The oceans play an important role in the flux of moisture. Large values of evaporation provide a source of moisture flux to regions with enhanced precipitation. Over South America, evaporation from the oceans exceeds precipitation throughout the Summer (Figs. 3.2 and 3.3). Along the coasts and over the Atlantic ITCZ, evaporation values are largest during February and March. Maximum values exceed 6 mm/day off the coast of Brazil at 15 S and 7 mm/day over the Atlantic along 10°N (Fig. 3.7) at a time when precipitation over South America is most pronounced. Fig. 3.7 shows strong evaporation over the Central and Western Pacific during January and February, coinciding with an enhanced SPCZ. Evaporation from the oceans is, therefore, a major source of vertically integrated moisture flux, and it contributes to evapotranspiration over the continent. Anomalies from the seasonal march are presented in Chapter 4 for cases of enhanced precipitation over tropical South America.

CHAPTER 4

NEGATIVE EVENTS

Periods of enhanced convection over the South Atlantic Convergence Zone have a pronounced effect not only over tropical South America but also in neighboring regions, where compensating sinking motions promote suppressed precipitation. This chapter documents the large-scale circulations associated with intensification of convection in the SACZ and examines the difference in local circulations resulting from different convective regimes in the Pacific Ocean. It is shown that strong SACZ events develop in about 10 days, with two different convective regimes over the Pacific Ocean, as shown in Fig. 1.1. Events with suppressed convection over the SPCZ (150°W, 20°S) and enhanced convection over Australia and the SACZ are components of a large-scale system that evolves from its opposite phase in about 10 days. In contrast, there is a second type of evolution of enhanced convection in the SACZ with roots over South America and the Pacific Ocean, without any apparent ties to the Pacific Ocean. Such cases are accompanied by an enhanced SPCZ.

The chapter is divided into five subsections as follows: first, OLR and precipitation fields are discussed; followed by a description of associated upper-level circulation anomalies; and a discussion on the possible role of synoptic-scale transients. The fourth section examines components of the atmospheric hydrological cycle for these events. Substantiation of results obtained from the ECMWF reanalysis is then presented by comparing ECMWF analysis composites obtained for events over a 6-year period with cloud coverage obtained from the ISCCP and OLR observations.

4.1 OLR and Precipitation Diagnostics

Rotated empirical orthogonal function (REOF) analyses of OLR anomalies, described in section 2.4, were used to identify periods of alternating wet and dry conditions over subtropical South America during summer. Two types of REOF analyses were conducted (NPM97). The first focused on South America, extending from 40°S to 10°N and from 100°W to the Greenwich Meridian (denoted as REOF A). The second was applied to a sector from 180°W to 20°E and from 40°S to 40°N (denoted as REOF B). Filtered data was projected onto these EOFs to obtain time series of principal components (PCs). An event was chosen when the magnitude of the PC was greater than 1.2 of its own standard deviation and lasted for 5 or more days. Events selected by REOF A and B are used to study SACZ cases with possible connections to atmospheric processes over the Pacific Ocean. These are referred to as "SACZ with SPCZ" (abbreviated "with SPCZ"). Events chosen with REOF A but not with REOF B are referred to as "SACZ only." The negative events (cases of enhanced SACZ) are listed in Table 4.1 and are shown to have an average duration (as defined in Chapter 2) of about a week. Events which occur during warm ENSO years are denoted by an asterisk. The analyses reveal that "with SPCZ" cases are more than twice as likely (64% versus 25%) to occur during warm ENSO years. NPM97 found that these events were three times more likely to occur during warm and cold ENSO years for the period 1973-1993.

Therefore, the two types of composites ("with SPCZ" and "SACZ only") were selected based on REOF analyses over different areas. The "with SPCZ" cases consider a large portion of the Pacific and an active SPCZ that is associated with SACZ events. The "SACZ only" cases have been selected based on intensification or suppression over the SACZ without regard to activity in the Pacific (the REOF area does not include a large portion of the Pacific). A third type of composite was also produced. It consists of events on the list for REOF B but not on the list for REOF A. These are denoted as "SPCZ only."

Table 4.1

Negative Events

"with SPCZ"	"SACZ only"
01/20-02/02 '77*	02/04-02/09 '75
01/23-01/28 '82	03/24-03/28 '76
03/03-03/07 '83*	01/14-01/23 '81
01/22-01/29 '84*	03/25-03/30 '81
03/08-03/12 '84*	03/08-03/12 '82
11/24-12/01 '85	01/17-01/30 '85
01/26-01/31 '87*	02/27-03/09 '85
02/15-02/20 '87*	11/03-11/08 '85
01/07-01/11 '88	12/23-12/28 '85
03/11-03/15 '89*	02/16-02/20 '86
03/22-03/30 '91	12/25-12/31 '86*
01/16-01/25 '92*	02/24-02/28 '90
03/26-03/31 '93*	11/11-11/16 '91*
03/03-03/09 '94	11/02-11/07 '92*
	03/05-03/13 '93*
	02/02-02/12 '95
Total=14	Total=16
Ave Time=7.1 dy	Ave Time=7.4 dy
64% Warm ENSO	25% Warm ENSO

* denotes events that occurred during warm ENSO years

Figure 4.1 Satellite-derived (Liebmann and Smith 1996) OLR composite anomalies (OLRA) for negative cases, 1974-1995, for (a) intraseasonal (retains variations between 10 and 90 days) "SACZ only," (b) low-pass (retains variations greater than 10 days) "SACZ only," (c) intraseasonal "with SPCZ," (d) low-pass "with SPCZ," (e) intraseasonal "SPCZ only," and (f) low-pass "SPCZ only" cases. The values are contoured and shaded every 5 W/m^2.

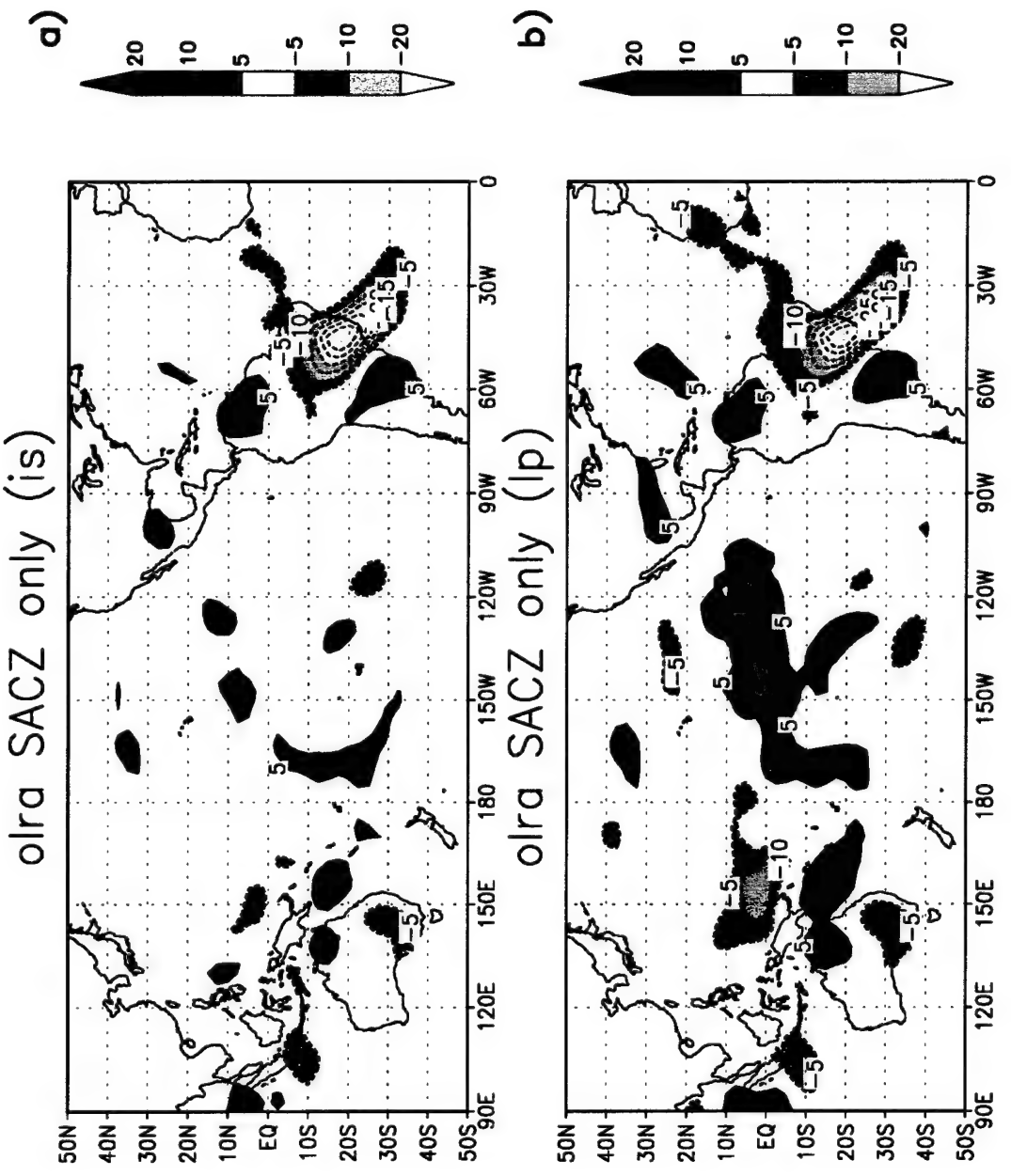
a)
20
10
5
-5
-10
-20
olra SACZ only (is)
b)
olra SACZ only (lp)
50N
40N
30N
20N
10N
EQ
10S
20S
30S
40S
50S
90E
120E
150E
180
150W
120W
90W
60W
30W
0

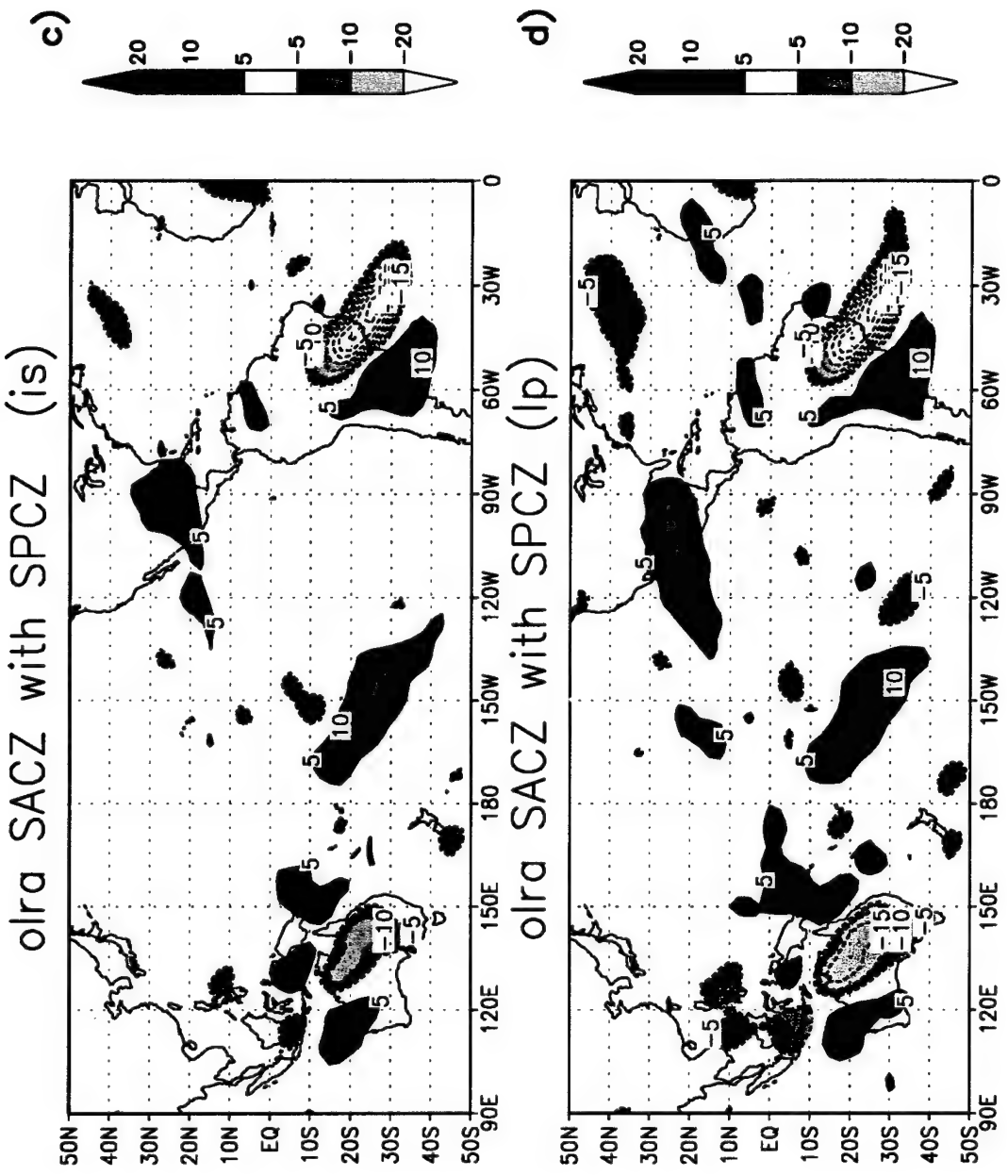

Figure 4.1 Continued

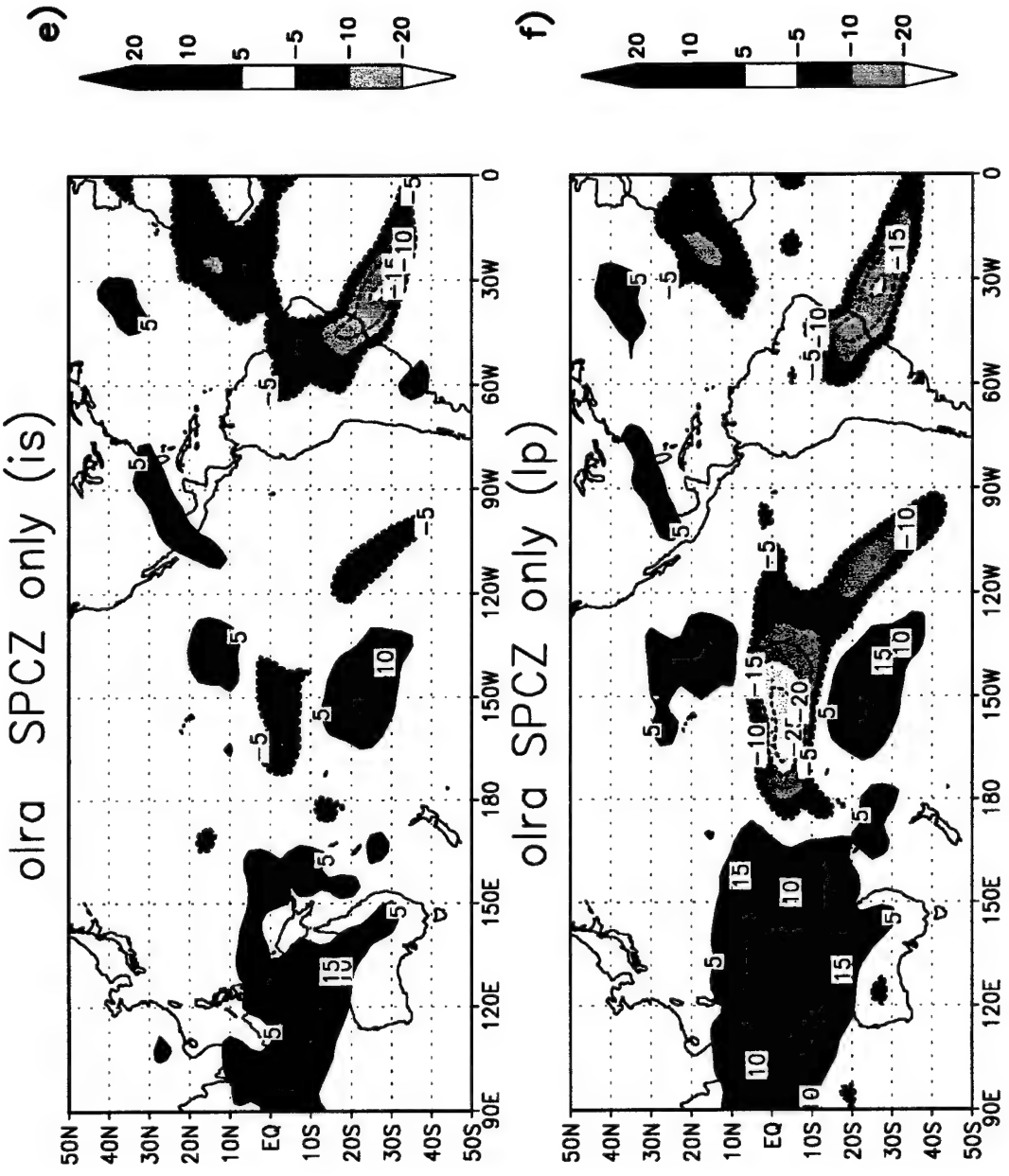

Figure 4.1 Continued

Contributions to the OLR anomaly composites from different frequency bands are shown in Fig. 4.1. The composites obtained from the intraseasonal (IS) or 10- to 90-day filter (Fig. 4.1 a,c,e) are compared to those obtained from a low pass (LP) filter that has removed time scales less than 10 days (Fig. 4.1 b,d,f). The contribution to the OLR anomaly composite from the interannual band (IA, 90 days and beyond) for each case is roughly the difference between the contribution from the LP (low frequency) band and the IS (10- to 90-day) band. Comparison of Fig. 4.1 a with b and c with d shows remarkable similarity between IS and LP filters, indicating the contribution from the IA band is small. However, contributions from the IA band to the "SPCZ only" case is large and gives an ENSO signal (compare Fig. 4.1 e with f). It shows an amplified OLR anomaly response west of South America for the LP filter (Fig. 4.1 f) that is not shown in the IS filter (Fig. 4.1 e). ENSO events favor this eastward displacement of the SPCZ, a feature associated with some cases of enhanced SACZ (as in Fig. 4.1 c). Cases with enhanced and suppressed convection over the SACZ average out any ENSO signal in that region, while there is a net ENSO signal flanking the SACZ region (to the north and south of the SACZ). The "SPCZ only" composites show well-defined ENSO-like signatures.

Fig. 4.2 displays the (ECMWF) evolution of the outgoing longwave radiation anomalies. Fig. 4.2 a through d compares well with the "seesaw" in precipitation over South America NPM97 identified using observed OLR anomalies obtained from National Environmental Satellite, Data, and Information System averages of individual satellite scans. They linked the evolution of the "seesaw" pattern to convection over the Pacific Ocean. Similar to the results of NPM97, Fig. 4.2 d shows that convection is supressed in the region of the SPCZ, while an enhancement in tropical convection occurs in the Central Pacific. Over Eastern Australia, similar sign reversals are seen in the OLR anomalies, evolving towards a regime of enhanced precipitation over Central Australia and suppressed convection toward the north. The suppressed convection over the Maritime Continent is apparent in the ENSO mode (Fig. 4.1 f), and this also tends to favor the occurrence of

Figure 4.2 ECMWF OLRA composite anomalies for negative cases (1979-1993) for (a) "with SPCZ" days -8 to -6, (b) "with SPCZ" days -6 to -4, (c) "with SPCZ" days -4 to -2, (d) "with SPCZ" days -1 to 1, (e) "SACZ only" days -8 to -6, (f) "SACZ only" days -6 to -4, (g) "SACZ only" days -4 to -2, and (h) "SACZ only" days -1 to 1. Intervals are 5 W/m^2 as indicated by the colorbars.

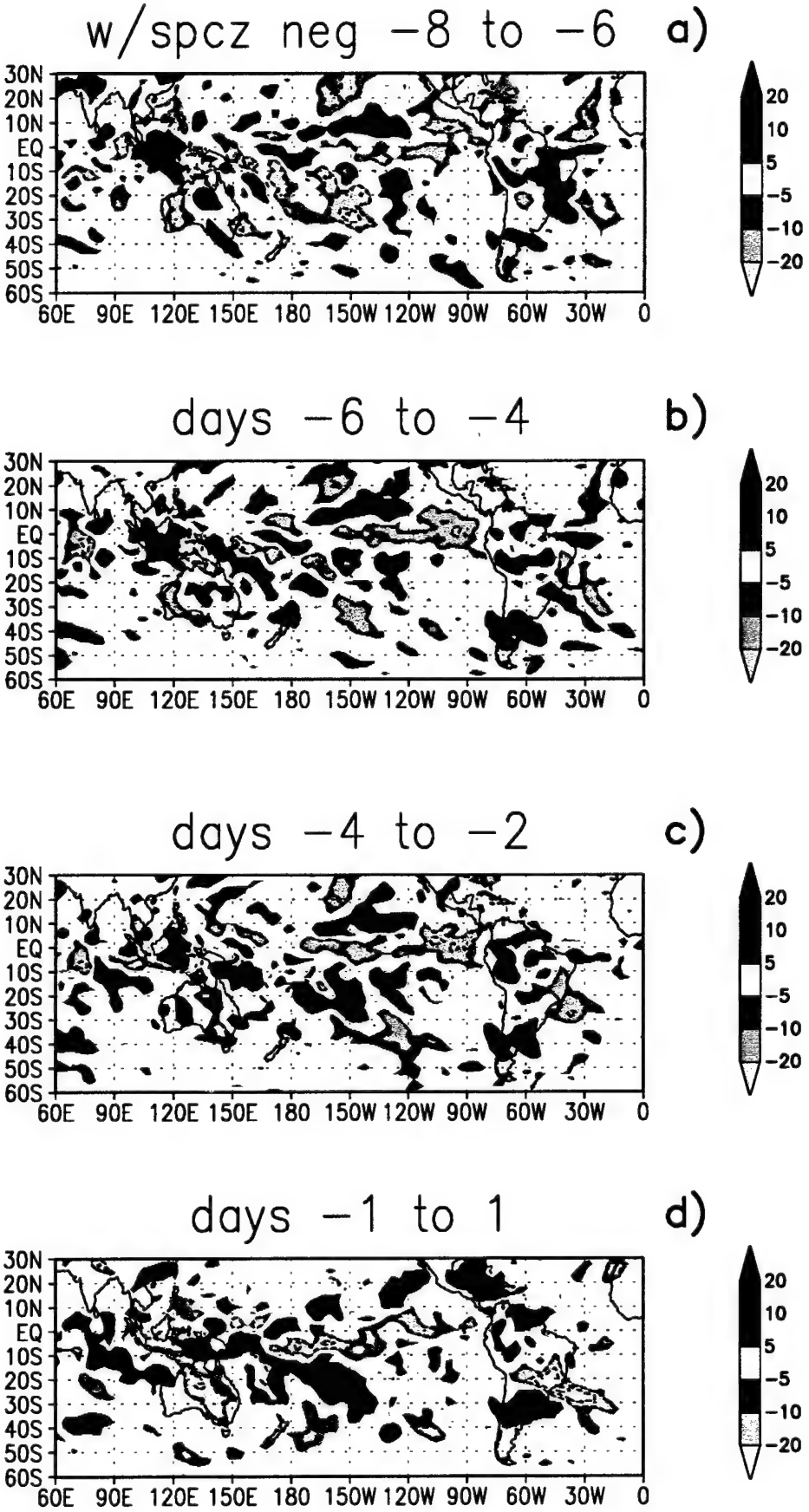
w/spcz neg −8 to −6
a)
days −6 to −4
b)
days −4 to −2
c)
days −1 to 1
d)
30N
20N
10N
EQ
10S
20S
30S
40S
50S
60S
60E 90E 120E 150E 180 150W 120W 90W 60W 30W 0
20
10
5
−5
−10
−20

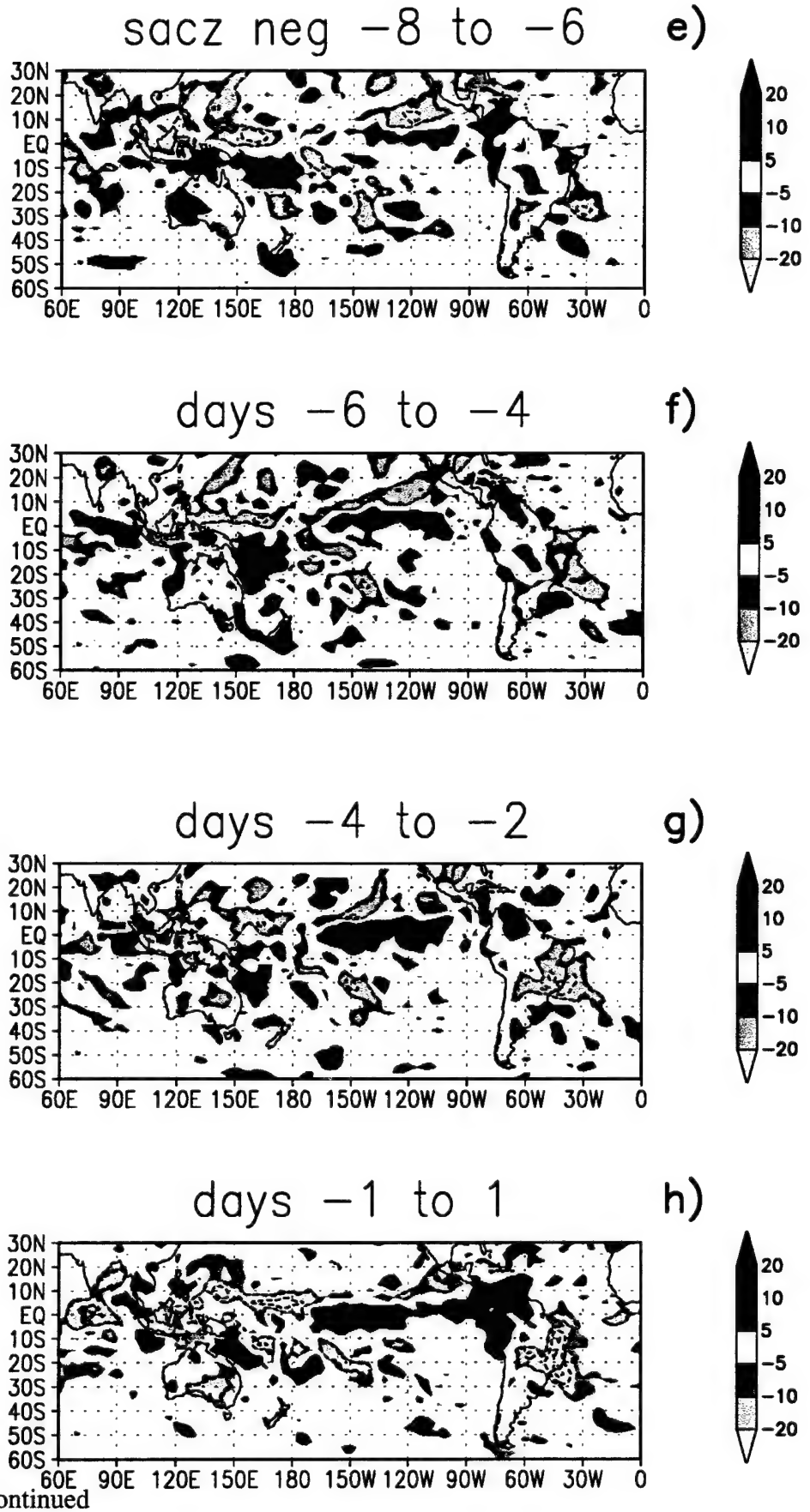

Figure 4.2 Continued

"with SPCZ" events during ENSO years. However, the signal seen in the interannual time scale (Fig. 4.1 f) is damped by intraseasonal variations (Fig. 4.1 c).

The "SACZ only" composites in Fig. 4.2 e through h reveal a stationary pattern over South America (no "seesaw" in precipitation), as the convective area over the SACZ builds with time. Signatures of low OLR anomalies are already present over the SACZ at day -8 from onset. The ITCZ weakens with time over Central America and the Gulf of Mexico as low OLR signatures shift northward. Over the SPCZ, activity is not suppressed as it is for "with SPCZ" cases. In contrast to the evolving amplification in low OLR over Australia, a more stationary, weaker area of low OLR anomalies over that region develops for "SACZ only" cases by day +1. Therefore, the mechanisms of formation for "SACZ only" cases appear to differ significantly from those of "with SPCZ" cases.

Analyses of OLRA have been offered as proxies of convection. A more realistic analysis follows, showing the precipitation fields derived by the assimilation system during the course of data insertion.

The OLR anomalies in Fig. 4.2 correspond well to enhanced precipitation patterns, as shown by the precipitation anomaly composites in Fig. 4.3. The "with SPCZ" composite (Figure 4.3 a) shows an enhanced SACZ with precipitation extending in an elongated arc into the Southwest Atlantic. The Pacific ITCZ is well-defined by an extensive area of precipitation. Four well-defined, northwest-to-southeast-oriented precipitation bands are evident (Fig. 4.3 a) in the Southern Hemisphere. They extend from the SACZ, eastward into the Central Pacific, and from the tropics into midlatitudes. These bands acquire a more zonally-oriented tilt as they merge into the westerly flow. The 200 mb horizontal convergence and divergence anomalies (contoured in Fig. 4.3) correspond well with areas of suppressed and enhanced precipitation, respectively. Over the SACZ, horizontal divergence values of up to 3×10^{-6} s^{-1} are present (Fig. 4.3a), while convergence values are high in the region of suppressed convection over the subtropical plains of South America. As shown in Fig. 4.2, high OLR anomalies strengthen in time over the subtropical plains

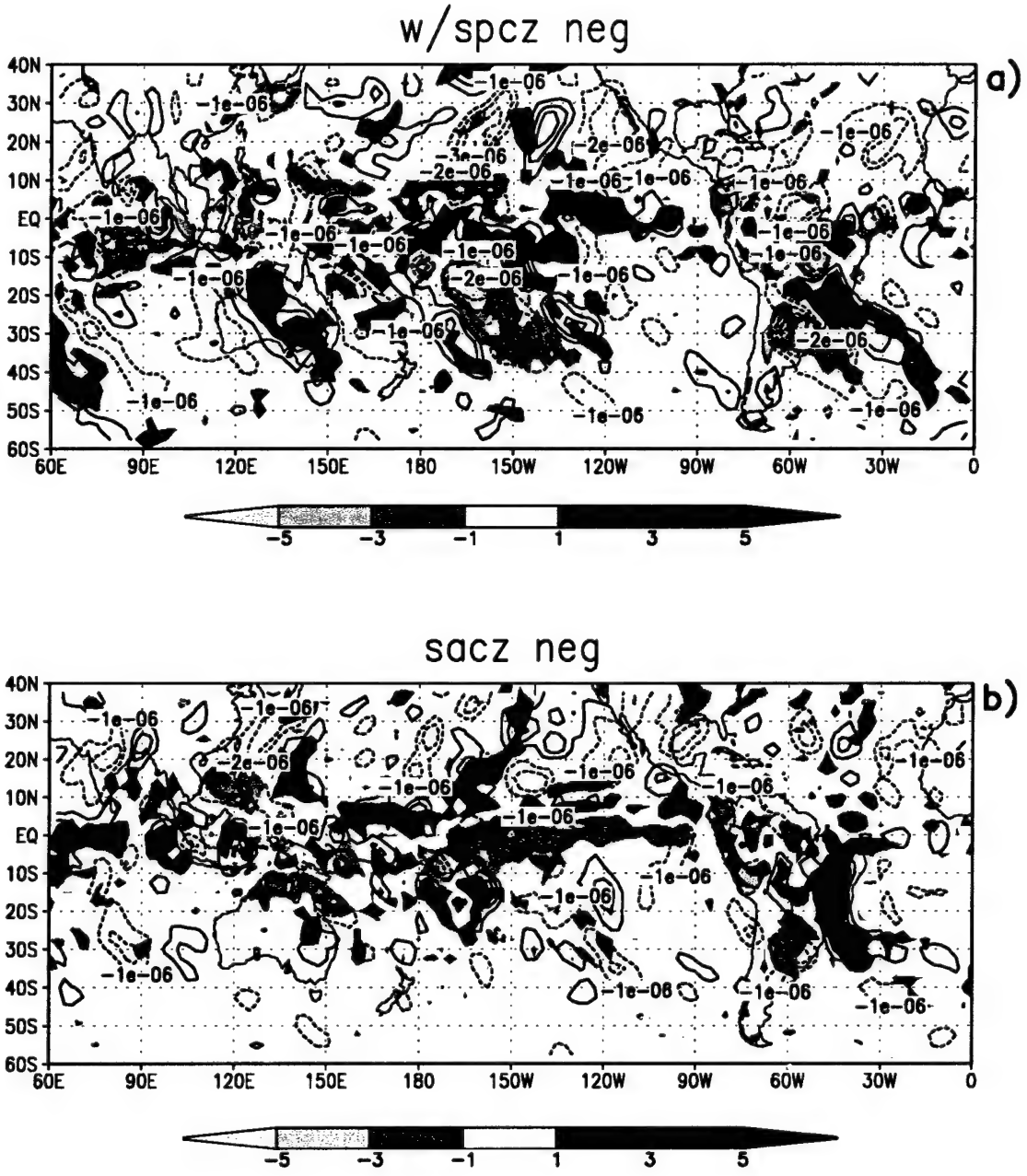

Figure 4.3 ECMWF composite precipitation anomalies (mm/day) and 200 mb horizontal divergence (s^{-1}) anomalies for (a) "with SPCZ" negative cases, and (b) "SACZ only" negative cases. Precipitation values are shaded as indicated by the colorbars.

as precipitation over the SACZ strengthens. In the region of the SPCZ, precipitation is suppressed and has been displaced eastward, corresponding to the OLR in Figure 4.2 d.

For the "SACZ only" composite (Fig. 4.3 b), precipitation is more continental in nature and stronger, extending uninterrupted into Northeast Brazil and with less protrusion into the Southwest Atlantic. Maximum anomalies exceeding 7 mm/day are found in the vicinity of 20°S, 45°W. Negative precipitation anomalies surround the convection over the SACZ. Compensating subsidence around the active SACZ appears more widespread for "SACZ only" cases, though negative precipitation anomalies are generally less intense over the subtropical plains of South America. Precipitation is in an opposite phase over the Pacific at the Equator compared to "with SPCZ" cases. The Pacific ITCZ is suppressed over the equator, and 200 mb horizontal divergence and precipitation extend farther northward. The SPCZ is also at a normal position over the Western Pacific (Fig. 4.3 b). Over the Eastern Pacific, off the coast of Central America, low OLR anomalies (Fig. 4.2 d) show evidence of cirrus blowoff (not precipitation) from convection to the south, as precipitation anomalies are not shown in the region. From this discussion of the two types of negative cases, differences in large-scale, organized convection for the two types of SACZ events are apparent. An analysis of the upper-level flow patterns provides further insight.

4.2 Influences on the Circulation

To diagnose the upper-level circulations during negative events, composites have been compiled for the 200 mb and 500 mb levels. Fig. 4.4 shows precipitation and 200 mb height anomalies for each case and the difference (Fig. 4.4 c) between the two types of enhanced SACZ. Approximately 5 waves are found in the 200 mb height anomaly pattern between 40°S and 50°S for "with SPCZ" cases, suggesting a possible link between the four precipitation bands in the Southern Hemisphere and height fields. This is confirmed in Fig. 4.4 d. It shows precipitation anomalies south of 20°S co-located with regions of negative height anomalies at 1000 mb. The 200 mb negative height anomalies are displaced

Figure 4.4 ECMWF precipitation anomalies (mm/day) and 200 mb height anomalies (m) are shown in (a) for "with SPCZ" negative cases, (b) "SACZ only" negative cases, and (c) "with SPCZ" minus "SACZ only (a-b). Precipitation anomalies are shaded as indicated in the colorbars, and 200 mb heights are contoured every 20 m. The 1000 mb height anomalies are shown with precipitation anomalies in (d) for "with SPCZ" negative cases, and (e) "SACZ only" negative cases. The 1000 mb height contours are every 5 m.

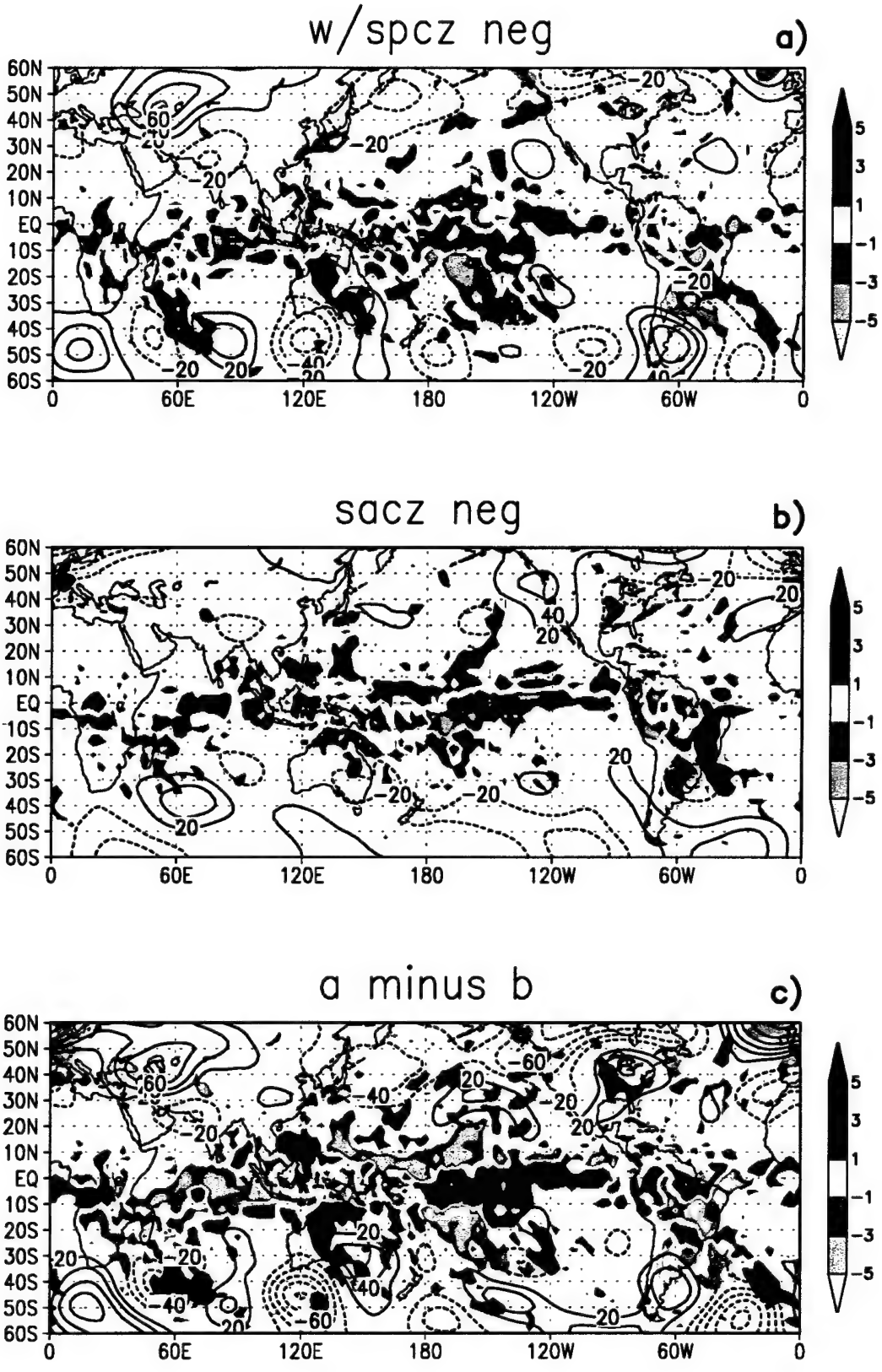
w/spcz neg
a)
sacz neg
b)
a minus b
c)
60N
50N
40N
30N
20N
10N
EQ
10S
20S
30S
40S
50S
60S
0
60E
120E
180
120W
60W
0
5
3
1
-1
-3
-5

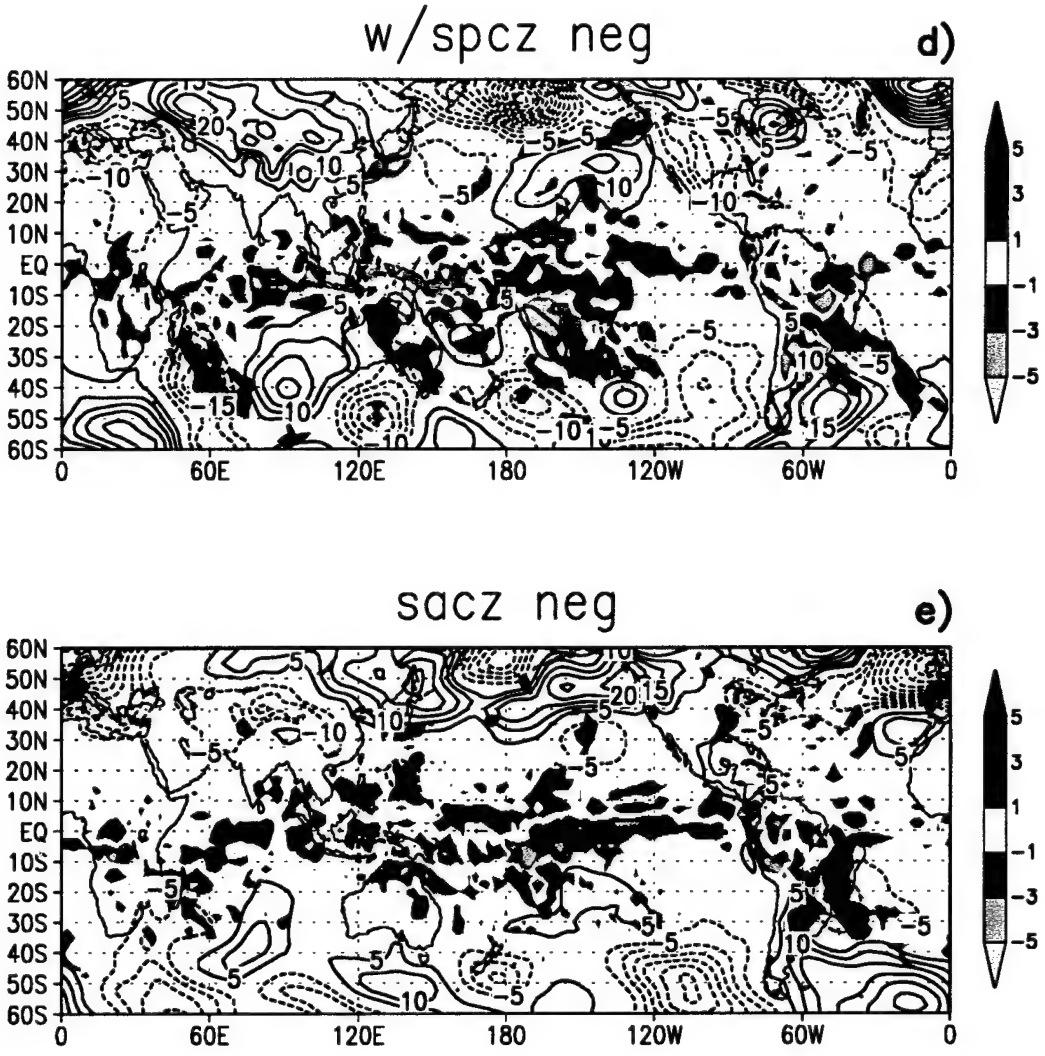

Figure 4.4 Continued

toward the west (or southwest) of the surface anomalies, as expected for baroclinic waves. In contrast, waves for "SACZ only" cases are longer (wave 2) and weaker. A wave 5 pattern is seen in the differences (Fig. 4.4 c), and values are generally higher than those of either Fig 4 a or b. This indicates the wave patterns are generally out of phase. An exception is the negative low height anomaly located over the South Pacific off the Southwest Coast of South America, which appears in both cases. The 1000 mb height field exhibits a more complex wave pattern than at 200 mb for the "SACZ only" composite (Fig. 4.4 e). The largest amplitudes are found at 50 S in the vicinity of South America.

Another characteristic of the upper-level flow field is the more active wave pattern over North America for the "SACZ only" composite (Fig. 4.4 b), showing high height anomalies over the Western U.S. and low height anomalies over the Eastern U.S. Convection over the Central and Eastern Pacific is shifted northward, possibly contributing to the amplification over North America. The possible association of the "SACZ only" negative patterns with the amplification over North America will be further examined in section 4.4.

Results presented in this section have linked "with SPCZ" tropical convergence zones to a baroclinic wave number 5, observed in the height anomalies. This is also substantiated by the vertical structure of wave height anomalies at 50°S, shown in Fig 4.5. In general, height anomalies maximize between 250 and 300 mb (Fig. 4.5 a), and large central values are observed in all waves. In contrast, the wave 2 pattern of "SACZ only" cases is weaker and appears to propagate upward eastward of 60°E (Fig. 4.5 b). Fig 4.5 c shows the structure of the stationary waves at 50°S, characterized by a strong wave number 1. This has been identified (e.g., Hoskins and Karoly 1981) with a meridionally-propagating Rossby wave generated by Antarctica. Both cases show deviations from the average pattern, indicating that the anomalies are not a result of an amplification of the climatological state. Therefore, the next question addresses event evolution, in an effort to quantify the degree of transience associated with each type of event.

Figure 4.5 ECMWF height anomalies for negative cases at 50°S from 1000 mb to 100 mb for (a) "with SPCZ" cases, (b) "SACZ only" cases, and (c) climatology. Contours are every 20 m.

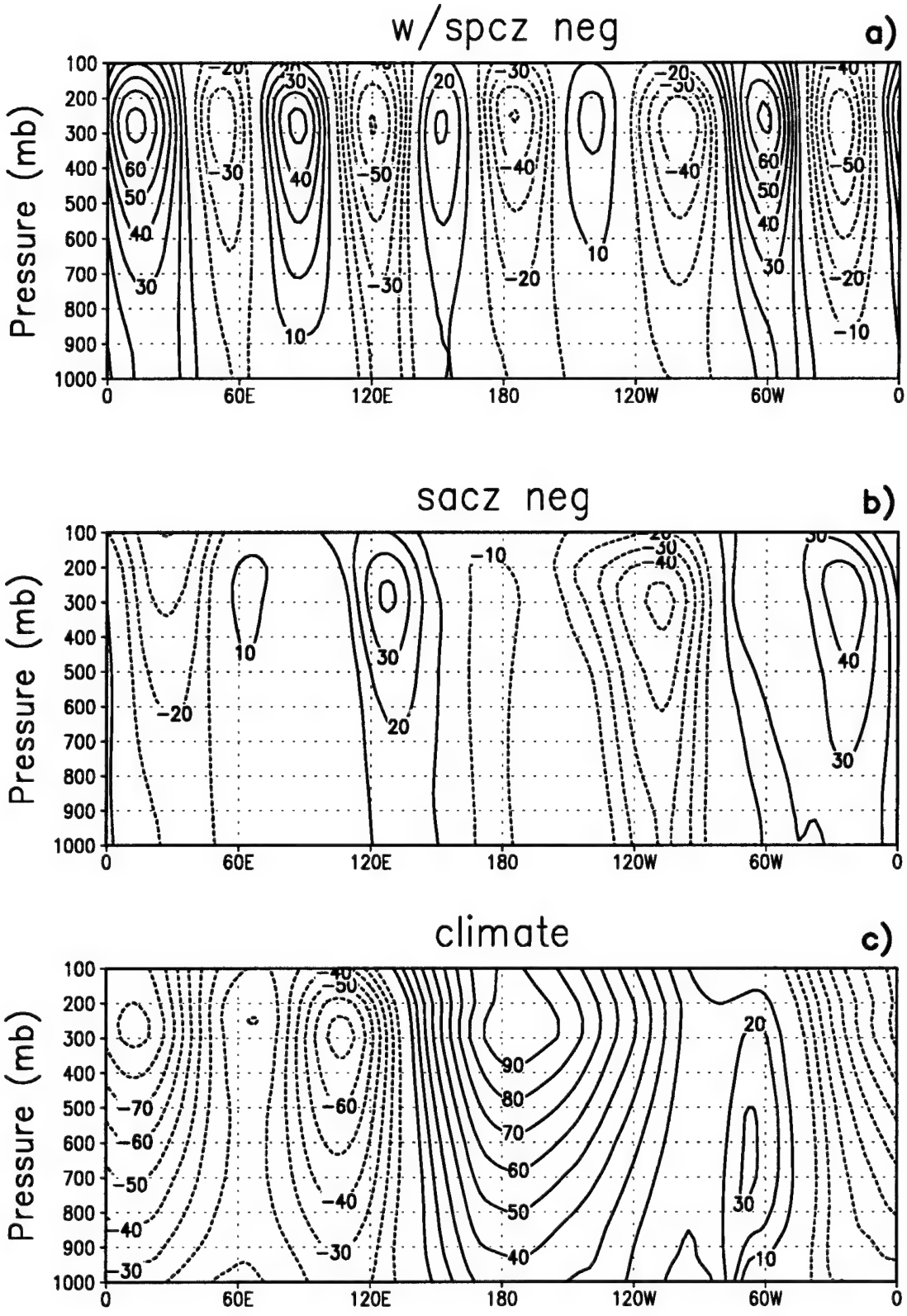
w/spcz neg
a)
sacz neg
b)
climate
c)
Pressure (mb)
100
200
300
400
500
600
700
800
900
1000
0
60E
120E
180
120W
60W
0

4.3 Transients

The strength of synoptic eddies is quantified by the variance of 200 mb heights within each event. The square root is then taken from the mean variance for all events. Fig. 4.6 a shows this quantity for "with SPCZ" cases. The Southern Hemisphere appears more variant than the Northern Hemisphere. When the "SACZ only" composite is subtracted from the "with SPCZ" composite (Fig. 4.6 b), the latter contributes more strongly to transient activity at midlatitudes. For example, high variability between the Greenwich Meridian and 30°W may be a reflection of more active synoptic patterns over the Southwestern Atlantic. In the average, this might also support the extensive, arc-like nature of the precipitation over this region (see Fig. 4.3 a). Similar associations may be established for other "with SPCZ" convergence zones discussed, previously.

The preceding discussion relates to the synoptic time variability contained within individual events. Here, the averaged composite evolution is shown with a Hovmöller diagram of 200 mb height anomalies along 50°S for "with SPCZ" cases (Fig. 4.7). An amplified (wave 5) pattern is shown, specifically during the onset (day 0) of the events. Southern South America is influenced by a broad area of high height anomalies which maximize at day 0. Near 120°E and south of Australia, strong negative anomalies reach a maximum by day +6. These anomalies are also visible in the horizontal composite (Fig. 4.4 a).

The more stationary nature of "SACZ only" cases is seen in the composite evolution of the 500 mb height anomaly in Fig. 4.8. The wave pattern over the southern Pacific Ocean is already evident 8 to 6 days prior to the onset. Largest values are found in association with the negative anomalies between 60°W and 120°W (Fig. 4.8 d). As revealed in Fig. 4.6 b, the region between 60°W and 120°W is also less transient than "with SPCZ" cases. Whether the precursors to the height anomalies in the 0 to 120°W region are found over the Pacific, or are associated with the strengthened SACZ pattern (Fig. 4.4 e) is

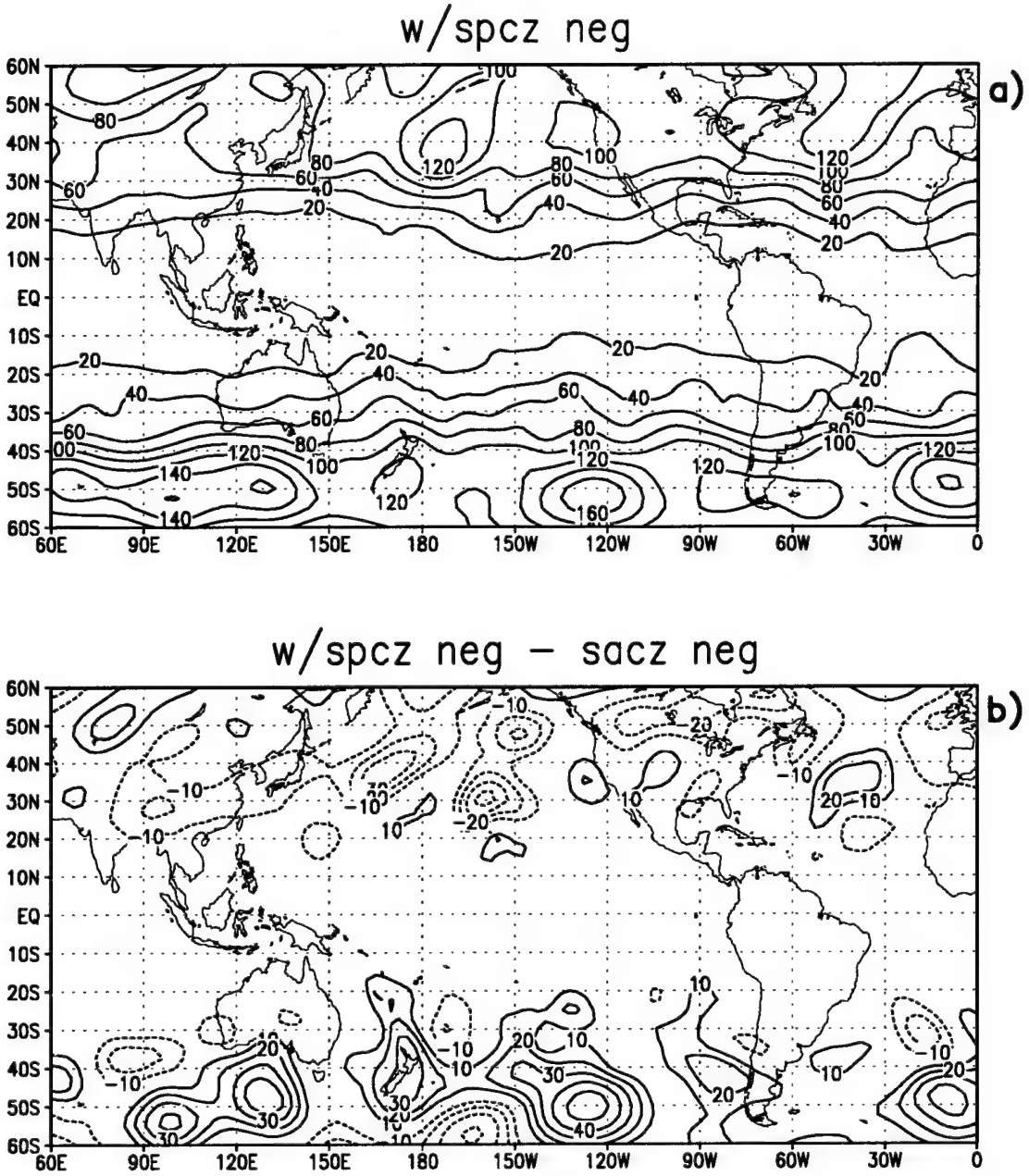

Figure 4.6 The square root of the variance in ECMWF 200 mb heights are shown for (a) "with SPCZ" negative cases, and (b) "with SPCZ" minus "SACZ only" negative cases. Contours in (a) are every 20 m; contours in (b) are every 10 m.

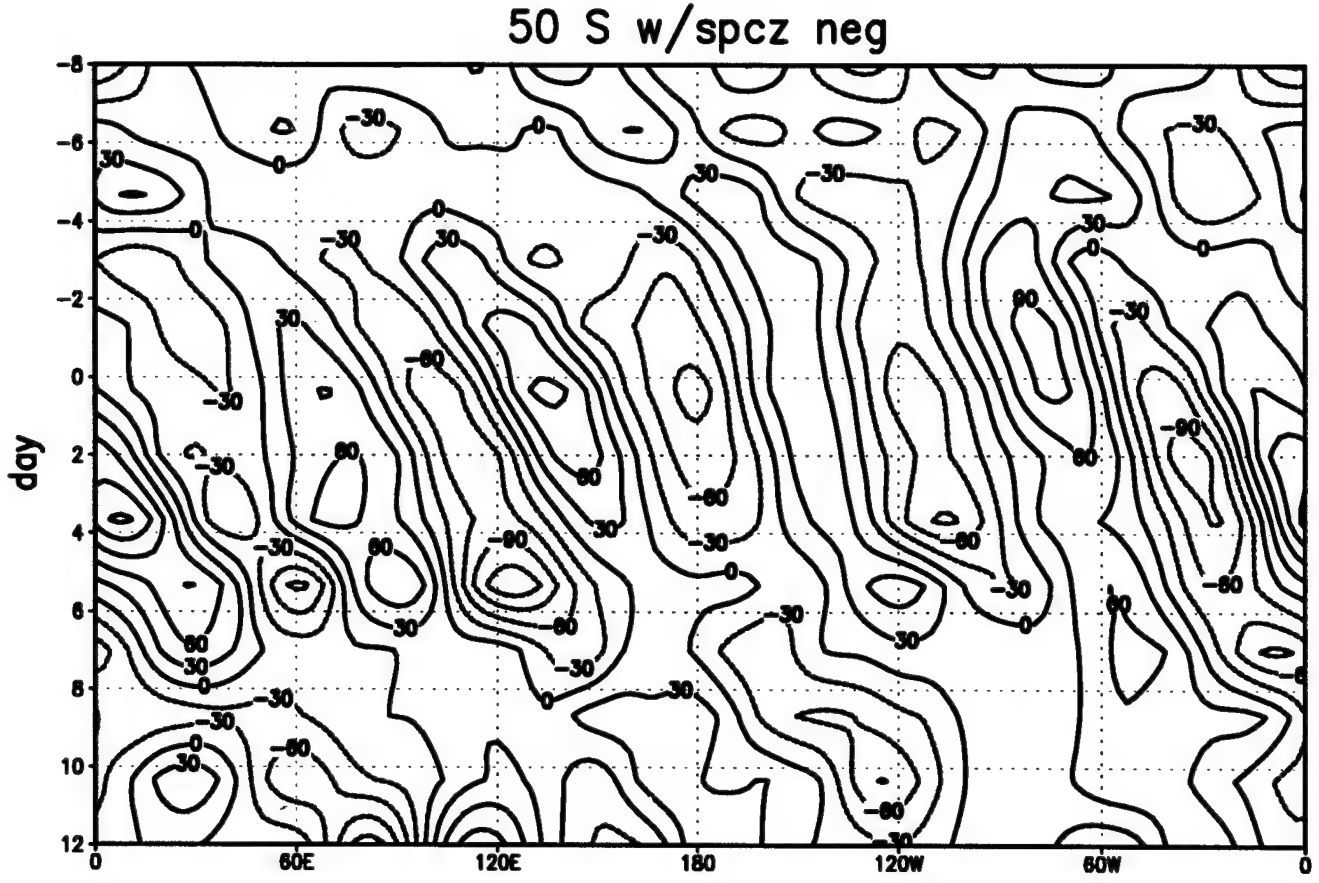

Figure 4.7 ECMWF 200 mb composite height anomalies along 50°S for "with SPCZ" negative cases. The y-axis shows time for 8 days preceding event onset (day -8), to event onsent (day 0), to 12 days following event onset (day +12). Contours are every 30 m.

Figure 4.8 ECMWF 500 mb height anomalies for "SACZ only" negative cases for (a) days -8 to -6, (b) days -6 to -4, (c) days -4 to -2, and (d) days -1 to 1. Contours are every 20 m.

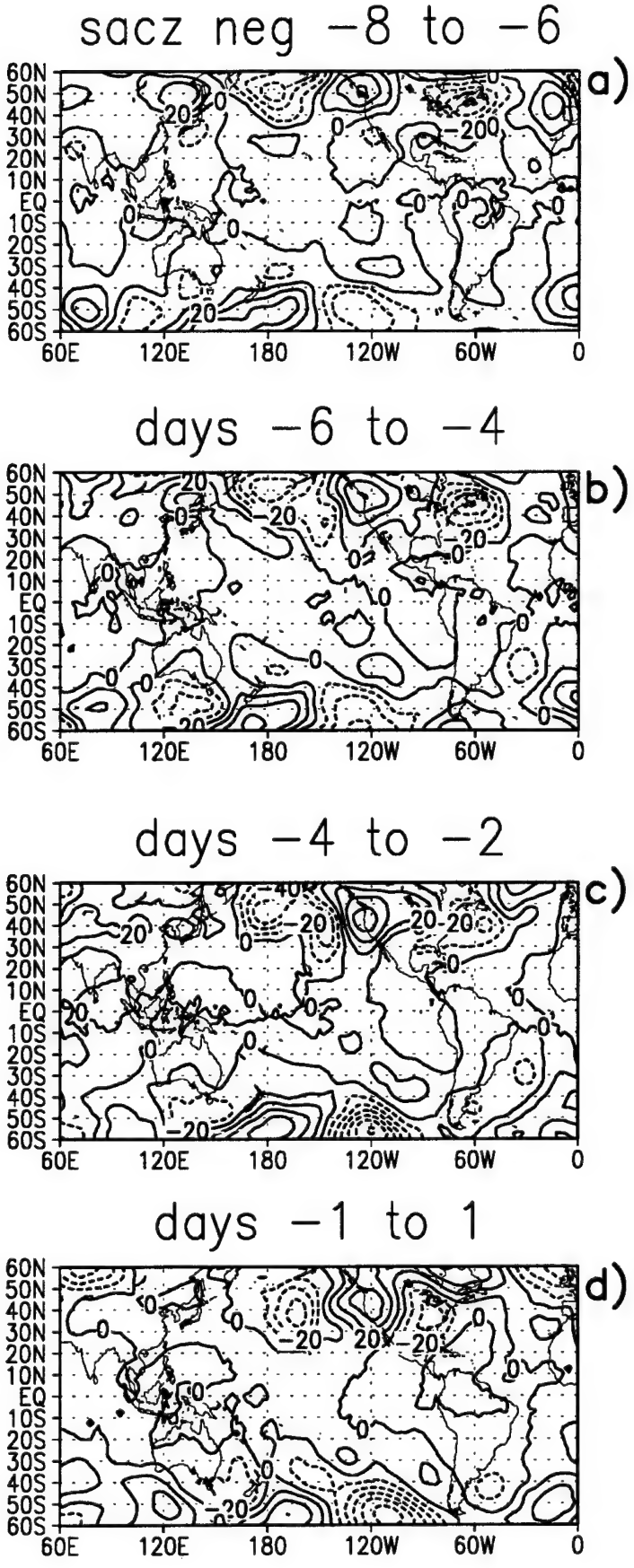
sacz neg −8 to −6
a)
days −6 to −4
b)
days −4 to −2
c)
days −1 to 1
d)
60N
50N
40N
30N
20N
10N
EQ
10S
20S
30S
40S
50S
60S
60E
120E
180
120W
60W
0

not clear at this time. An examination of the hydrological cycle for the negative cases follows.

4.4 Moisture Sources

This section examines the moisture sources contributing to the two cases in which the SACZ is enhanced. Differences in precipitation are linked to different moisture sources. Fig. 4.9 shows the 850 mb wind field and precipitation anomalies for "with SPCZ" and the difference between the two types of negative cases considered. Precipitation differences show that it is more intense over tropical South America for "SACZ only" cases, but it is more intense over the Pacific ITCZ for "with SPCZ" cases. Features of the low-level circulation include subtropical highs located to the east and west of South America, zonal westerly winds at midlatitudes, and a strong easterly flow of tradewinds into the interior of Northern South America.

In examining the differences between "with SPCZ" and "SACZ only," several features are apparent. The Pacific subtropical high appears stronger for "SACZ only" cases (Fig. 4.9 b). The cool southerly flow over the west coast of South America is much different from the warm, moist, northerly flow associated with the subtropical high on the east coast. Over the Southwestern Atlantic, the westerly return flow in the region of precipitation anomalies is stronger for "with SPCZ" cases. At around 40°W, 30°S, Fig. 4.9 b shows increased meridional flow closer to the coast for "SACZ only" events, producing an anticyclone in the differences. This supports the more continental nature of the precipitation for "SACZ only" events. The orientation of the Atlantic subtropical high differs between the two cases. For "with SPCZ," the ridge axis is northwest-to-southeast, while for "SACZ only," the ridge axis is more zonal. This is consistent with the general northwest-to-southeast-prevailing orientation found in the convergence zones for "with SPCZ" cases.

Flow regimes also differ over the Equatorial Pacific. The "with SPCZ" composite shows a stronger easterly component over the Pacific ITCZ. For "SACZ only" cases,

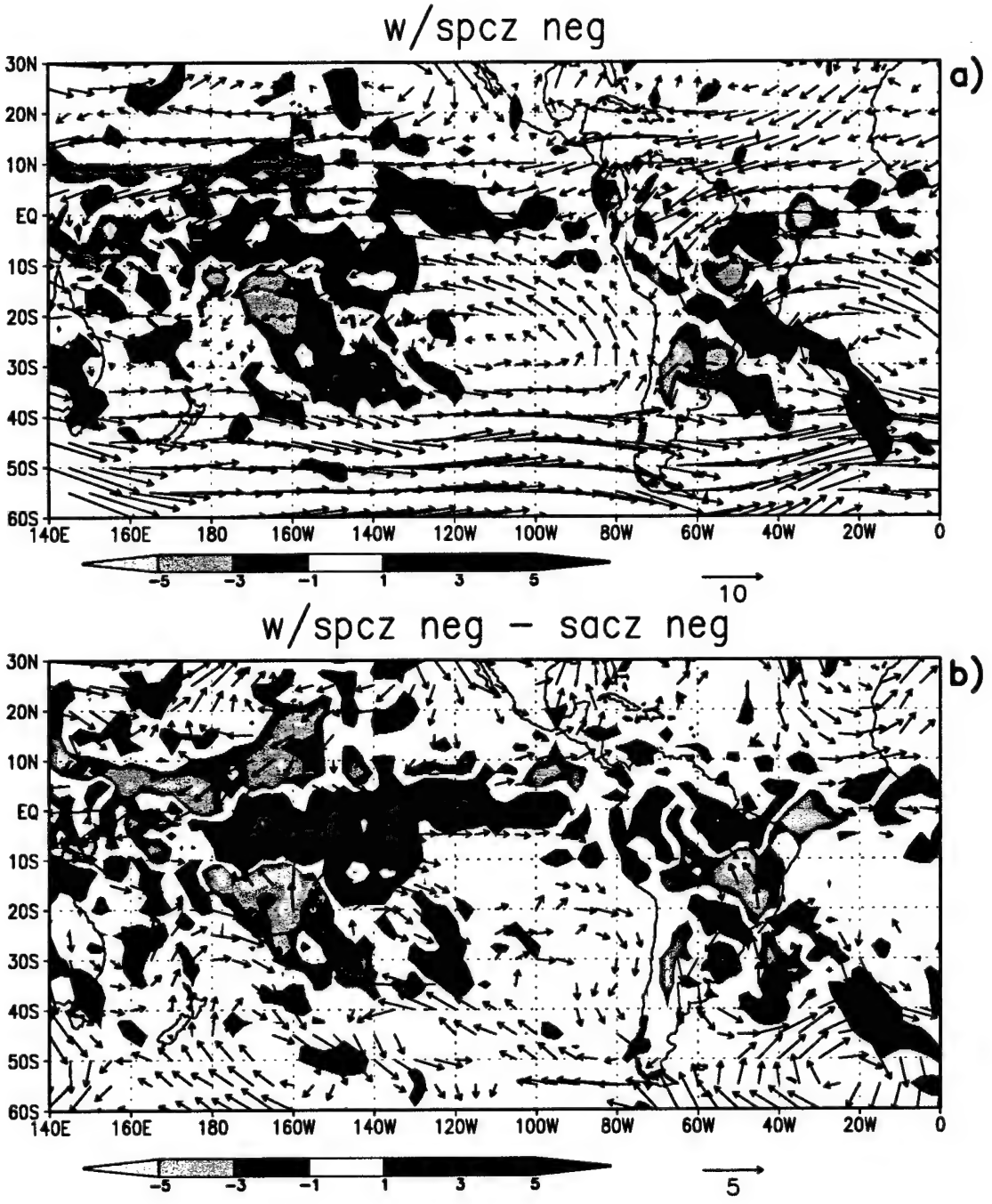

Figure 4.9 The 850 mb wind vectors (m/s) and precipitation anomalies (mm/day) for (a) "with SPCZ" negative cases, and (b) "with SPCZ" minus "SACZ only" negative cases. Precipitation values are shaded with intervals indicated by the colorbars.

easterly flow is not as intense but remains zonal for a longer distance. Low-level flow turns toward the south at about 180°W for "with SPCZ" cases, in an area of precipitation anomalies between the Equator and 10°S. Farther south, in the region of the SPCZ, the easterly flow has a stronger meridional component for "SACZ only" cases. In the Northern Hemisphere, at about 170°W, 20°N, meridional components also appear in the difference between the cases (Fig. 4.9 b). The meridional component for "SACZ only" cases is stronger. This is also a region where precipitation anomalies have shifted northward.

In section 4.2, the upper-level height anomalies for "SACZ only" cases (Fig. 4.4) showed an amplification in the flow over North America, with lower height anomalies over the Eastern U.S. The 850 mb composite temperatures and precipitation anomalies (used as a reference) in Fig. 4.10 also show the influence from "SACZ only" cases. Between 20°N and 30°N, a two degree temperature anomaly (Fig. 4.10 c) appears over the Gulf of Mexico, showing cooler temperatures for "SACZ only" cases. Such cold anomalies may be related to cold outbreaks from the winter hemisphere. They possibly sustain the anomalous precipitation pattern seen in the Eastern Pacific Ocean between 90°W and 105°W (Fig. 4.10 e). In contrast, the low-level winds for "with SPCZ" cases are very different in the vicinity of North America. Southerly flow is increased (Fig. 4.10 d), associated with low anomalies in the height field over the continental U.S. and Mexico. Low-level wind and precipitation anomalies over equatorial latitudes over Northeastern Brazil suggest the continental precipitation anomaly is supported by southerly continental air masses (Fig. 4.10 d). At the same time, the displacement over the oceans results from northerly flow (Fig 4.10 e). These relationships are further explored by considering the role evaporation and vertically integrated moisture fluxes play in maintaining precipitation anomalies.

Fig. 4.11 shows evaporation and precipitation composite anomalies for the two cases. For both, the region of the SACZ is characterized by negative evaporation anomalies, while regions of suppressed convection (over the SPCZ in Fig. 4.11 a, for example) tend to have

Figure 4.10 ECMWF 850 mb temperature anomalies and precipitation anomalies for (a) "with SPCZ" negative cases, (b) "SACZ only" negative cases, and (c) "with SPCZ" minus "SACZ only (a minus b)." Temperature anomalies are contoured every 0.5 K, and precipitation anomalies are shaded with intervals indicated by the colorbars. ECMWF 925 mb vector wind anomalies are plotted with the shaded precipitation anomalies in (d) for "with SPCZ" negative cases, and (e) "SACZ only" negative cases.

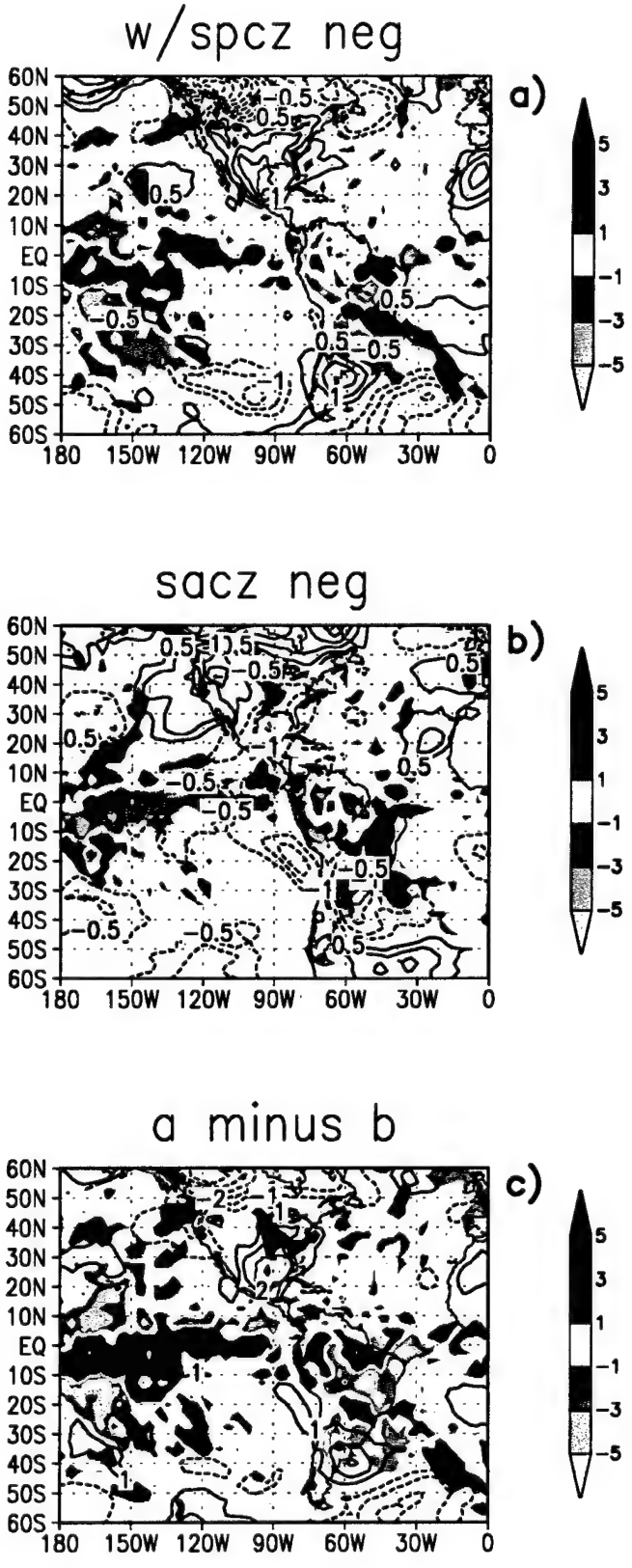
w/spcz neg
a)
sacz neg
b)
a minus b
c)
60N
50N
40N
30N
20N
10N
EQ
10S
20S
30S
40S
50S
60S
180
150W
120W
90W
60W
30W
0
5
3
1
-1
-3
-5

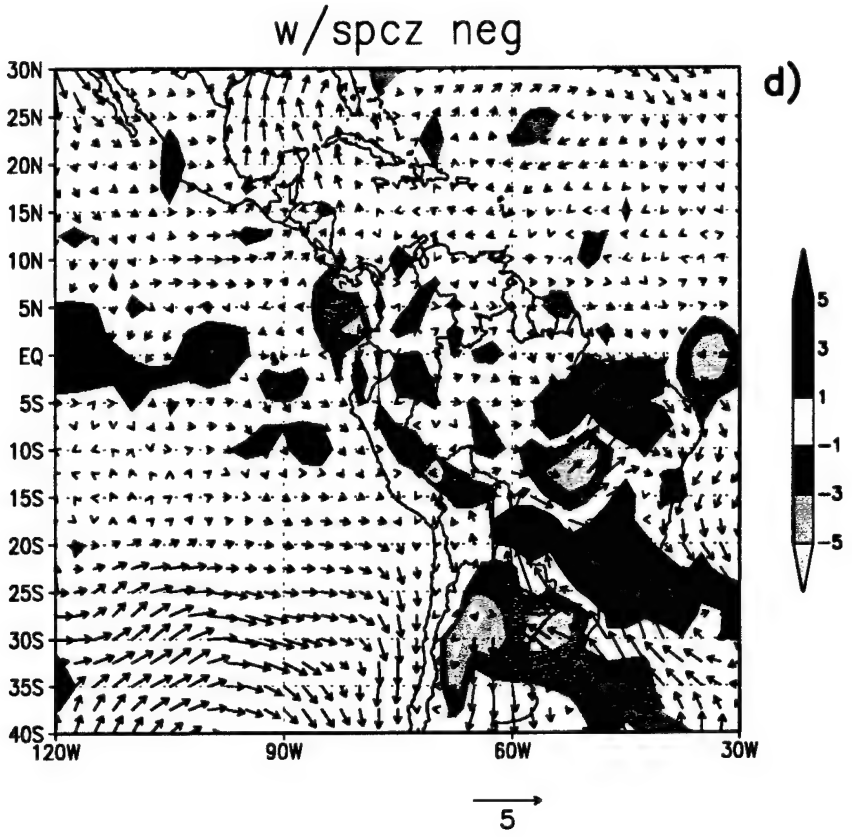

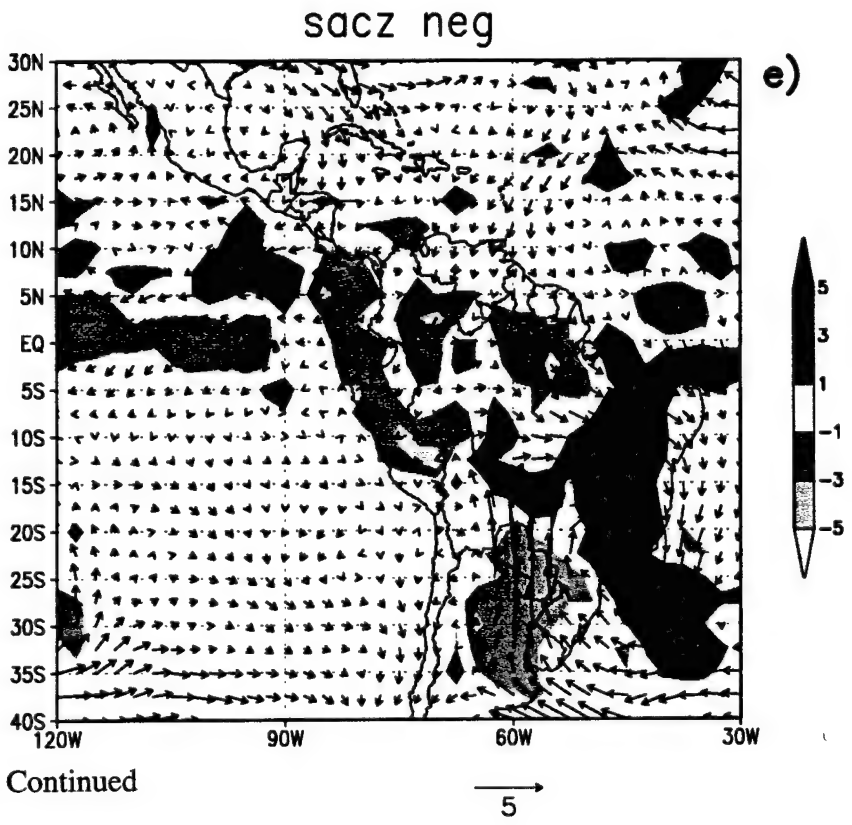

Figure 4.10 Continued

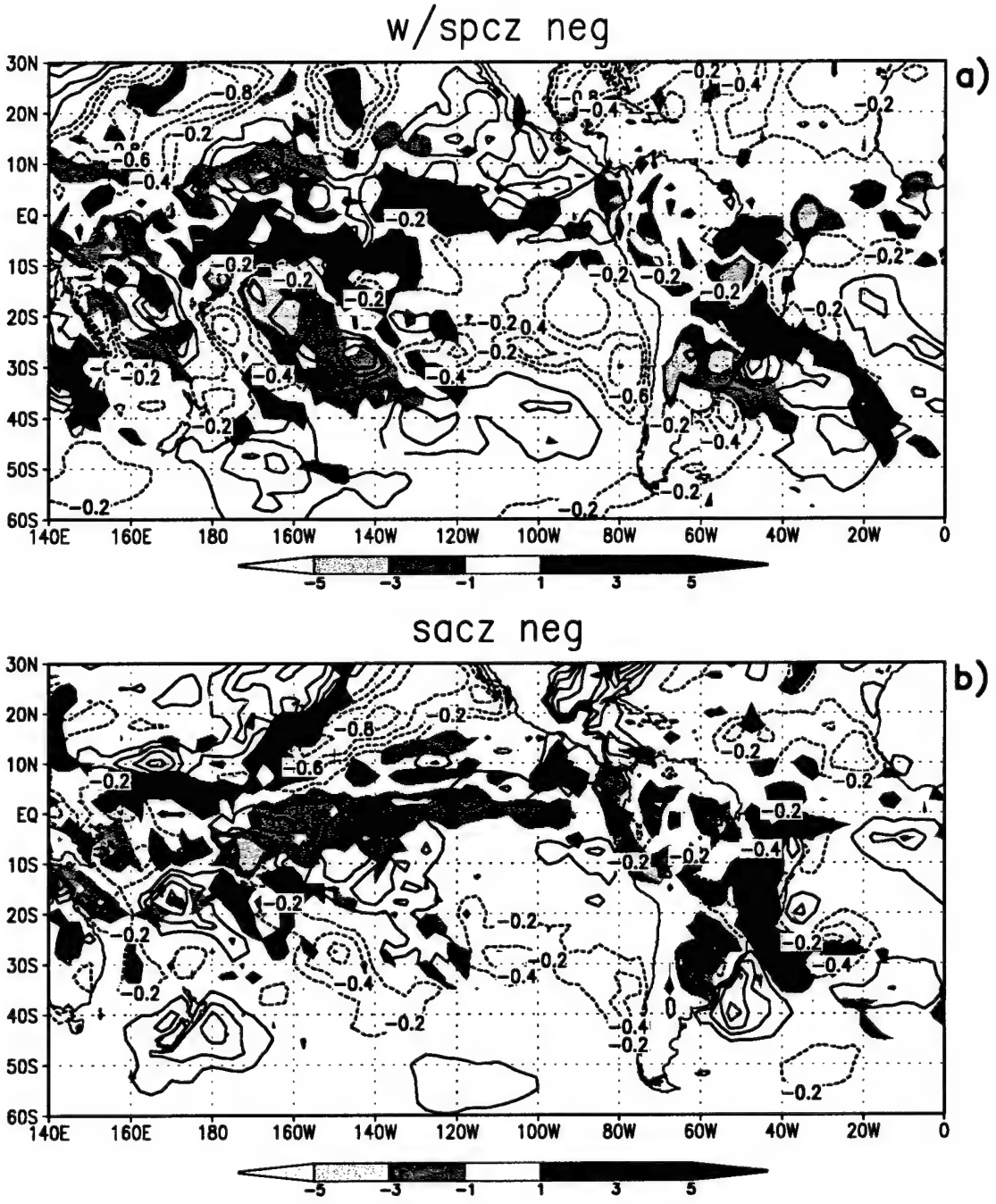

Figure 4.11 ECMWF composite evaporation anomalies and precipitation anomalies for (a) "with SPCZ" negative cases, and (b) "SACZ only" negative cases. Evaporation anomalies are contoured every 0.2 mm/day, and precipitation anomalies are shaded as indicated by the colorbars.

positive evaporation anomalies. This suggests a lack of feedback between precipitation anomalies and the underlying surface fluxes. Whether this is true for the time scales of the anomalies considered here, or an artifact of the assimilating model physics, remains to be determined. Overall, the evaporation anomalies shown in the ECMWF analysis are small, at least an order of magnitude smaller than the precipitation anomalies. This suggests evaporation has a small role as a moisture source for these events. Therefore, precipitation anomalies must be primarily maintained by convergence of moisture flux.

In Fig. 4.12, moisture flux convergence is generally co-located with precipitation anomalies (seen in Fig. 4.4). The extensive arc of convection defining the SACZ for "with SPCZ" cases (Fig. 4.12 a) is apparent in the convergence of moisture flux, which extends southeastward to about 15°W. In the Eastern Pacific ITCZ, flux convergence is strong for the "with SPCZ" composite (where precipitation anomalies are located), while it is absent for the "SACZ only" composite (Fig. 4.12 b). Over the West Pacific, "SACZ only" convergence of moisture flux is well-defined over the SPCZ and north of the Equator. Similarly, for "with SPCZ" cases, flux convergence coincides with precipitation anomalies. Correspondence between the four precipitation bands in the Southern Hemisphere (Fig. 4.4 a) and the areas of vertically integrated moisture flux convergence is not exact, since the full composites of moisture flux convergence (not the flux convergence anomalies) are being compared to precipitation anomalies. Off the west coast of South America, moisture transport is weak for both "with SPCZ" and "SACZ only" cases (weaker for "with SPCZ"), in contrast to the strong moisture flux on the eastern side of the continent. The moisture flux vectors appear to follow the low-level winds. This suggests the main contributor to the convergence of moisture flux is given by the wind convergence multiplied by the specific humidity rather than moisture advection.

Differences in moisture transport between the two cases are illustrated in Fig. 4.12 c. Moisture transport differences are large, as maximum arrows are greater than 50% of the original values. At midlatitudes, the reflection of higher wavenumbers for "with SPCZ"

Figure 4.12 ECMWF vertically integrated moisture flux vectors and contours of horizontal convergence of moisture flux for (a) "with SPCZ" negative cases, and (b) "SACZ only" negative cases. Vectors are mulitiplied by 10 g cm^{-1} s^{-1}, and values less than 75 are not plotted in (a) or (b). Convergence of moisture flux is contoured every 5 X 10^{-8} s^{-1}. Differences in vertically integrated moisture flux vectors and differences in horizontal convergence of moisture flux (a minus b) are shown in (c). Differences in horizontal convergence of moisture flux are contoured every 2 X 10^{-8} s^{-1}. Vectors less than 25 (multiplied by 10 g cm^{-1} s^{-1}) are not plotted in (c). For reference, the shading in (c) shows the horizontal convergence of moisture flux for "with SPCZ" negative cases (as contoured in a).

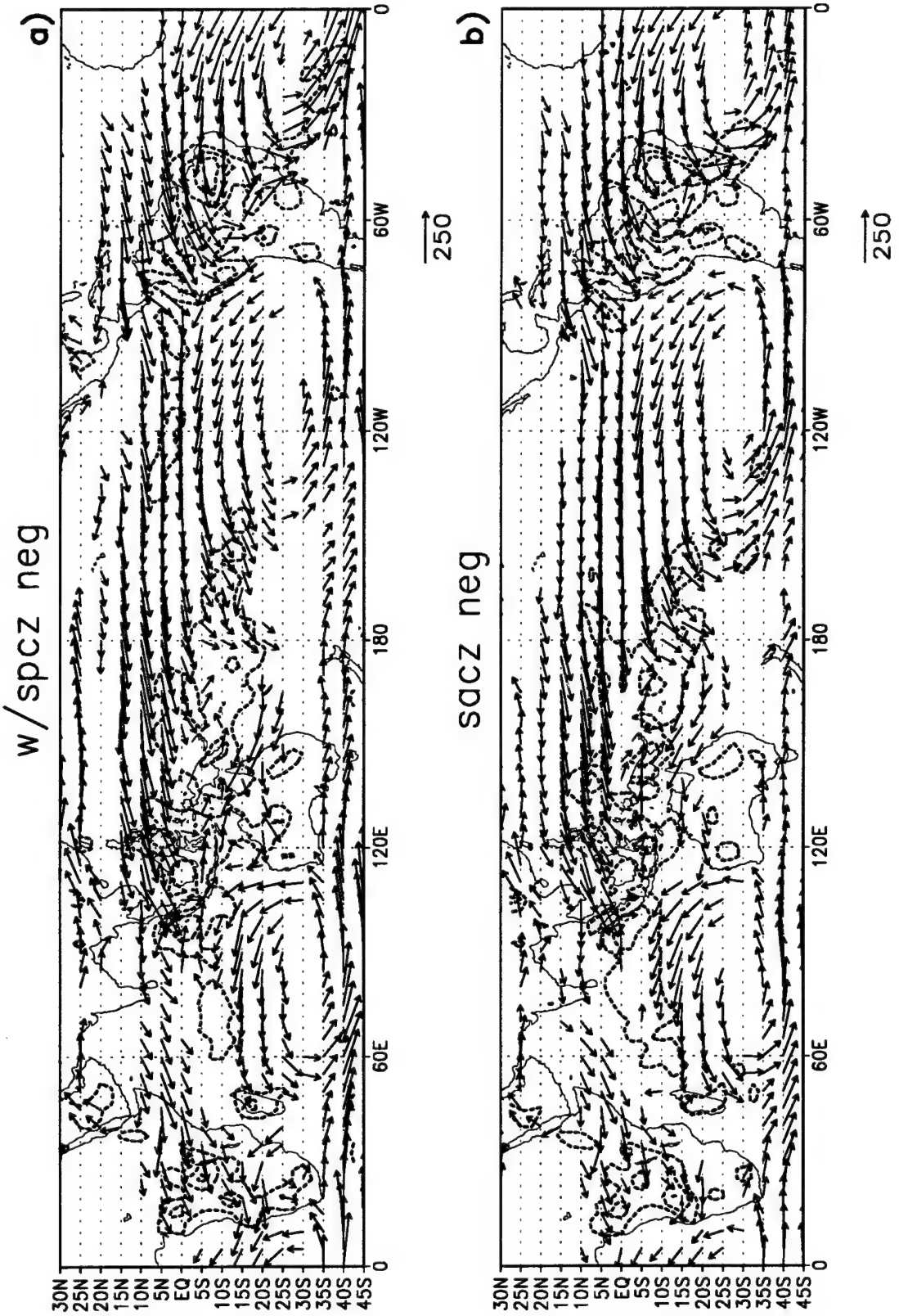
a)
w/spcz neg
b)
sacz neg
30N
25N
20N
15N
10N
5N
EQ
5S
10S
15S
20S
25S
30S
35S
40S
45S
0
60E
120E
180
120W
60W
0
250
250

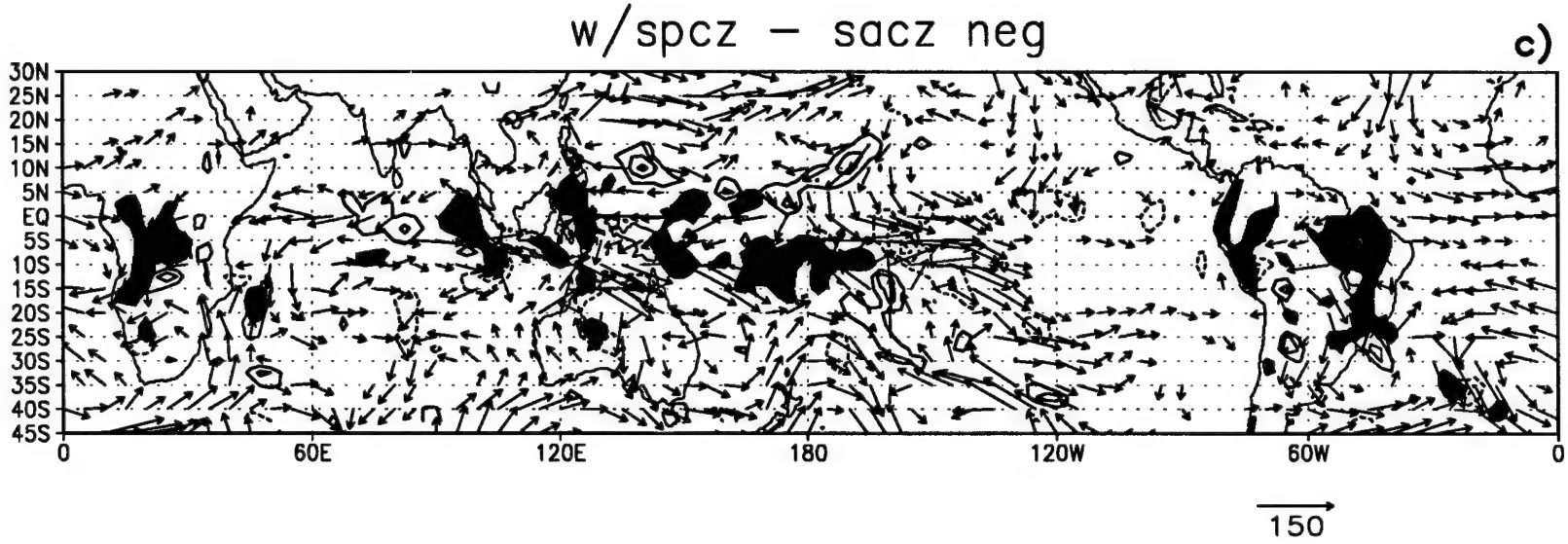

Figure 4.12 Continued

cases is shown in the vector wave pattern. Over South America, the continental nature of the anomalous convection for "SACZ only" cases is shown (as flux divergence), similar to the precipitation anomalies. Over the Southwest Atlantic, "with SPCZ" cases show significant moisture flux convergence (for example, near 35°W, 40°S). The zonal component of moisture flux dominates convergence over the Pacific ITCZ. Oceanic moisture transport is stronger in this region for "with SPCZ" events. Over the SPCZ and in the Northern Hemisphere (around 180°W), larger areas of moisture convergence from "SACZ only" cases are shown as flux divergence. Over Australia, the precipitation anomalies observed for "with SPCZ" events are accompanied by strong moisture flux (110°E). These composites show that the major moisture source for the anomalous precipitation events may be associated with moisture flux convergence.

A description of two different patterns of enhanced convection over the SACZ has been given based on the ECMWF reanalysis. Some of the quantities, such as precipitation and evaporation, are derived by the assimilation system. They may deviate from reality, depending on the accuracy of the physical parameterizations of the assimilating model. Next, data obtained from satellite measurements are used to ascertain, to the extent possible, the veracity of the convective patterns discussed above.

4.5 ISCCP Comparisons

To look at the reliability of the ECMWF assimilated data, composites of total cloud cover have been assembled from the ISCCP dataset. Composites of satellite-derived OLR (Liebmann and Smith 1996) have also been assembled. The composites are for negative events that occurred from January 1985 to March 1991. The ECMWF reanalysis global precipitation field has been used to make several conclusions, but one way to verify the validity of the data set is to compare it to observed cloud data. This is possible since the ECMWF analysis sytem carries prognostic equations for cloud water and cloud cover (Tiedke 1993). Cloud water/ice losses result from cloud evaporation and precipitation processes. The approach in this section is 1) to compare precipitation patterns with cloud

coverage derived from satellite measurements, and 2) to compare ECMWF derived OLR fields with those obtained from satellites. Approach 1) is accomplished to offer some validation of the ECMWF. Approach 2) involves radiation calculations as well as cloud processes, and it gives an overall assessment of the veracity of both parameterizations.

Fig. 4.13 shows the precipitation and OLR from the ECMWF, as well as deviations from observed OLR (Fig. 4.13 c), and Fig. 4.14 shows differences between "with SPCZ" and "SACZ only" negative events. The model-derived precipitation and OLR fields tend to correspond well with low OLR values and high precipitation estimates over the Southern Hemisphere convergence zones. Differences exhibit consistent signals, though the ECMWF OLR is apparently about 20 to 40 W/m^2 too high over regions of convection (Fig. 4.13 c). Over South America, for example, "with SPCZ" cases have lower precipitation and higher OLR values. Fig. 4.14 c shows the difference in observed OLR (Liebmann and Smith 1996) between the two types of cases. The ECMWF differences (Fig. 4.14 b) tend to match observations over South America and over the SPCZ. Corresponding to observations, the SACZ extends over the Southwest Atlantic for "with SPCZ" events, and it remains more confined to the continent for "SACZ only" events. The differences over Australia are similar for both the assimilated and the observed data. Over the Equatorial Pacific, the ECMWF differences appear too large compared with observations; but over the Northern Hemisphere, the observations pick up on the displaced OLR for the "SACZ only" cases.

Composites of ISCCP cloud data for negative events are shown in Figs. 4.15 and 4.16. They show cloud percentages for high, middle and low clouds (prepared by Johnson 1996). The main feature of the low clouds is the large area observed off the West Coast of South America, which occurs predominantly for "with SPCZ" cases (Fig 4.16 c). Cloud climatologies for the austral summer (e.g., Johnson 1996) show pronounced low stratus decks in this region. However, the broad area covered in Fig. 4.16 c exceeds the climatological amount. Fig. 4.11 shows pronounced negative evaporation anomalies

Figure 4.13 Average composite fields of "with SPCZ" negative events for the years 1985-1991, showing (a) ECMWF precipitation (contoured every 3 mm/day), (b) ECMWF OLR (contoured every 20 W m^{-2}), and (c) ECMWF OLR minus satellite-derived OLR observations (Liebmann and Smith 1996) (contoured every 20 W m^{-2}).

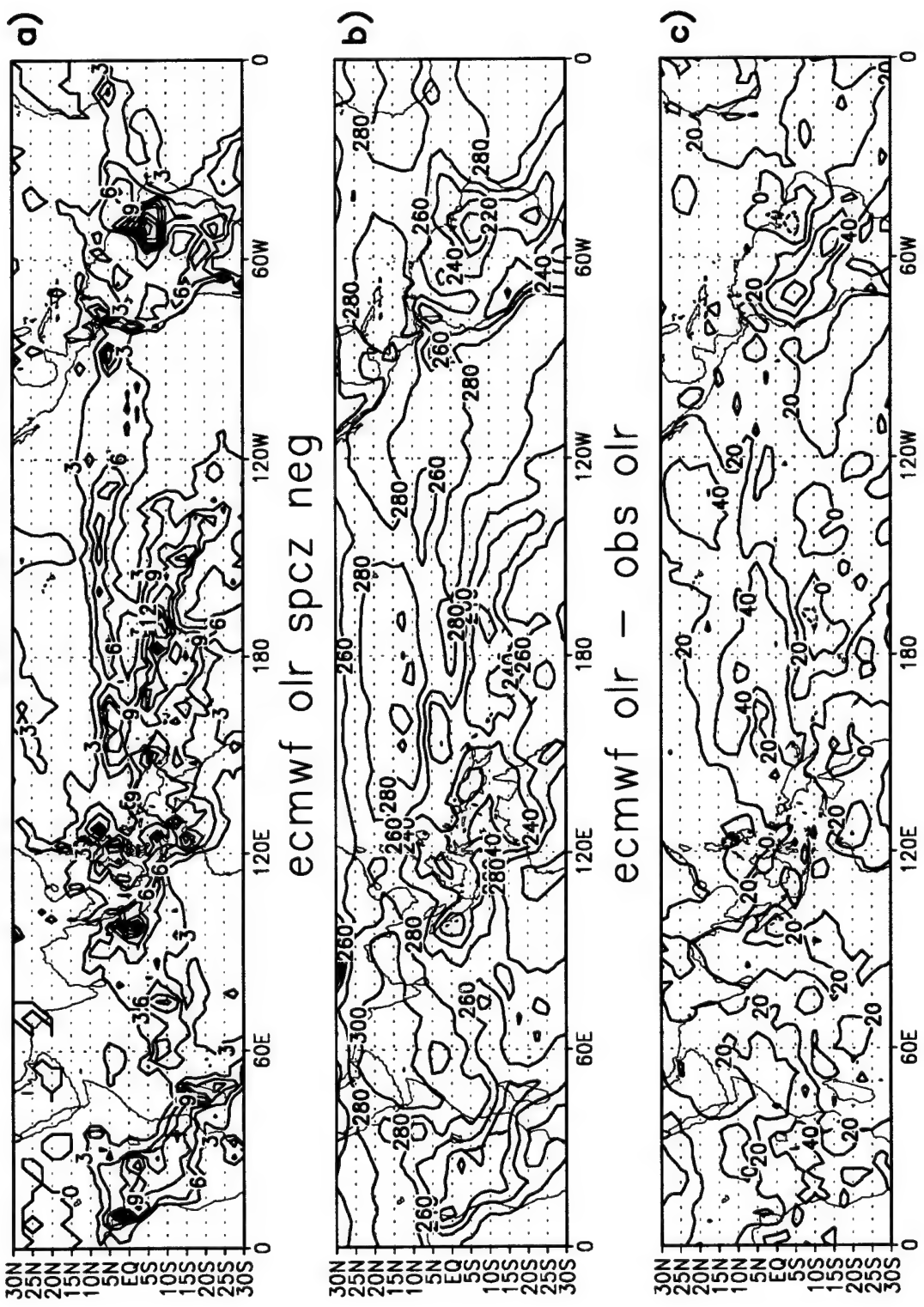
a)
ecmwf precip. spcz neg
b)
ecmwf olr spcz neg
c)
ecmwf olr – obs olr
30N
25N
20N
15N
10N
5N
EQ
5S
10S
15S
20S
25S
30S
0
60E
120E
180
120W
60W
0

Figure 4.14 Average composite differences between "with SPCZ" and "SACZ only" negative events for the years 1985-1991, showing (a) ECMWF precipitation (contoured every 3 mm/day), (b) ECMWF OLR (contoured every 10 W m^{-2}), and (c) satellite-derived OLR observation differences (Liebmann and Smith 1996) (contoured every 10 W m^{-2}).

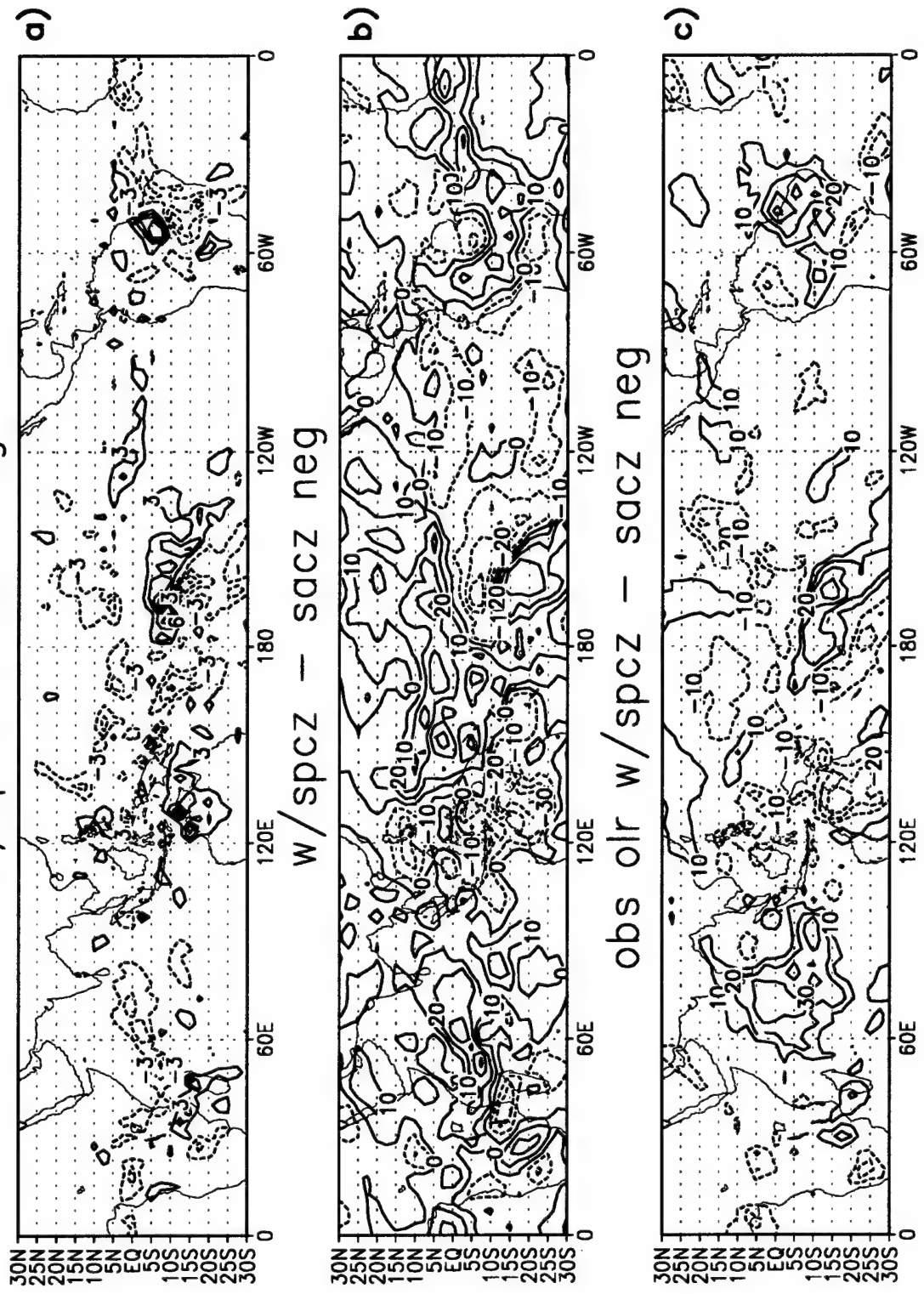
a)
w/spcz – sacz neg
b)
w/spcz – sacz neg
c)
obs olr w/spcz – sacz neg
30N
25N
20N
15N
10N
5N
EQ
5S
10S
15S
20S
25S
30S
0
60E
120E
180
120W
60W
0

Figure 4.15 Composite ISCCP data for "with SPCZ" negative events (1985-1991) for (a) high, (b) medium, and (c) low cloud percentages. Contours are every 10%.

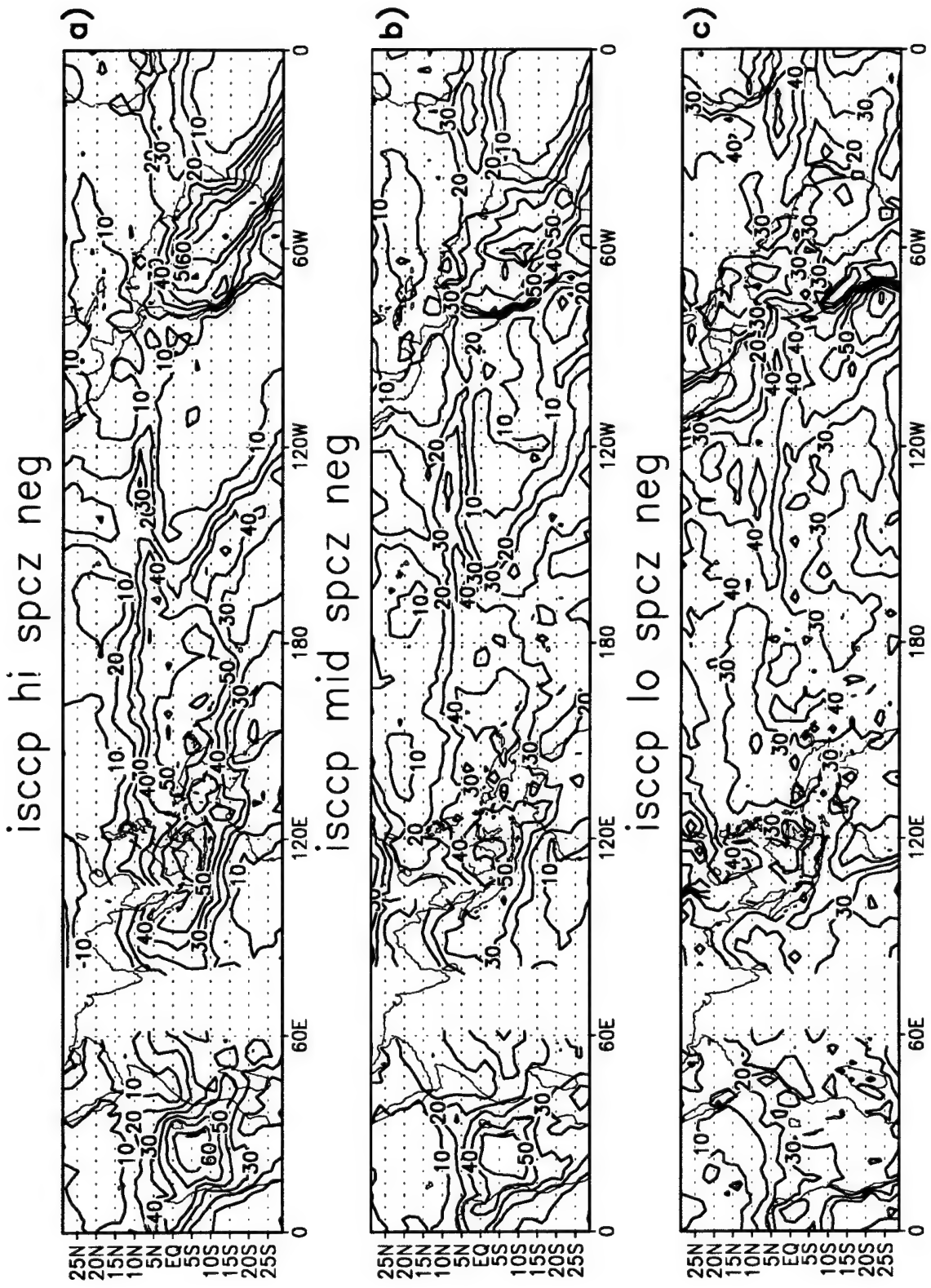
a)
isccp hi spcz neg
b)
isccp mid spcz neg
c)
isccp lo spcz neg
25N
20N
15N
10N
5N
EQ
5S
10S
15S
20S
25S
0
60E
120E
180
120W
60W
0

Figure 4.16 Composite ISCCP cloud differences for "with SPCZ" and "SACZ only" negative events (1985-1991) for (a) high, (b) medium, and (c) low cloud percentages. Contours are every 5%.

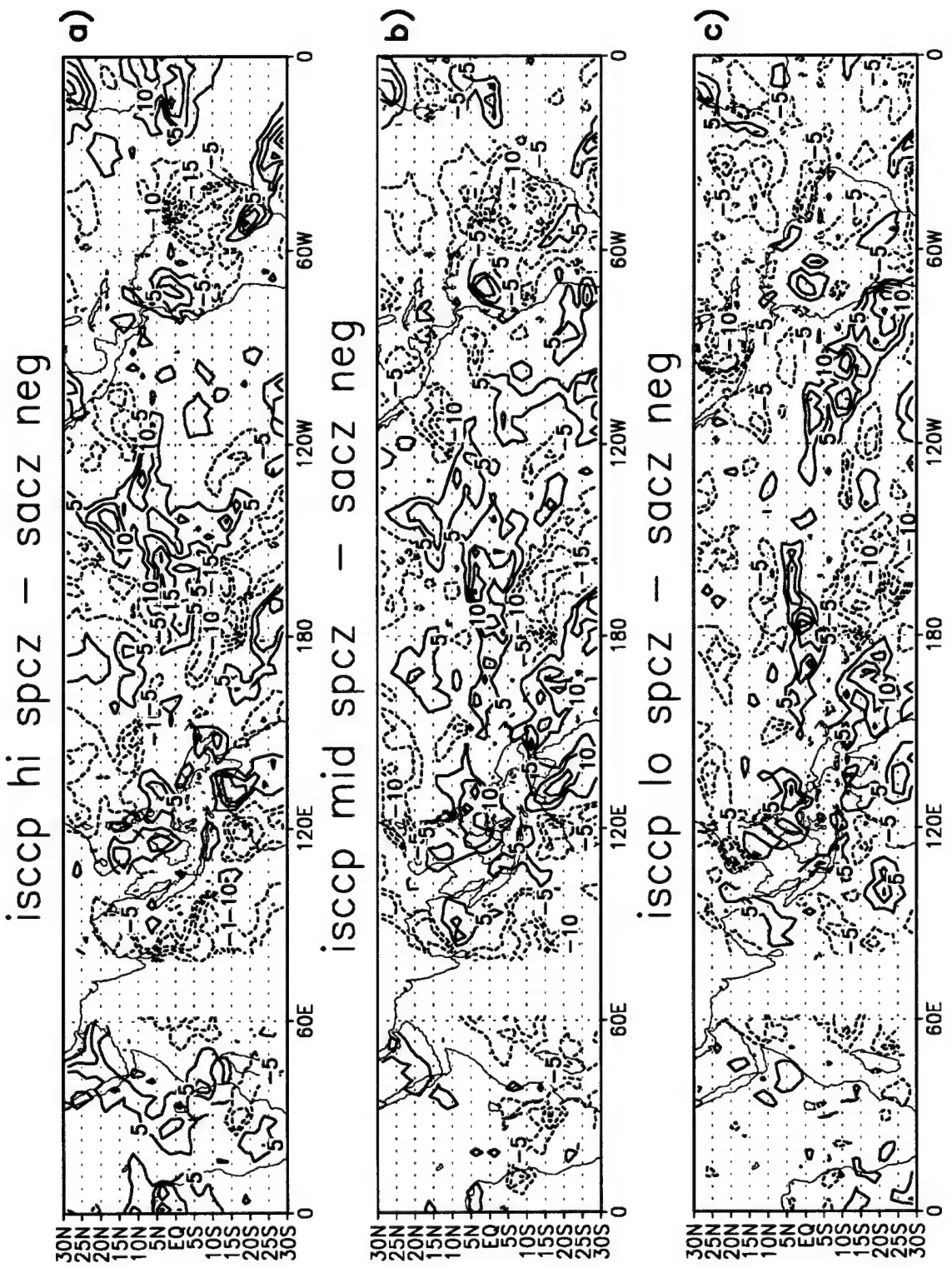
a)
isccp hi spcz – sacz neg
b)
isccp mid spcz – sacz neg
c)
isccp lo spcz – sacz neg
30N
25N
20N
15N
10N
5N
EQ
5S
10S
15S
20S
25S
30S
0
60E
120E
180
120W
60W
0

over the Southeastern Pacific, especially for "with SPCZ" cases. Extensive cloudiness (contributing to lower amounts of evaporation) over this region plays a role in the earth radiation budget, as solar radiation becomes less influential with the insulating layer of clouds. Due to the cool waters and predominant southerly flow, the low clouds in this region are generally layer clouds (stratus), associated with warm air over a cold surface (Wallace and Hobbs 1977). The stratus decks are more extensive and persistent for "with SPCZ cases," consistent with the warmer air temperatures observed at low levels. Differences in temperature between "with SPCZ" and "SACZ only" at 80°W are positive in the lower half of the atmosphere, with values of 3 Kelvin found at 850 mb and 22.5°S (not shown). These warmer temperatures and concommitant higher static stability at low levels are consistent with the more extensive stratus decks off the Chilean coast.

Results presented in this section confirm the adequacy of the ECMWF assimilated data in describing atmospheric patterns related to two different classes of SACZ enhancement. The primary source of remaining uncertainty is with the evaporation field. A question remains as to whether the lack of local feedback between evaporation and precipitation is a realistic feature of the hydrological cycle over time scales of 1 to 2 weeks (the period of focus for this study).

This chapter has evaluated two types of enhanced SACZ through an analysis of OLR and precipitation fields, upper-level and surface circulation anomalies, transients and hydrologic processes. "With SPCZ" events are related to the Pacific through intraseasonal oscillations, in agreement with the "seesaw" in precipitation found by NPM97. For these events, the region over the SPCZ becomes suppressed when the SACZ becomes enhanced. A 200 mb wave 5 pattern is evident in the Southern Hemisphere along with 4 NW-SE-oriented precipitation bands. The biweekly evolution of the "SACZ only" events has no apparent relation to activity in the Pacific. The signal over the SACZ appears 8 days from event onset and slowly amplifies. These cases are associated with longer waves in the Southern Hemisphere (wave 2 pattern) and more intense precipitation over South America.

The convergence of moisture flux is the major moisture source for both types of enhanced SACZ. Chapter 5 examines cases of suppressed SACZ.

CHAPTER 5

POSITIVE EVENTS

Rainfall patterns over the subtropical plains of South America have important agricultural and economic factors during the austral summer. This chapter focuses on periods of suppressed convection over the SACZ in which precipitation is abundant over the plains. As shown in Chapter 4, an intensified SACZ results in compensating subsidence that locally suppresses convection in surrounding regions. It is shown that increased precipitation over the plains occurs at the other extreme, when the SACZ weakens, on a similar timescale of about 10 days. This chapter examines two cases of suppressed convection over the SACZ (shown in Fig. 1.2). One type of event evolves with ties to the larger scale system, representing the opposite phase of the "seesaw" described in Chapter 4 (Fig. 1.2 a). The other regime originates more locally and with more intense local characteristics (Fig 1.2 b).

The chapter is divided into five subsections as follows: OLR and precipitation fields are discussed; followed by a description of associated upper-level circulation anomalies; third, a discussion of the possible role of synoptic-scale transients; fourth, components of the atmospheric hydrological cycle are examined; and finally, event composites from the ECMWF reanalysis for a 6-year period are compared with cloud coverage obtained from ISCCP and OLR observations.

5.1 OLR and Precipitation Diagnostics

The "with SPCZ" and "SACZ only" cases (see section 4.1) are identified by REOF analyses of OLR anomalies (see section 2.4), as in Chapter 4. Table 5.1 lists the positive events, and they are shown to have an average duration of about a week. Events that

Table 5.1

Positive Events

"with SPCZ"	"SACZ only"
03/07-03/12 '76	02/15-02/19 '75
01/12-01/16 '77*	12/06-12/11 '75
02/09-02/14 '77	01/16-01/21 '76
12/20-12/25 '80	03/24-03/30 '80
02/15-02/19 '81	01/30-02/04 '81
02/13-02/23 '82	12/20-12/25 '81
02/16-02/26 '83*	11/01-11/08 '84
01/10-01/18 '84*	02/04-02/10 '85
02/13-02/22 '85	12/08-12/13 '85
11/12-11/20 '85	01/18-01/22 '86
01/05-01/10 '87*	11/18-11/25 '86*
02/23-03/03 '87*	03/06-03/13 '90
01/15-01/23 '88	11/22-11/26 '91*
03/26-03/31 '88	01/01-01/05 '93*
12/07-12/12 '88	11/11-11/16 '93*
01/25-02/02 '89	02/02-02/06 '94
02/16-02/23 '92*	11/05-11/10 '94
01/27-01/31 '93*	12/11-12/17 '94
02/23-03/02 '95	01/14-01/18 '95
Total=19	Total=19
Ave Time=7.6 dy	Ave Time=6.2 dy
37% Warm ENSO	21% Warm ENSO

* denotes events that occurred during warm ENSO years

occurred during warm ENSO years are denoted by an asterisk. Although not nearly as strong as for the negative events, the positive "with SPCZ" events are more closely associated with warm ENSO events than are the "SACZ only" cases (37% versus 21%). "With SPCZ" positive events are one phase of the "seesaw" from enhanced to suppressed convection over the SACZ (the positive signal has been shown to occur 8 days from onset of a negative event). Results in Chapter 4 show that the opposite phase (negative "with SPCZ" composite) has a much stronger ENSO signal. To further examine these relationships, OLRA composites from the intraseasonal filter (IS) are compared to those obtained from a low pass filter (LP) that removes time scales less than 10 days. The "SPCZ only" composite is also produced (see section 4.1). The cases are shown in Fig. 5.1. Comparison of Fig. 5.1 a with b and c with d shows that interannual variations are more pronounced, especially over the Pacific Ocean. This indicates strong contributions to these events from interannual variations. For "with SPCZ" cases (c and d), the lack of an ENSO signal over the SACZ is supported by the intraseasonal "seesaw," which tends to average out any signal. Over the subtropical plains, low OLR anomalies indicate abundant precipitation south of the suppressed SACZ. This is a region Ropelewski and Halpert (1996) identify as exhibiting Southern-Oscillation-related precipitation relationships. Enhanced precipitation in this region matches a warm ENSO signal. Comparison of e) with f) supports the higher correlation of positive "with SPCZ" events to warm ENSO events. Over the plains in Fig. 5.1 e, OLR anomalies are weaker than those of Fig. 5.1 f. Positive events for the intraseasonal time scales are not apparent when compared to the interannual signal (Fig. 5.1 f), which also exhibits ENSO characteristics.

The evolution of the positive cases is shown in Fig. 5.2. A transition is evident (Fig. 5.2 a through d) over the SACZ from low to high OLR anomalies for "with SPCZ" cases. By 4 days prior to event onset, the SACZ becomes suppressed, with anomalies up to 25 W/m^2. By day 0 (Fig. 5.2 d), the signal is pronounced over the SACZ, while a weaker sign of increased convection over the subtropical plains is evident. At higher latitudes,

Figure 5.1 Satellite-derived (Liebmann and Smith 1996) OLR composite anomalies (OLRA) for positive cases, 1974-1995, for (a) intraseasonal (retains variations between 10 and 90 days) "SACZ only," (b) low-pass (retains variations greater than 10 days) "SACZ only," (c) intraseasonal "with SPCZ," (d) low-pass "with SPCZ," (e) intraseasonal "SPCZ only," and (f) low-pass "SPCZ only" cases. The values are contoured and shaded every 5 W/m^2.

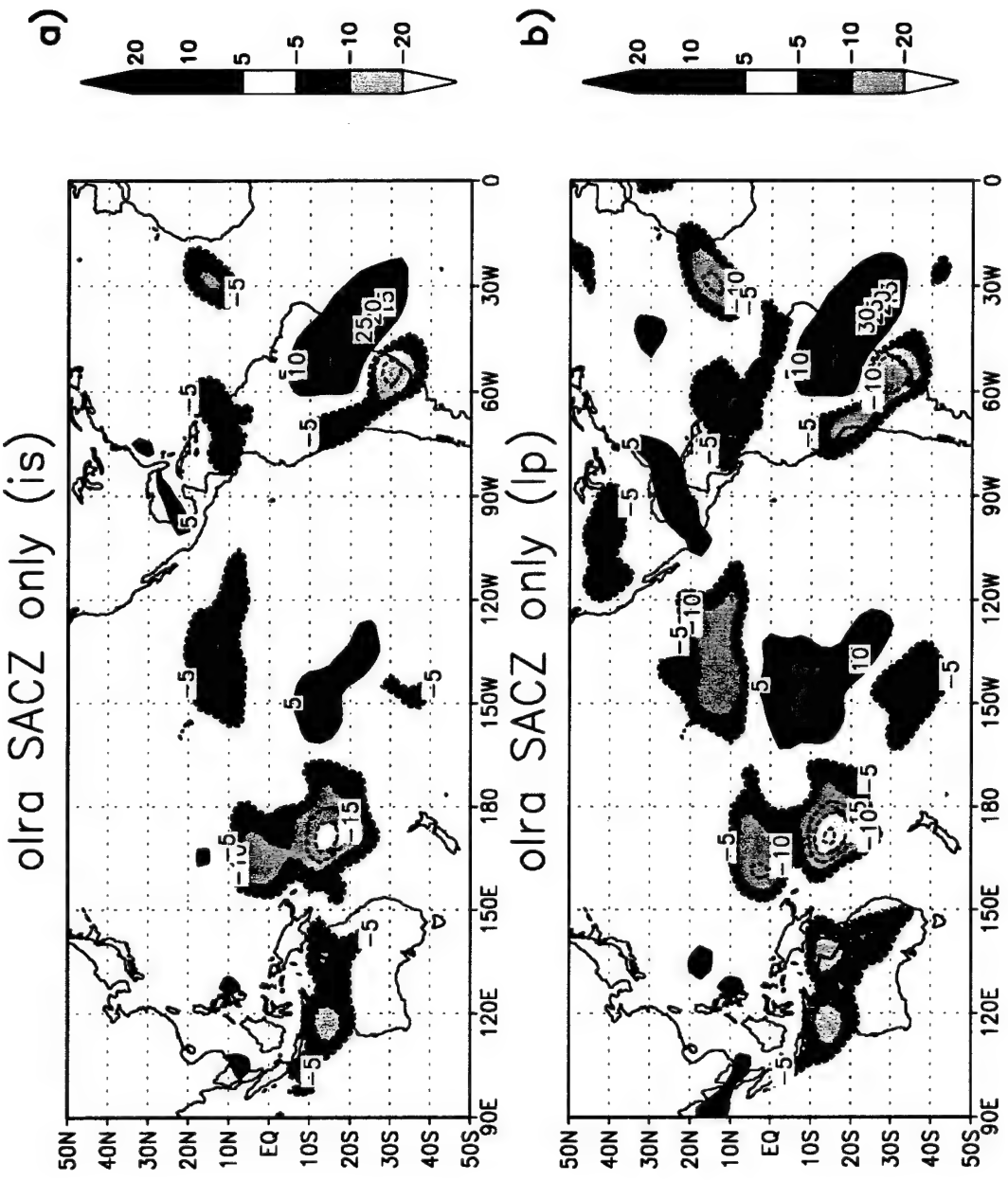
a)
20
10
5
-5
-10
-20
olra SACZ only (is)
b)
olra SACZ only (lp)
50N
40N
30N
20N
10N
EQ
10S
20S
30S
40S
50S
90E
120E
150E
180
150W
120W
90W
60W
30W
0

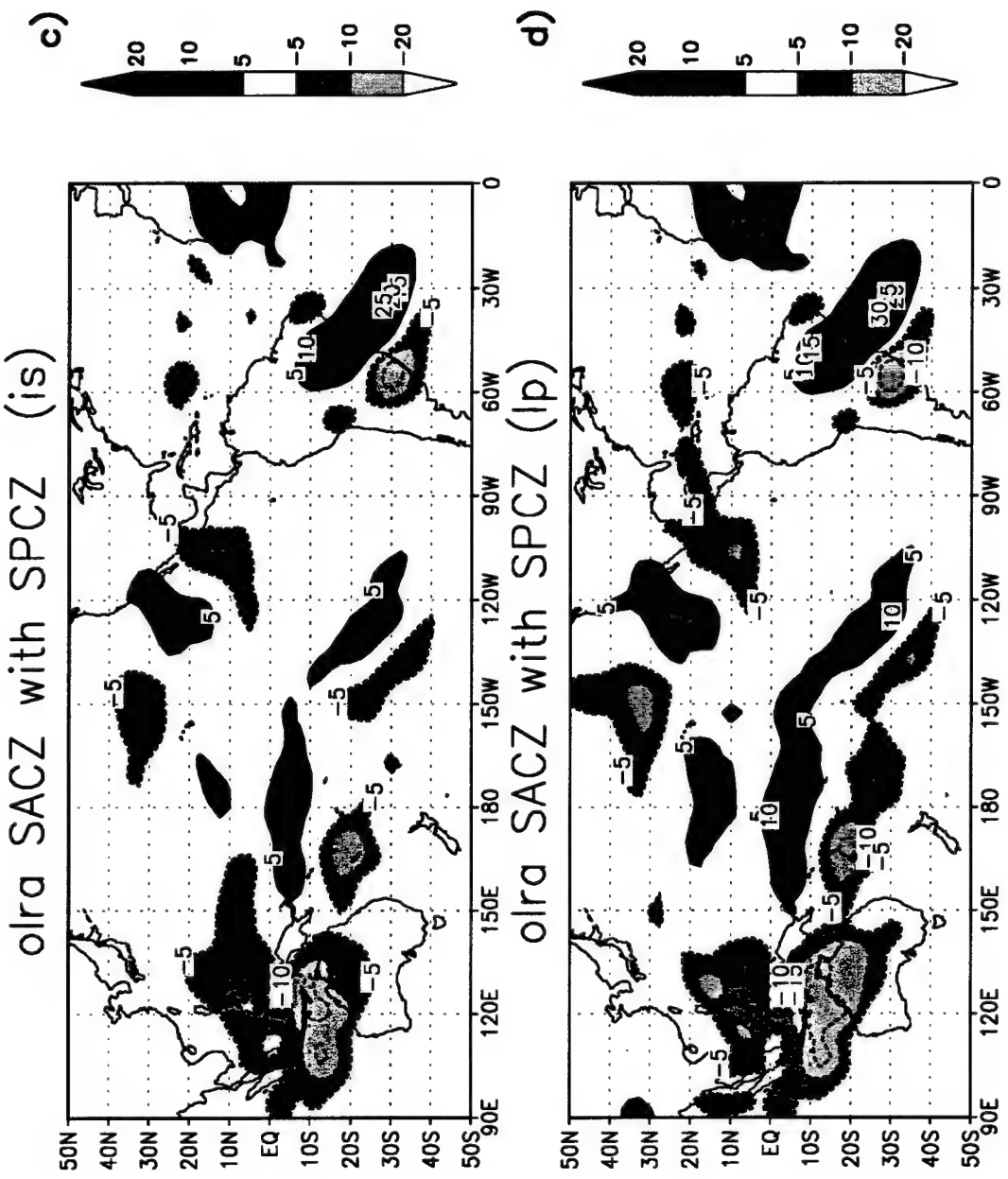

Figure 5.1 Continued

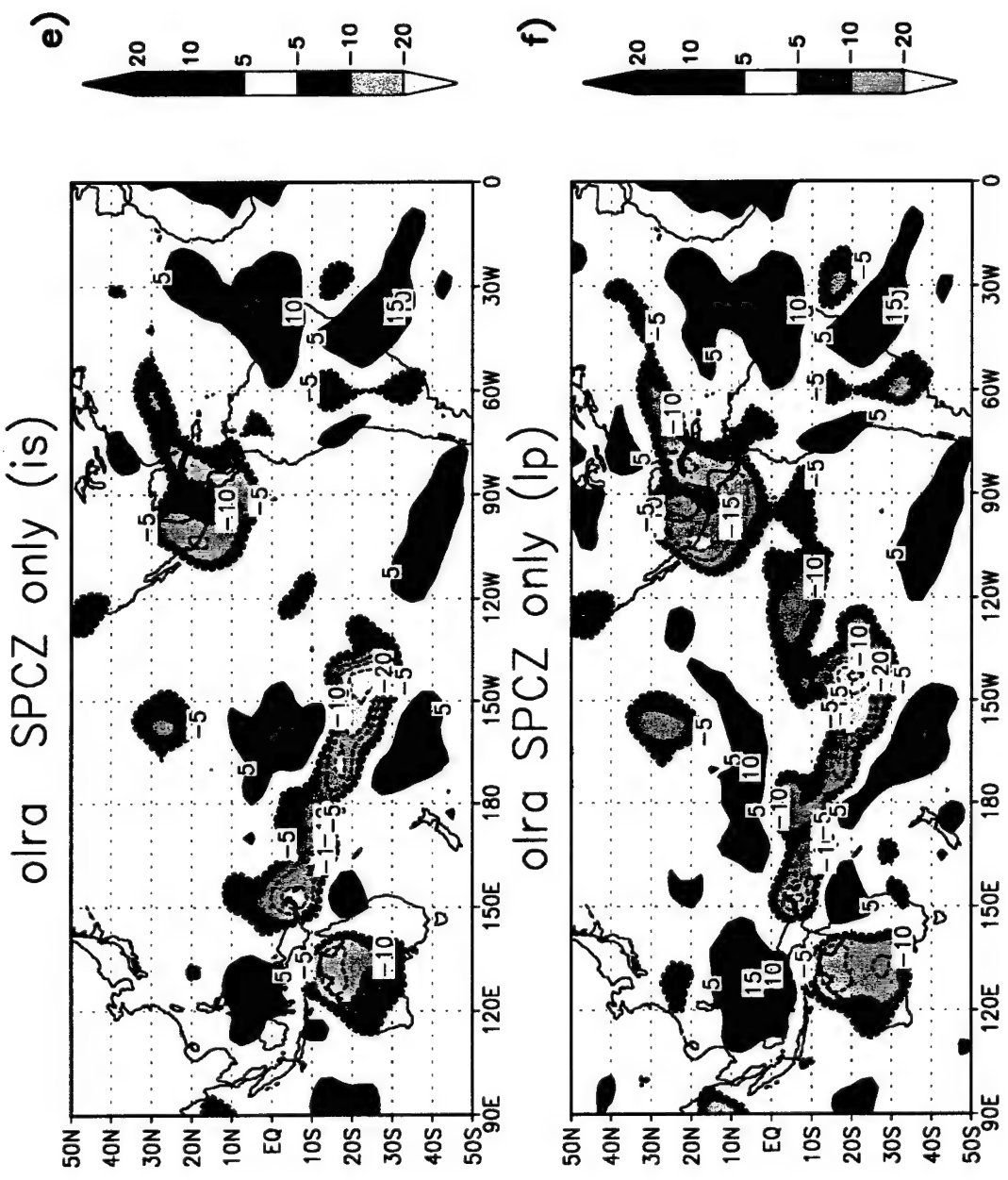

Figure 5.1 Continued

Figure 5.2 ECMWF OLRA composite anomalies for positive cases (1979-1993) for (a) "with SPCZ" days -8 to -6, (b) "with SPCZ" days -6 to -4, (c) "with SPCZ" days -4 to -2, (d) "with SPCZ" days -1 to 1, (e) "SACZ only" days -8 to -6, (f) "SACZ only" days -6 to -4, (g) "SACZ only" days -4 to -2, and (h) "SACZ only" days -1 to 1. Intervals are 5 W/m^2 as indicated by the colorbars.

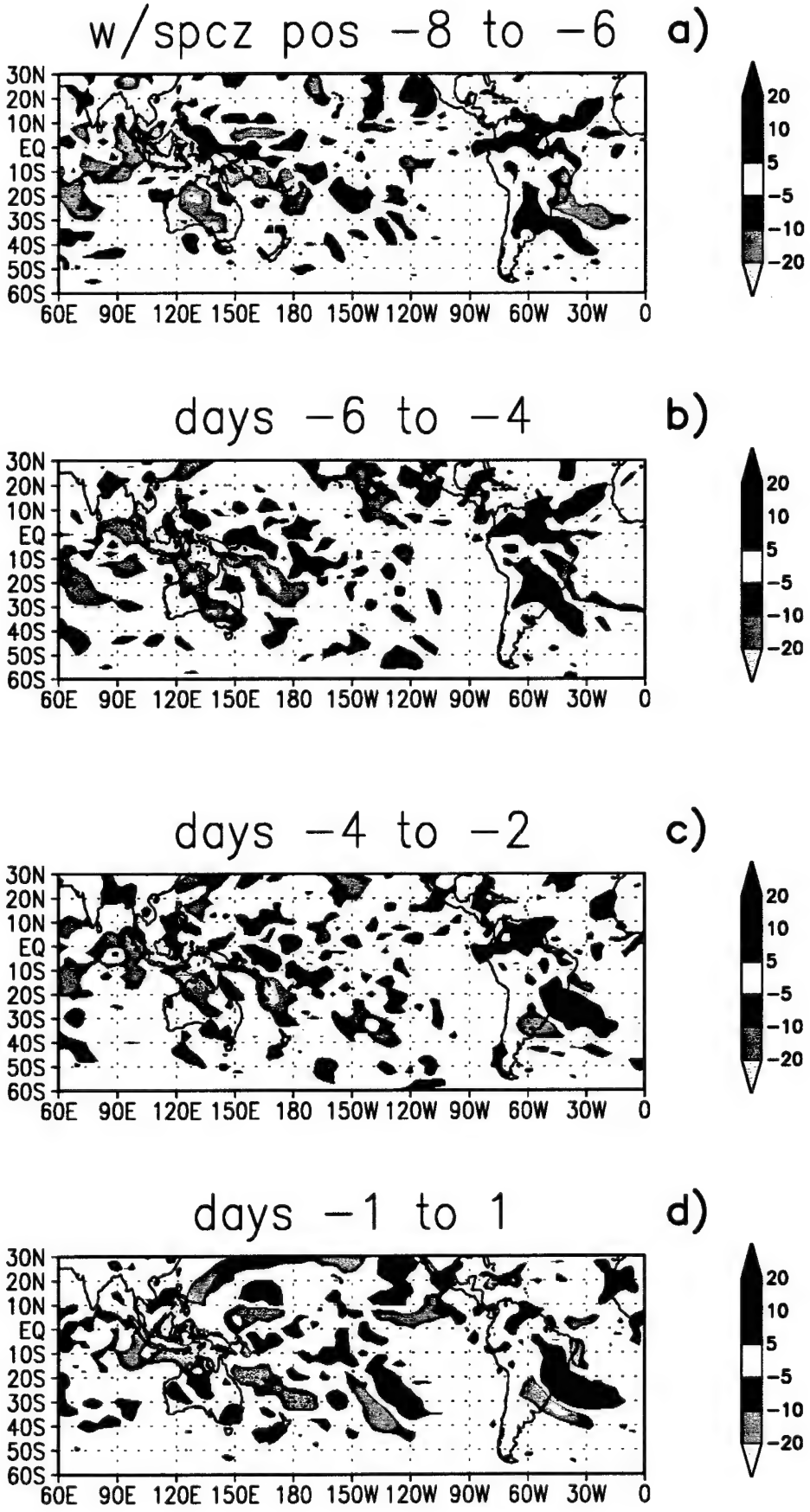
w/spcz pos −8 to −6
a)
days −6 to −4
b)
days −4 to −2
c)
days −1 to 1
d)
30N
20N
10N
EQ
10S
20S
30S
40S
50S
60S
60E 90E 120E 150E 180 150W 120W 90W 60W 30W 0
20
10
5
−5
−10
−20

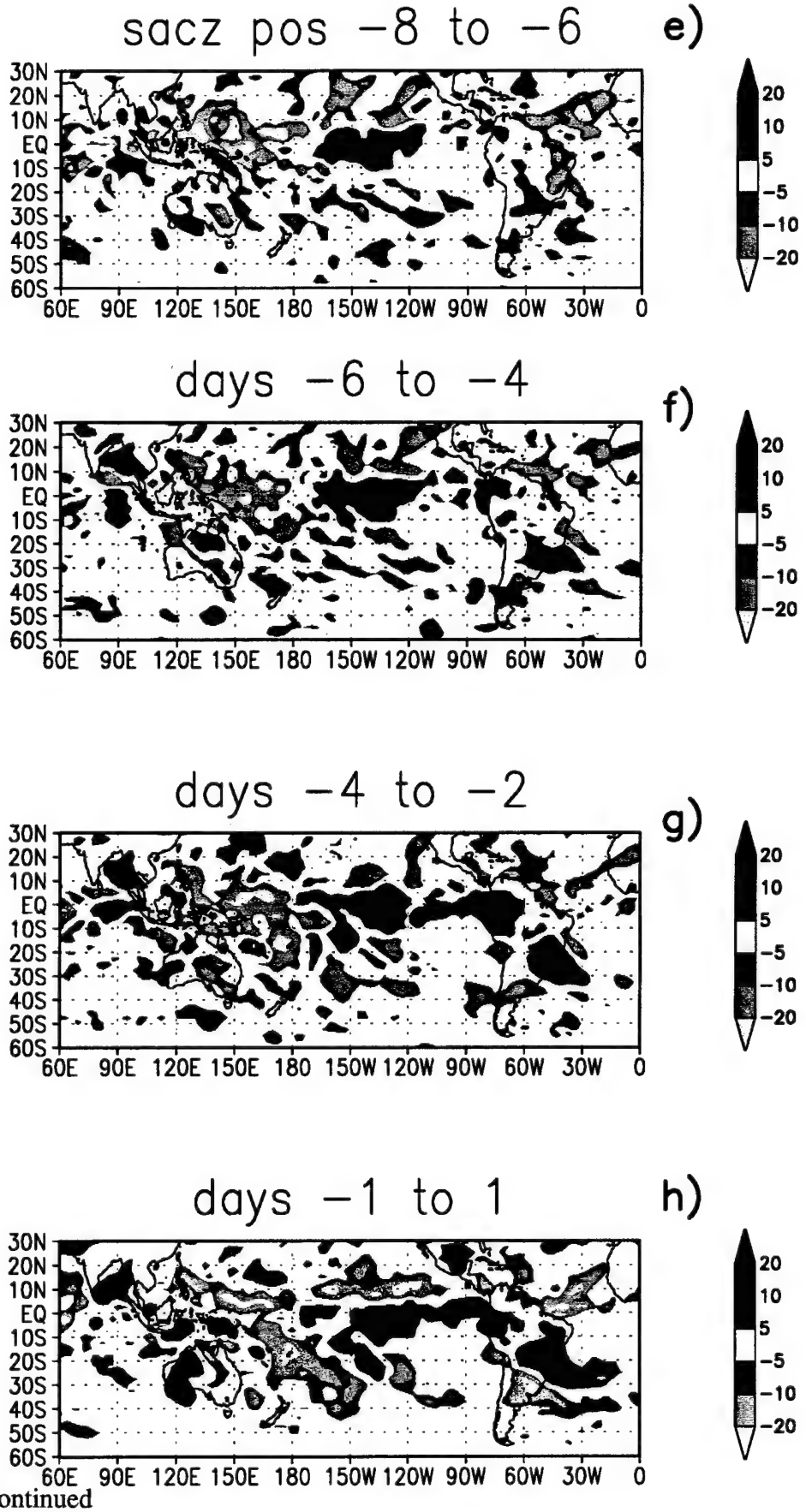

Figure 5.2 Continued

OLR becomes a less reliable proxy of convection (the composites in Fig. 1.2 c and d show a stronger signal over the subtropical plains). Analysis of the precipitation field will show that the convective activity over the plains is more enhanced than what may be inferred from Fig. 5.2 d. Similar to the evolving conditions over the SACZ, the low OLR anomalies over Australia at day -8 (reminiscent of the negative phase) weaken by day 0, and the SPCZ becomes more pronounced in its normal position by event onset.

The "SACZ only" events (Fig. 5.2 e through h) develop in a more stationary manner, similar to the negative cases (Fig. 4.2 e through h). Over the SACZ, high OLR values are evident at day -6 and slowly build with time, as do the low OLR anomalies over the subtropical plains to the south. High OLR anomalies are located over the Equatorial Pacific as convection is displaced northward into the Northern Hemisphere. Anomalies over South America are stronger than they are for "with SPCZ" events. As with the negative cases, the mechanisms of formation for the two types of positive cases differ. A validation of the OLR anomalies as proxies of convection is shown with the following analysis of the precipitation fields.

Three bands of positive precipitation anomalies appear in the Southern Hemisphere for "with SPCZ" events (Fig. 5.3), coinciding areas of 200 mb horizontal divergence. Precipitation is pronounced over the subtropical plains of South America, in the SPCZ and over Australia. Over Australia, precipitation is not as intense as it is for the the negative (enhanced SACZ) phase of the "seesaw" in precipitation over South America. OLR anomalies in Fig. 5.2 d correspond well with the precipitation. The region over the SACZ is well-defined (Fig. 5.3 a), with negative precipitation anomalies exceeding 5 mm/day, and high values of upper-level convergence. This composite shows the counterpart to negative "with SPCZ" events. With roots to the large-scale circulation, precipitation and divergence anomalies do not show as significant a signal as do the more locally-oriented "SACZ only" cases in Fig. 5.3 b.

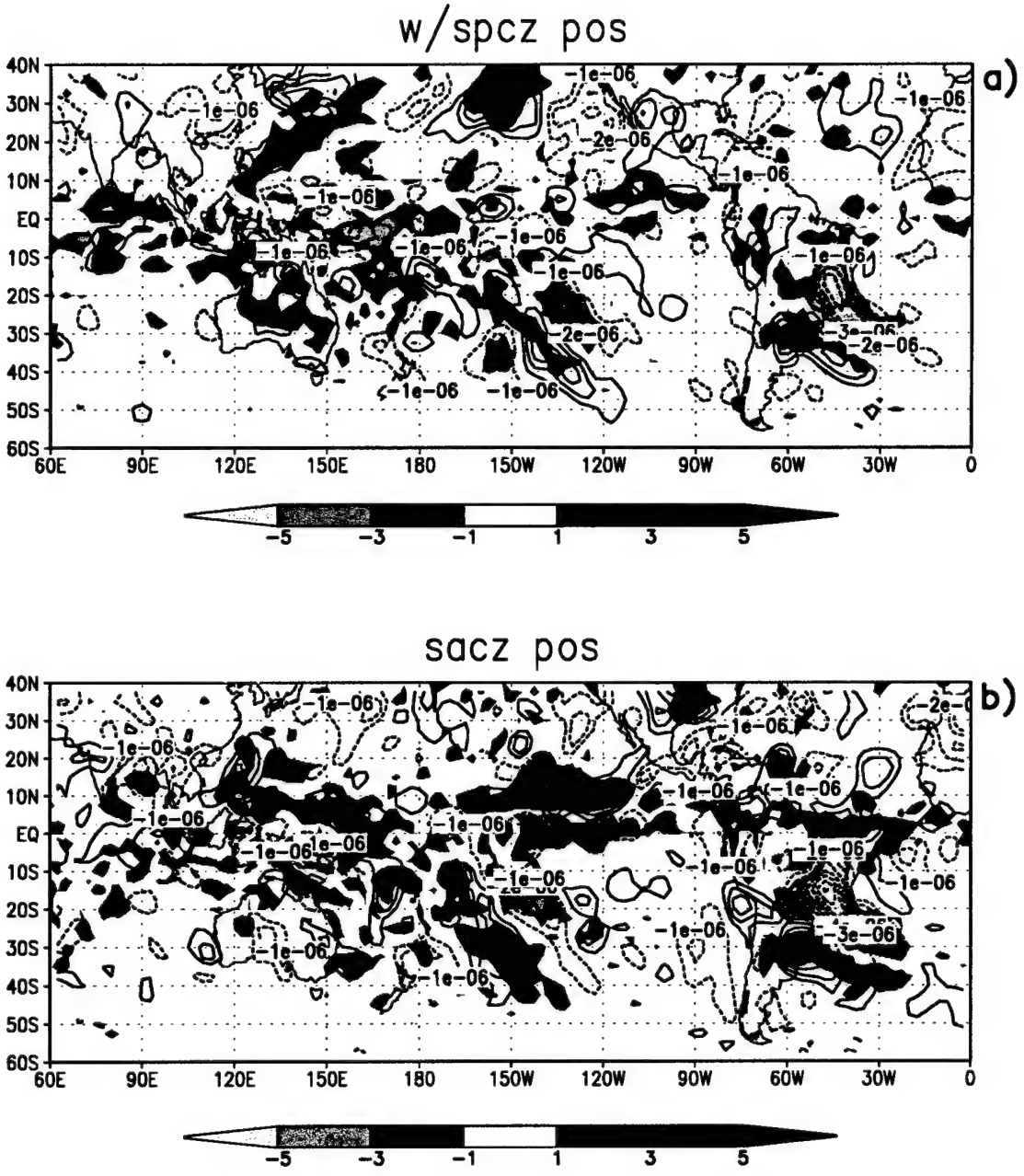

Figure 5.3 ECMWF composite precipitation anomalies (mm/day) and 200 mb horizontal divergence (s^{-1}) anomalies for (a) "with SPCZ" positive cases, and (b) "SACZ only" positive cases. Precipitation values are shaded as indicated by the colorbars.

Precipitation anomalies for "SACZ only" cases (Fig. 5.3 b) are much stronger, particularly over the SPCZ and over South America (two main bands of precipitation extend from NW to SE in the Southern Hemisphere). They show more pronounced negative precipitation and upper-level convergence anomalies over the SACZ, and an intense, more extensive band of precipitation anomalies to the south over the plains (precipitation anomalies are greater than 6 mm/day at about 50°W). In the Equatorial Eastern Pacific, a belt of enhanced precipitation is displaced northward to about 10°N. The pattern has characteristics of the warm ENSO phase. Therefore, as with the negative events (Chapter 4), the nature of the two types of positive cases differ. An analysis of composite upper-level circulations follows.

5.2 Influences on the Circulation

Composites of 200 mb and 1000 mb height and precipitation anomalies are shown in Fig. 5.4. An upper-level wave number 3 pattern is shown in the Southern Hemisphere at midlatitudes (Fig. 5.4 a, "with SPCZ" composite), with the most pronounced high at 100°W. Southeast of Africa, wave activity is suppressed and negative precipitation anomalies over Madagascar contrast with the anomalous precipitation band seen with the negative cases (see Fig. 4.4 a). This shows, again, how "with SPCZ" positive cases are the opposite phase of the "seesaw." Strong signals seen with the negative phase weaken in the positive phase. At 1000 mb (Fig. 5.4 d), the wave pattern is strongly amplified near South America, and low height anomalies are tied to positive precipitation anomalies (for instance, over Australia). Surface ridges are in place over the SACZ, co-located with negative precipitation anomalies.

The wave pattern for "SACZ only" cases (Fig. 5.4 b) is weaker over the Eastern Pacific than it is for the "with SPCZ" cases. Two waves are evident from 100°W downstream to 80°E. Near South America, the midlatitude 1000 mb height field shows a trough-ridge-trough pattern in Fig. 5.4 d, while "SACZ only" events (Fig. 5.4 e) show a ridge and a very intense trough over the Southwest Atlantic. The height field is amplified

Figure 5.4 ECMWF precipitation anomalies (mm/day) and 200 mb height anomalies (m) are shown in (a) for "with SPCZ" positive cases, (b) "SACZ only" positive cases, and (c) "with SPCZ" minus "SACZ only (a-b). Precipitation anomalies are shaded as indicated in the colorbars, and 200 mb heights are contoured every 20 m. The 1000 mb height anomalies are shown with precipitation anomalies in (d) for "with SPCZ" negative cases, and (e) "SACZ only" negative cases. The 1000 mb height contours are every 5 m.

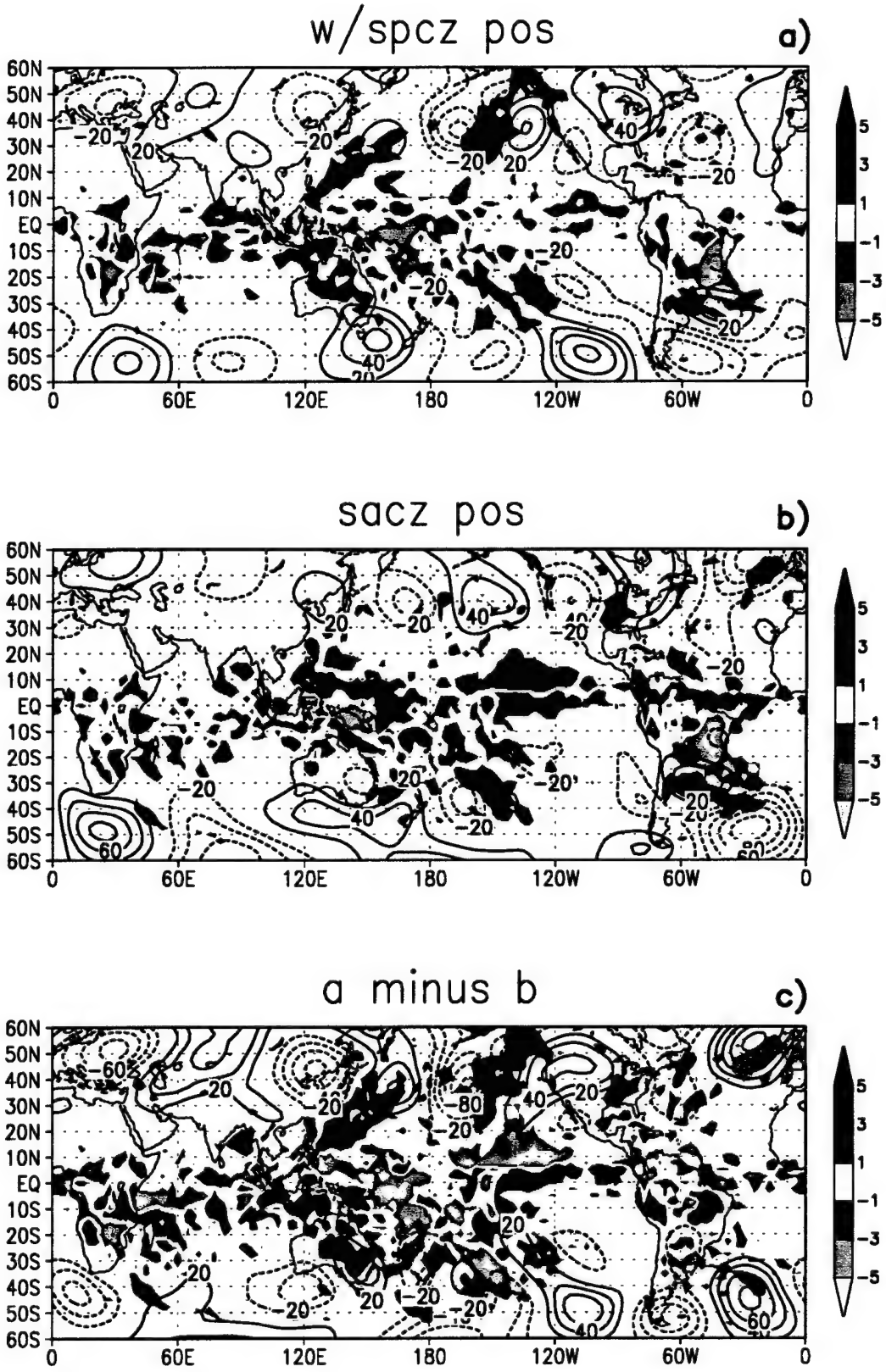
w/spcz pos
a)
sacz pos
b)
a minus b
c)
60N
50N
40N
30N
20N
10N
EQ
10S
20S
30S
40S
50S
60S
0
60E
120E
180
120W
60W
5
3
1
-1
-3
-5

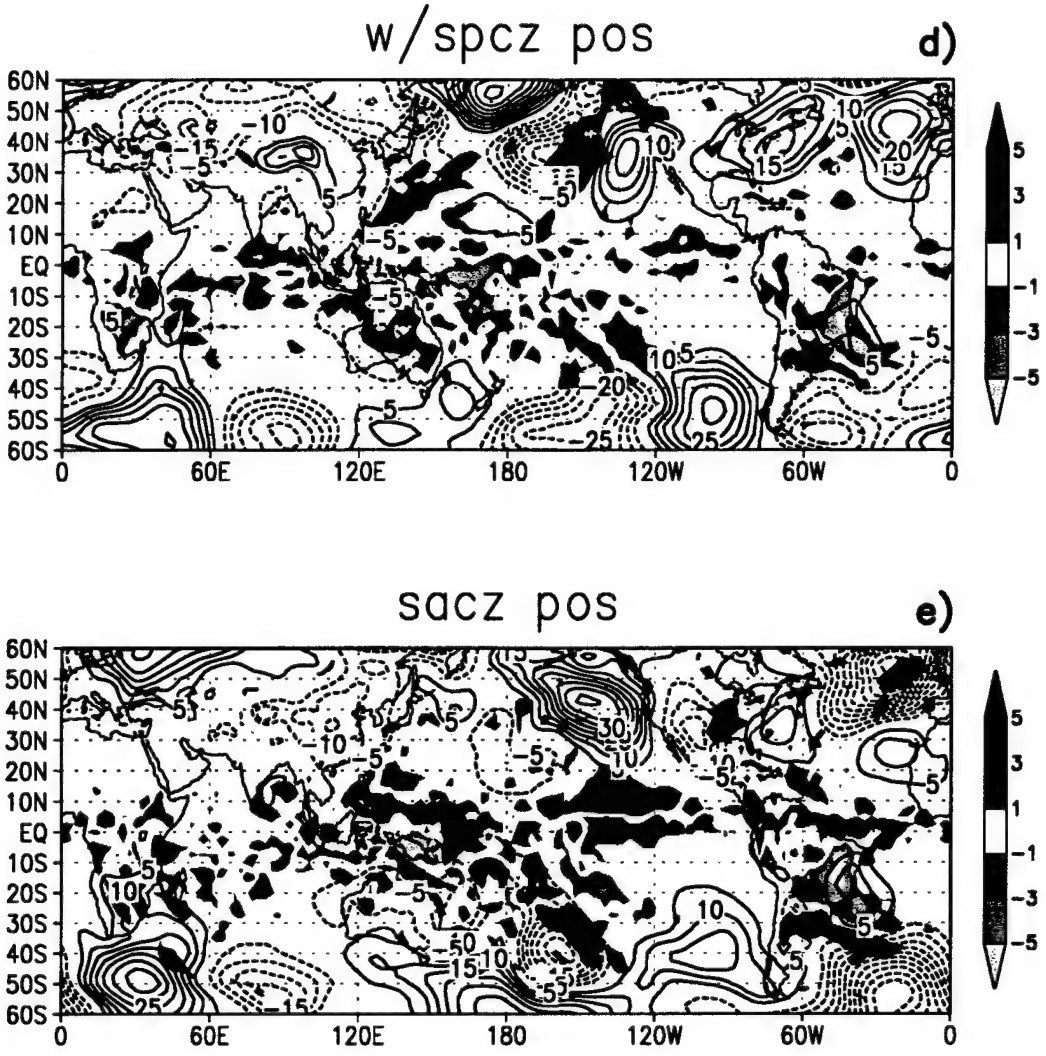

Figure 5.4 Continued

(see Fig. 5.4 b and e) with very low anomalies in the height field at 30°W. Garreaud and Wallace (1997) found that summertime incursions of midlatitude air are predominant features of the South American circulation. They move equatorward at about 10 m/s and maintain identities for about 5 days. These incursions are preceded by an approaching upper-level trough that deepens the surface low over the central plains. The southward advection of moist air makes conditions favorable for deep convection over central and southern Argentina. The localized nature of "SACZ only" events suggests the passage of these strong frontal systems may play a role in the observed signature. The composites in Fig. 5.2 suggest a northward migration of OLR anomalies from midlatitudes to the subtropics, moving at a much slower rate of about 10 degrees latitude in 10 days. Over the SPCZ, 200 mb negative height anomalies are displaced toward the west of the surface anomalies, as expected for baroclinic waves. The difference in height and precipitation anomalies (Fig. 5.4 c) is well-defined and suggests the patterns are somewhat out of phase. The higher magnitude of "SACZ only" precipitation anomalies in the Southern Hemisphere is also illustrated. Over the Northern Hemisphere, the wave pattern is much more active at midlatitudes for both cases than was found for the negative cases. At 1000 mb over the Midwestern U.S., "SACZ only" cases show positive precipitation anomalies and southerly flow over the Eastern U.S., as indicated by the position of the height anomalies (Fig. 5.4 e).

The upper-level analyses thus show that large-scale circulations for "with SPCZ" events are more active, while "SACZ only" events have more locally amplified features near South America. This can also be shown with cross sections of meridional flow anomalies at 60°W (Fig. 5.5). A low-level northerly jet which transports moisture southward is established parallel to the Andes at midlatitudes (this will be discussed in further detail in subsection 5.4), and northerlies aloft maximize at 35°S. The upper-level northerlies are associated with the approaching trough off the west coast of South-America. Meridional anomalies for "SACZ only" events are stronger at low-levels and extend farther

Figure 5.5 Cross sections of ECMWF meridional wind anomalies along 60°W from 1000 mb to 100 mb for (a) "with SPCZ" positive cases, (b) "SACZ only" positive cases, and (c) climatology. Values are contoured every m/s.

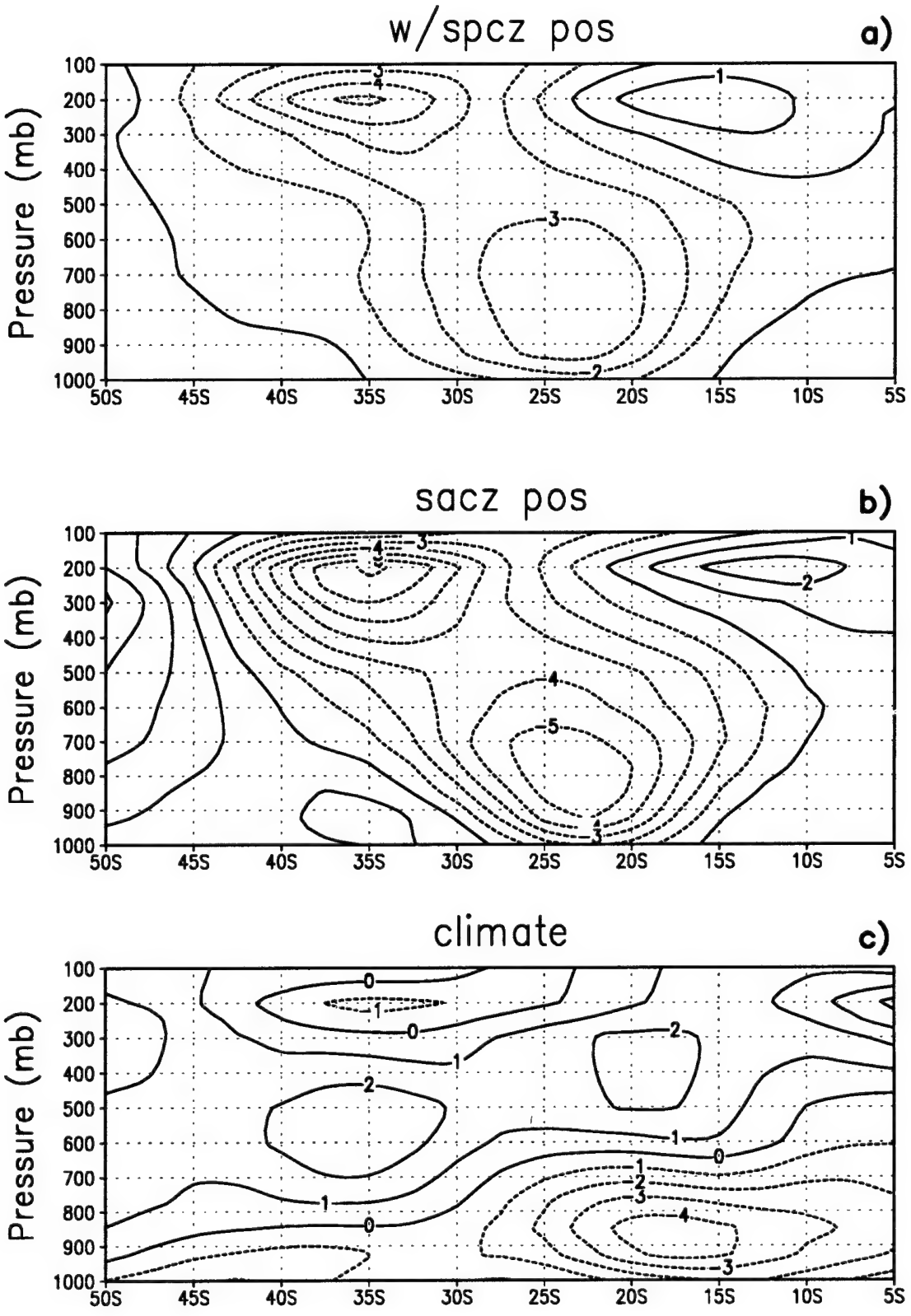
w/spcz pos
a)
Pressure (mb)
100
200
300
400
500
600
700
800
900
1000
50S
45S
40S
35S
30S
25S
20S
15S
10S
5S
sacz pos
b)
climate
c)

south aloft than those for "with SPCZ" events, with values up to 6 m/s at 300 mb (at 35°S, Fig. 5.5 b). The upper-level flow implies substantial differences from climatology. Fig. 5.5 c depicts prevailing southerlies at upper-levels associated with an upper-level anticyclone (Fig. 3.4). The next section looks at transient activity and the evolution of the events.

5.3 Transients

As in Chapter 4.3, the strength of the synoptic eddies is quantified by the variance of 200 mb heights within each event (Fig. 5.6). Then, the square root is taken from the mean variance for all events. This quantity is shown in Fig. 5.6 a for "with SPCZ" cases. The Northern and Southern Hemispheres both appear considerably variant at midlatitudes. In the Southern Hemisphere, when the "SACZ only" composite is subtracted from the "with SPCZ" composite (Fig. 5.6 b), both cases tend to contribute to transient activity at midlatitudes, though "with SPCZ" cases are predominant. While "with SPCZ" cases are more transient over the Pacific (as in the negative cases in Fig. 4.6), "SACZ only" cases show transient activity over the Southwest Atlantic (as noted by the -20 m difference). This supports conclusions in section 5.2 that strong cold air outbreaks may play a role in the signal over South America for "SACZ only" events. Over North America, transient activity is much more pronounced than was found for the negative events.

The averaged composite evolution is now shown with Hovmöller diagrams of the 200 mb height anomalies along 50°S for both types of cases (Figs. 5.7 and 5.8). For the "with SPCZ" composite, a wave pattern is in place from 180°W eastward by day -4. In support of the "seesaw" concept, this is a similar type of amplification observed for the negative cases at day 0 (see Fig. 4.7). Near Indonesia (from 120°E to the dateline), the strengthening of the high height anomalies after event onset is evident, as perturbations over the South Pacific maximize from days 2 to 4.

For "SACZ only" cases (Fig. 5.8), low height anomalies are located at about 90°W at day -6 from onset, and they gradually shift eastward and strengthen. By day 5, maximum

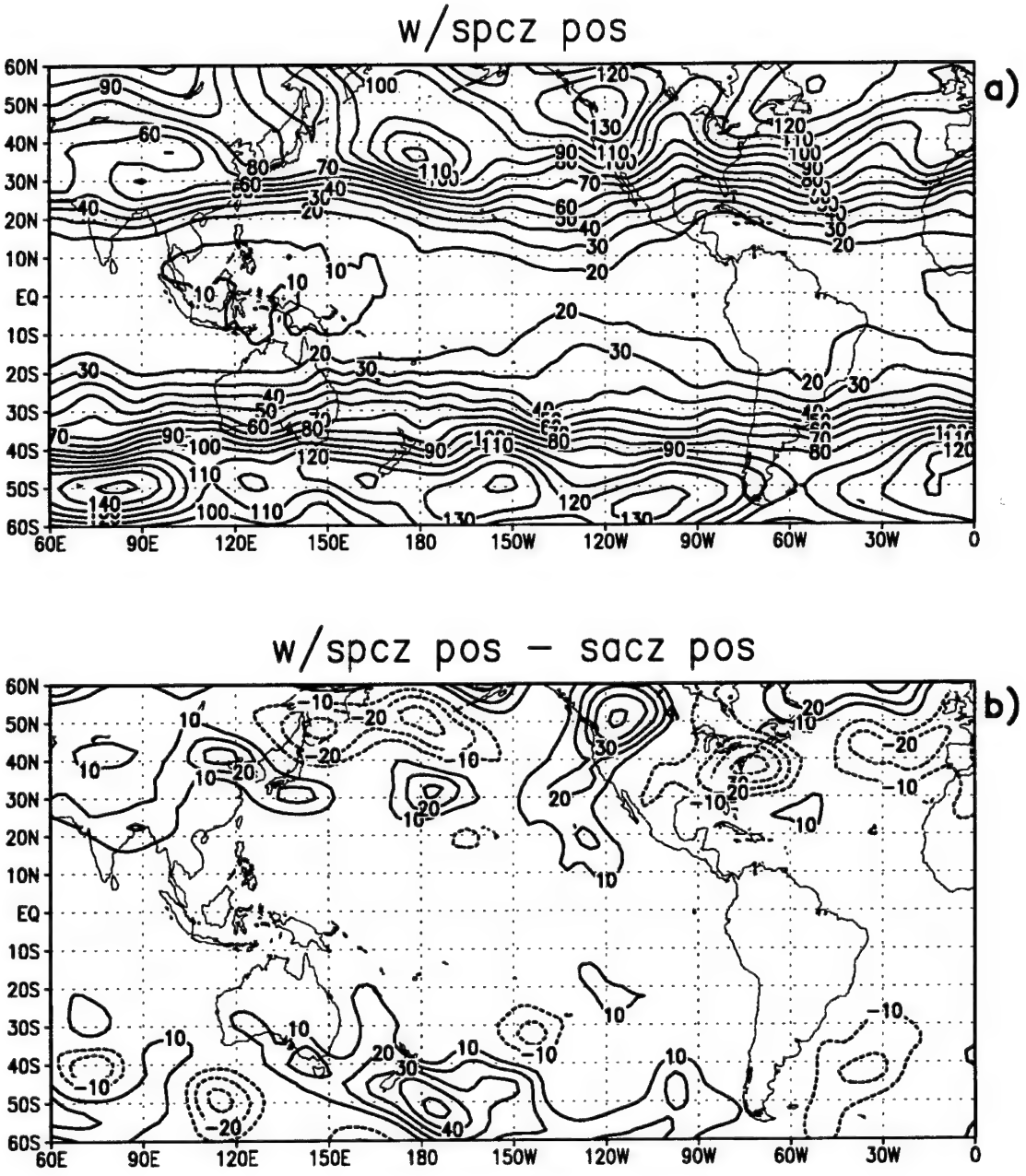

Figure 5.6 The square root of the variance in ECMWF 200 mb heights are shown for (a) "with SPCZ" positive cases, and (b) "with SPCZ" minus "SACZ only" positive cases. Contours in (a) are every 20 m; contours in (b) are every 10 m.

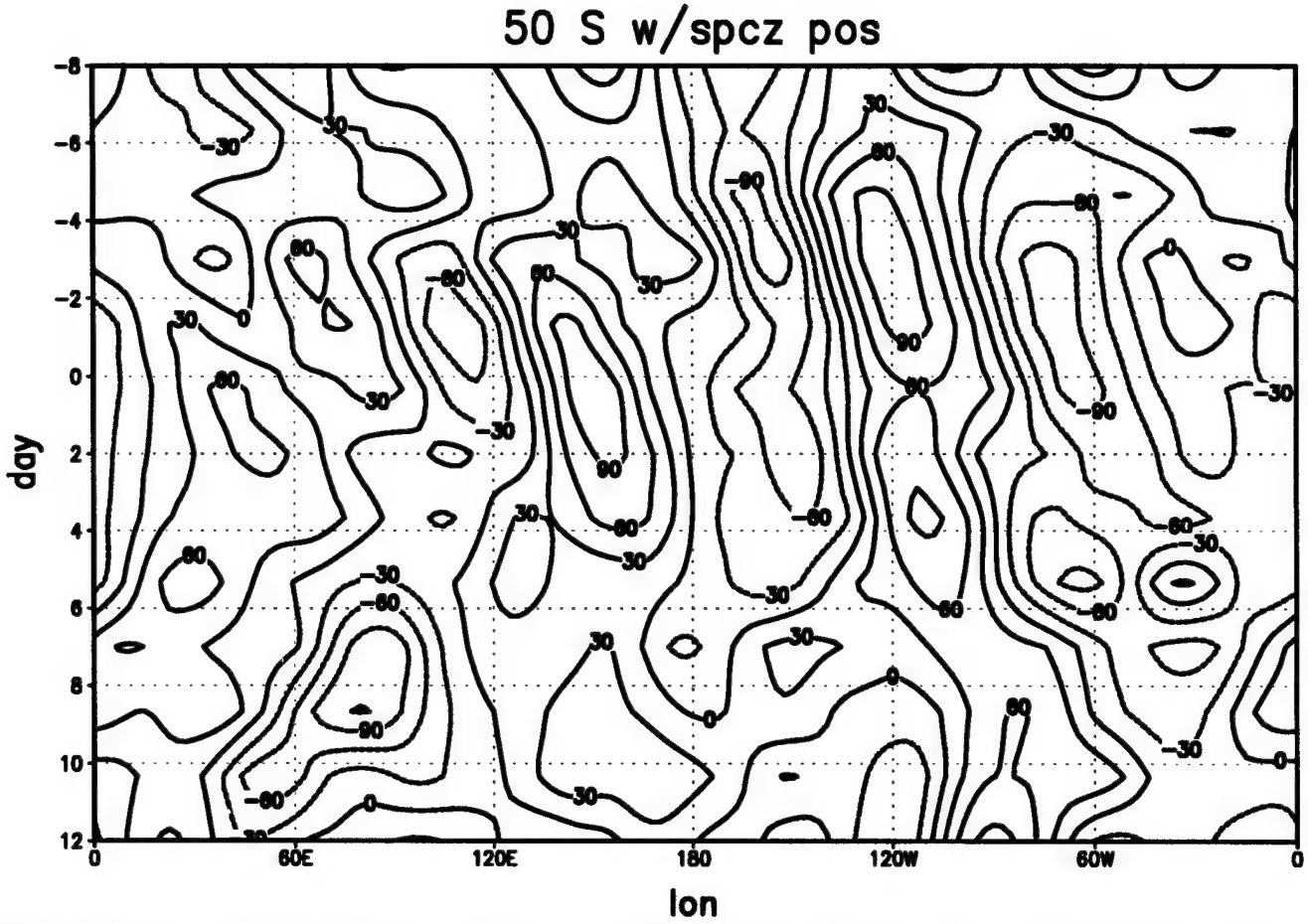

Figure 5.7 ECMWF 200 mb composite height anomalies along 50°S for "with SPCZ" positive cases. The y-axis shows time for 8 days preceding event onset (day -8), to event onsent (day 0), to 12 days following event onset (day +12). Contours are every 30 m.

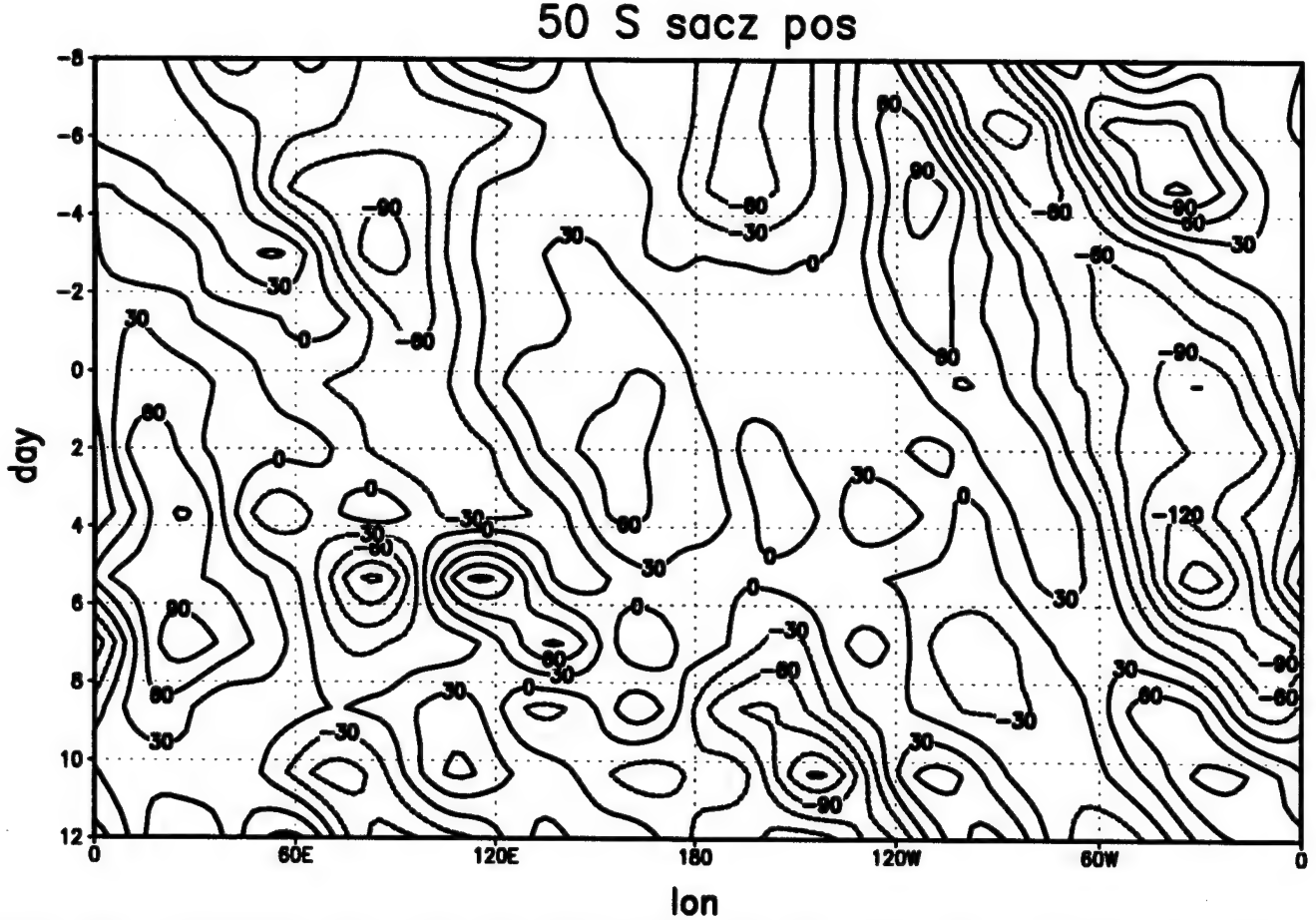

Figure 5.8 ECMWF 200 mb composite height anomalies along 50°S for "SACZ only" positive cases. The y-axis shows time for 8 days preceding event onset (day -8), to event onsent (day 0), to 12 days following event onset (day +12). Contours are every 30 m.

values are at 30°W with magnitudes up to -150 m. The upper-level low anomalies become established to the southeast of the high anomalies over the plains (see Fig. 5.4). This evolution matches the increased magnitude and extent (from the subtropical plains over the Southwest Atlantic) of the precipitation for "SACZ only" cases. A more localized, intense circulation is shown. The wave activity over the South Pacific appears weaker than in Fig. 5.7 (also seen if Fig. 5.4), but it intensifies over the Indian Ocean. From that region, waves propagate faster towards the east at approximate speeds of 10 m/s. Such faster propagation rates are not observed for "with SPCZ" cases. An examination of the hydrological processes for the positive cases follows.

5.4 Moisture Sources

This section examines the moisture sources contributing to the two cases of suppressed SACZ. Different moisture sources, as for cases of enhanced SACZ (Chapter 4), are responsible for differences in precipitation. The description starts with low-level fields. To describe the low-level flow field in relation to the precipitation anomalies, Fig. 5.9 references the 850 mb winds and shows the difference between the two types of positive cases (Fig. 5.9 b).

The precipitation anomalies are plotted with the low-level winds in Fig. 5.9 a for the "SACZ only" composite. Comparison with OLR anomalies in Fig. 5.2 h shows good correlation between the OLR and precipitation fields. The distribution of positive and negative precipitation (and OLR) anomalies over the Pacific and South America shows characteristics of a warm ENSO signature. Precipitation over the Eastern Pacific is enhanced, and a strong precipitation signal flanks the suppressed SACZ over Northeastern and Southeastern South America (e.g., Ropelewski and Halpert 1996). Low-level circulation features (Fig. 5.9 a) include the subtropical high over the South Pacific, a displaced subtropical high over the Southwestern Atlantic whose western periphery flows southward parallel to the Andes, zonal westerly winds at midlatitudes, and a strong easterly flow of tradewinds into the interior of Northern South America.

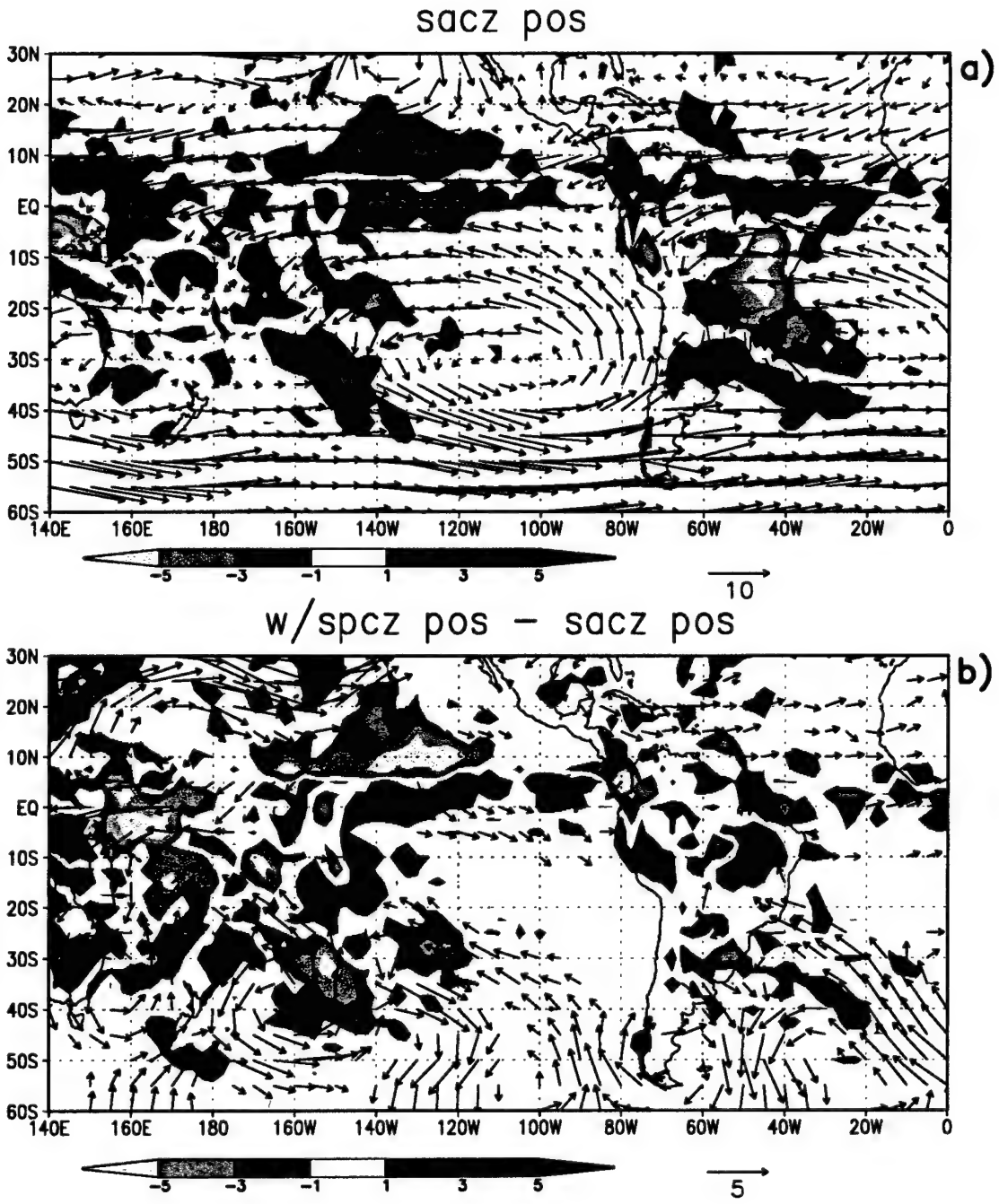

Figure 5.9 The 850 mb wind vectors (m/s) and precipitation anomalies (mm/day) for (a) "SACZ only" positive cases, and (b) "with SPCZ" minus "SACZ only" positive cases. Precipitation values are shaded with intervals indicated by the colorbars.

Differences in wind and precipitation (Fig. 5.9 b) show several features. Both the Atlantic and Pacific subtropical highs are displaced to the southwest. Precipitation is more intense over the SPCZ, over the Pacific ITCZ along 10°N, over the Atlantic ITCZ, and over the subtropical plains of South America for "SACZ only" events. Off the coast of South America, the low-level trough is stronger, as shown with the extension of precipitation from the plains. The "with SPCZ" cases show stronger precipitation anomalies over Northern South America, the Equatorial Pacific and over the region flanking the SPCZ to the east (150°W, 20°S). The northerly jet over the subtropical plains of South America is stronger for "SACZ only" cases (seen with a positive vector in Fig. 5.9 b). Over the Equatorial Pacific, the main difference is in the meridional component, with a stronger southerly contribution for the "SACZ only" composite. This may be associated with convergence in the area of positive precipitation anomalies along 10°N, (to be further investigated with an examination of moisture flux differences). In the Pacific at about 20°N, the "SACZ only" composite is stronger in the zonal direction. This is a region where precipitation is more suppressed compared to "with SPCZ" cases.

Precipitation anomalies over the western hemisphere are similar for both cases, with an amplified signal for "SACZ only" cases. Main circulation differences are found at midlatitudes. This is also apparent in the temperature field, shown in Fig. 5.10. Over the South Pacific and Southwest Atlantic, "SACZ only" cases have cold anomalies. Over the Atlantic, this corresponds to enhanced precipitation extending from the subtropical plains. The presence of these anomalies may suggest a role that cold surges have in locally intense frontal passages over South America. This was attributed, earlier, to the "SACZ only" composite in reference to the findings of Garreaud and Wallace (1997) (see section 5.2). In Fig. 5.10 a, the temperature anomalies in the Southern Hemisphere are in an opposite phase to those shown in Fig. 4.10 a (for the "with SPCZ" negative cases), particularly over the South Pacific. This further supports the "seesaw" nature of "with SPCZ" events, as shown in the low-level temperature field. Over South America at about 25°S, the

Figure 5.10 ECMWF 850 mb temperature anomalies and precipitation anomalies for (a) "with SPCZ" positive cases, (b) "SACZ only" positive cases, and (c) "with SPCZ" minus "SACZ only (a minus b)." Temperature anomalies are contoured every 0.5 K, and precipitation anomalies are shaded with intervals indicated by the colorbars. ECMWF 925 mb vector wind anomalies are plotted with the shaded precipitation anomalies in (d) for "with SPCZ" positive cases, and (e) "SACZ only" positive cases.

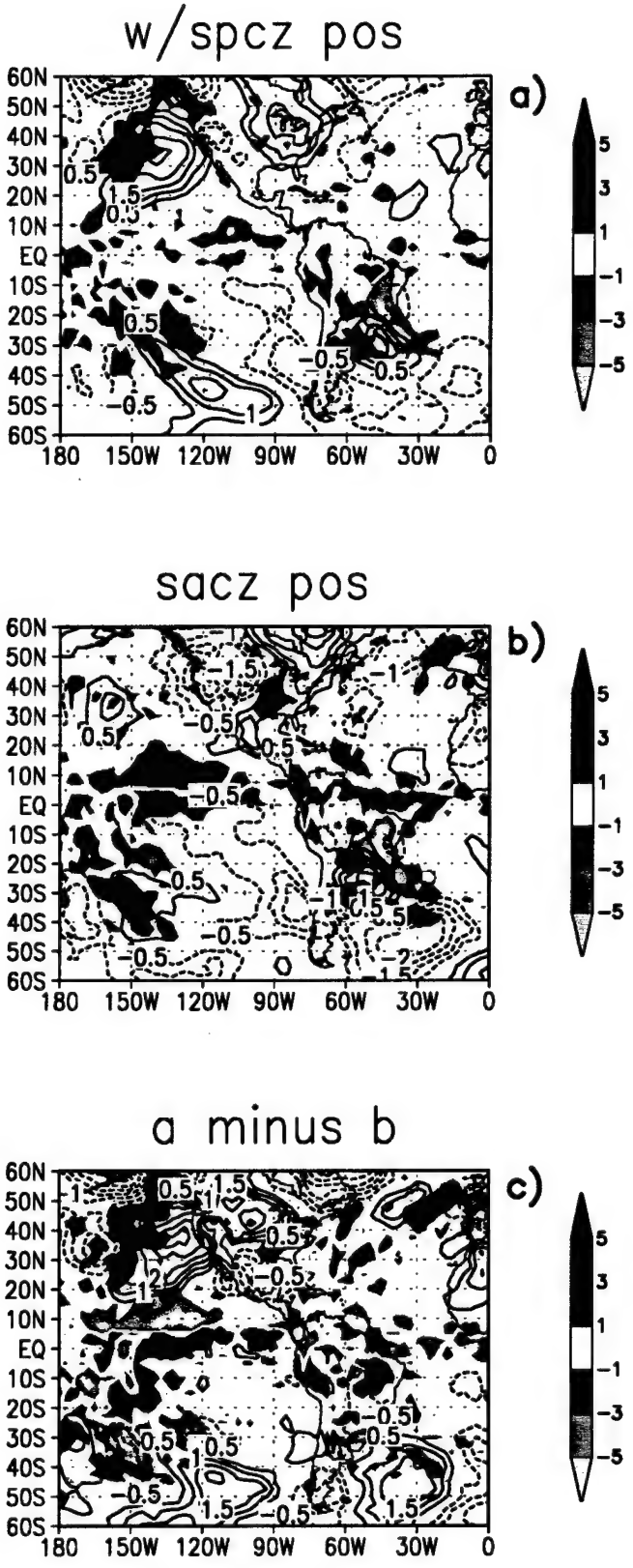
w/spcz pos
a)
sacz pos
b)
a minus b
c)
60N
50N
40N
30N
20N
10N
EQ
10S
20S
30S
40S
50S
60S
180
150W
120W
90W
60W
30W
0
5
3
1
−1
−3
−5

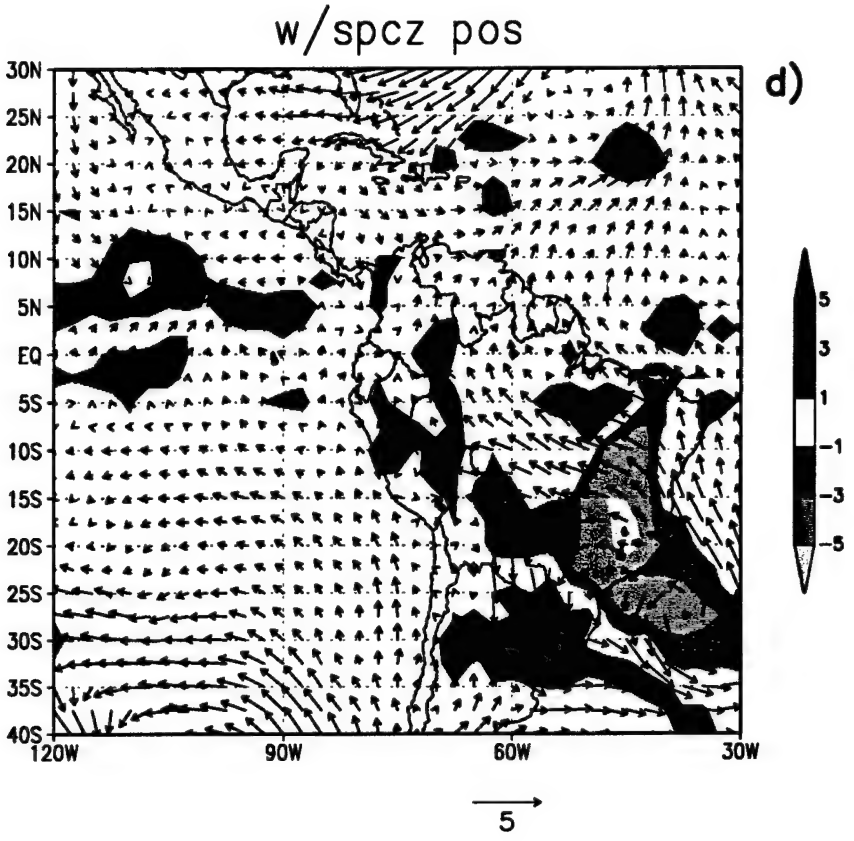

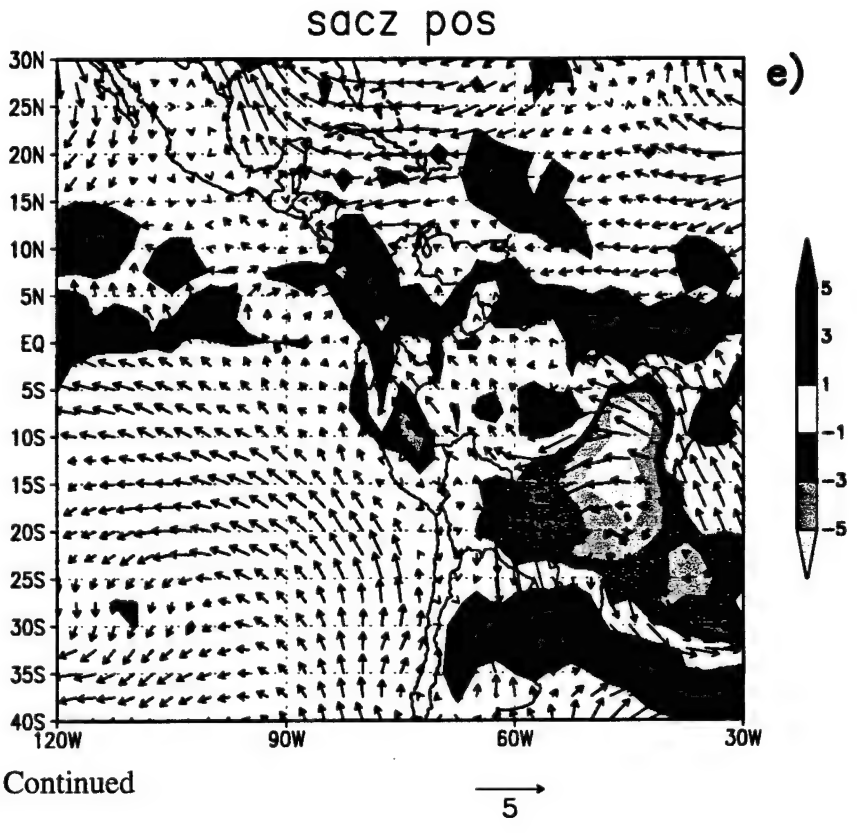

Figure 5.10 Continued

temperature differences between the two cases are small, as both show warm temperature anomalies flanking the dry and wet precipitation anomalies. In general, "with SPCZ" events are warmer than "SACZ only" events over the western hemisphere.

Temperature anomaly differences are also evident near North America, and this lends to correlations of the events with activity in the winter hemisphere. The "with SPCZ" composite shows significantly warmer temperatures over the Eastern Pacific accompanying positive precipitation anomalies and a strong low-level trough (see Fig. 5.4 d). For the negative cases, a cold anomaly was evident over the Gulf of Mexico for "SACZ only" cases (see Fig. 4.10 c), while for the positive composite, a warm anomaly (the opposite) is shown in the same region near 25°N (Fig. 5.10 c). The position of the low height anomaly (see Fig. 5.4 e) also suggests warm, southerly flow over the Gulf of Mexico. This is verified with Fig. 5.10 e, which shows pronounced anomalous southerly flow at 925 mb. The "with SPCZ" composite shows weak easterly flow in the Gulf of Mexico (Fig. 5.10 d), in contrast to southerly anomalies observed for "with SPCZ" negative events.

The precipitation patterns in the tropics and over South America are similar for the two cases, but as Fig. 5.10 d and e shows, low-level flow patterns differ significantly. For "with SPCZ" cases, precipitation anomalies over the subtropical plains of South America can be tied to the low-level jet and moisture supply from the Amazon Basin. Eltahir and Bras (1993) described contributions to the hydrologic cycle through a recycling of water vapor from the Amazon. They estimated a 35% recycling ratio. The availability of moisture through evapotranspiration is important to surrounding regions, as illustrated in Fig. 5.10 d. For "SACZ only" events (Fig. 5.10 e), transport of Amazonian moisture is also important over the plains, but low-level flow from the suppressed SACZ (southward) appears to play an even stronger role in the enhanced anomalous convection. The 925 mb winds turn southward from the suppressed region and approach the plains more directly for "SACZ only" cases (Fig. 5.10 e) than they do for "with SPCZ" cases (Fig. 5.10 d).

Evaporation and moisture flux are two possible sources of moisture for these cases.

Anomalies of evaporation are plotted with precipitation anomalies in Fig. 5.11. For both types of positive cases, positive precipitation anomalies are generally associated with negative evaporation anomalies, as less solar radiation is available for solar heat flux. As shown for the negative cases, the anomalies are small. They are at least an order of magnitude smaller than the precipitation anomalies. Thus, the main source of moisture is not from evaporation, but from moisture flux. For the negative cases, negative evaporation anomalies are widespread over the Southeastern Pacific (see Fig. 4.11). Positive evaporation anomalies dominate this region for the positive cases (Fig. 5.11 a,b). A relation of stratus decks to the temperature field is suggested in section 5.5. However, the role of evaporation in the cloud processes over this region, as assimilated by the reanalysis, is unclear at this time. An examination of the moisture flux reveals that it is the source of moisture for these events.

The moisture flux is the major source of moisture, similar to conclusions in Chapter 4. Fig. 5.12 shows the moisture flux for both types of positive cases, with values less than 75 g cm^{-1} s^{-1} not plotted. For both cases, convergence of moisture flux is pronounced in regions corresponding to positive precipitation anomalies. An example of this is over the Pacific at 10°N in Fig. 5.12 b, where strong precipitation anomalies are also located. Over the subtropical plains of South America, north-to-south vectors parallel the Andes. They correspond with moisture transported by the low-level jet that sets up as the Atlantic subtropical high shifts westward. Moisture flux convergence is weak over the SACZ where convection is suppressed. For "SACZ only" cases, significant convergence of moisture flux extends from the South American continent well into the Atlantic. Over the Western Atlantic basin, the westward-flowing branch of the subtropical high brings in Atlantic air that is channeled southward by the Andes.

The differences in moisture flux show the nature of the anomalies for the two types of cases. Differences are significant, as maximum arrows are greater than 50% of the original values (Fig. 5.12 c). Values of moisture flux less than 25 g cm^{-1} s^{-1} are not plotted.

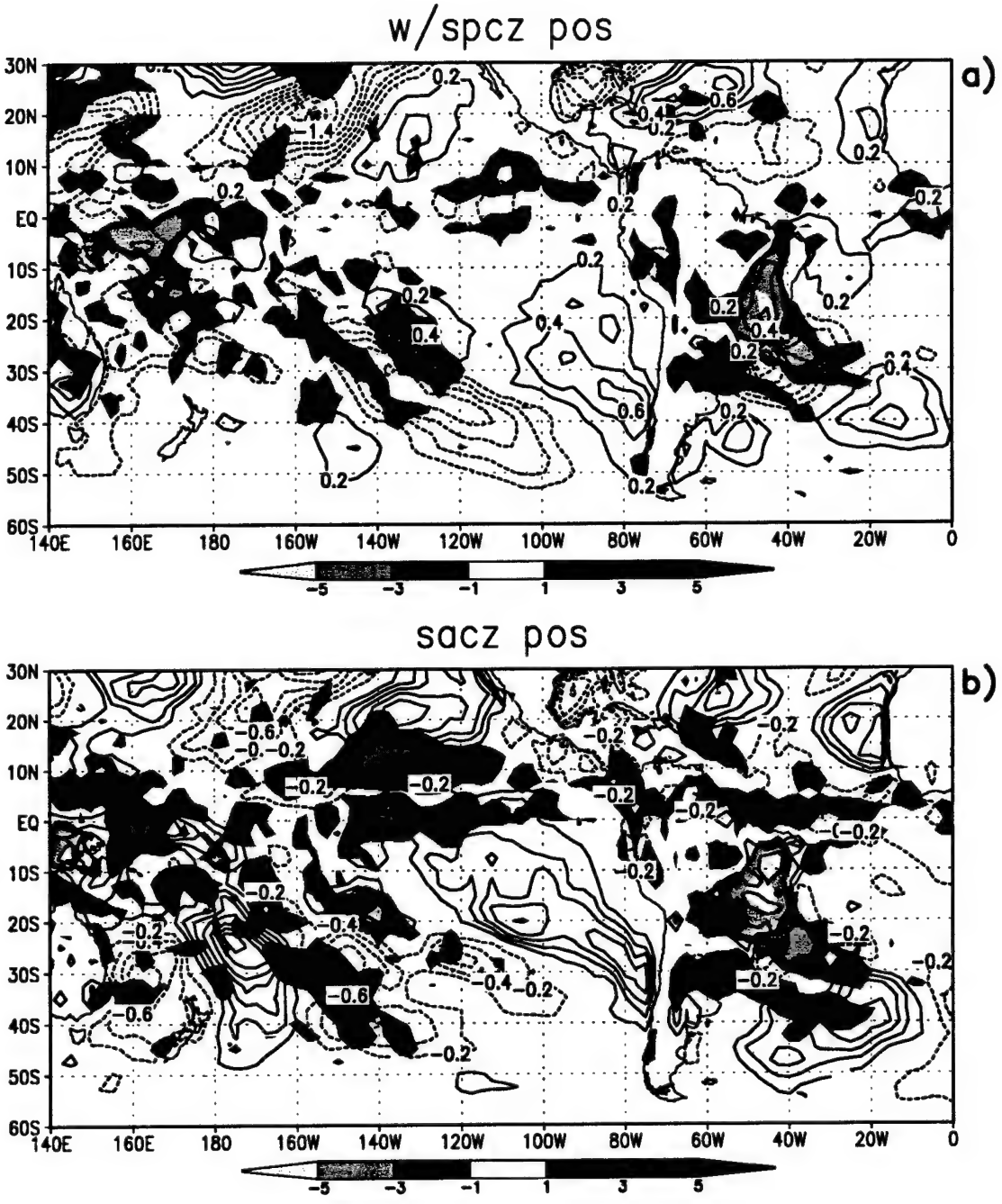

Figure 5.11 ECMWF composite evaporation anomalies and precipitation anomalies for (a) "with SPCZ" positive cases, and (b) "SACZ only" positive cases. Evaporation anomalies are contoured every 0.2 mm/day, and precipitation anomalies are shaded in mm/day as indicated by the colorbars.

Figure 5.12 ECMWF vertically integrated moisture flux vectors and contours of horizontal convergence of moisture flux for (a) "with SPCZ" positive cases, and (b) "SACZ only" positive cases. Vectors are mulitiplied by 10 g cm^{-1} s^{-1}, and values less than 75 are not plotted in (a) or (b). Convergence of moisture flux is contoured every 5 X 10^{-8} s^{-1}. Differences in vertically integrated moisture flux vectors and differences in horizontal convergence of moisture flux (a minus b) are shown in (c). Differences in horizontal convergence of moisture flux are contoured every 2 X 10^{-8} s^{-1}. Vectors less than 25 (multiplied by 10 g cm^{-1} s^{-1}) are not plotted in (c). For reference, the shading in (c) shows the horizontal convergence of moisture flux for "with SPCZ" positive cases (as contoured in a).

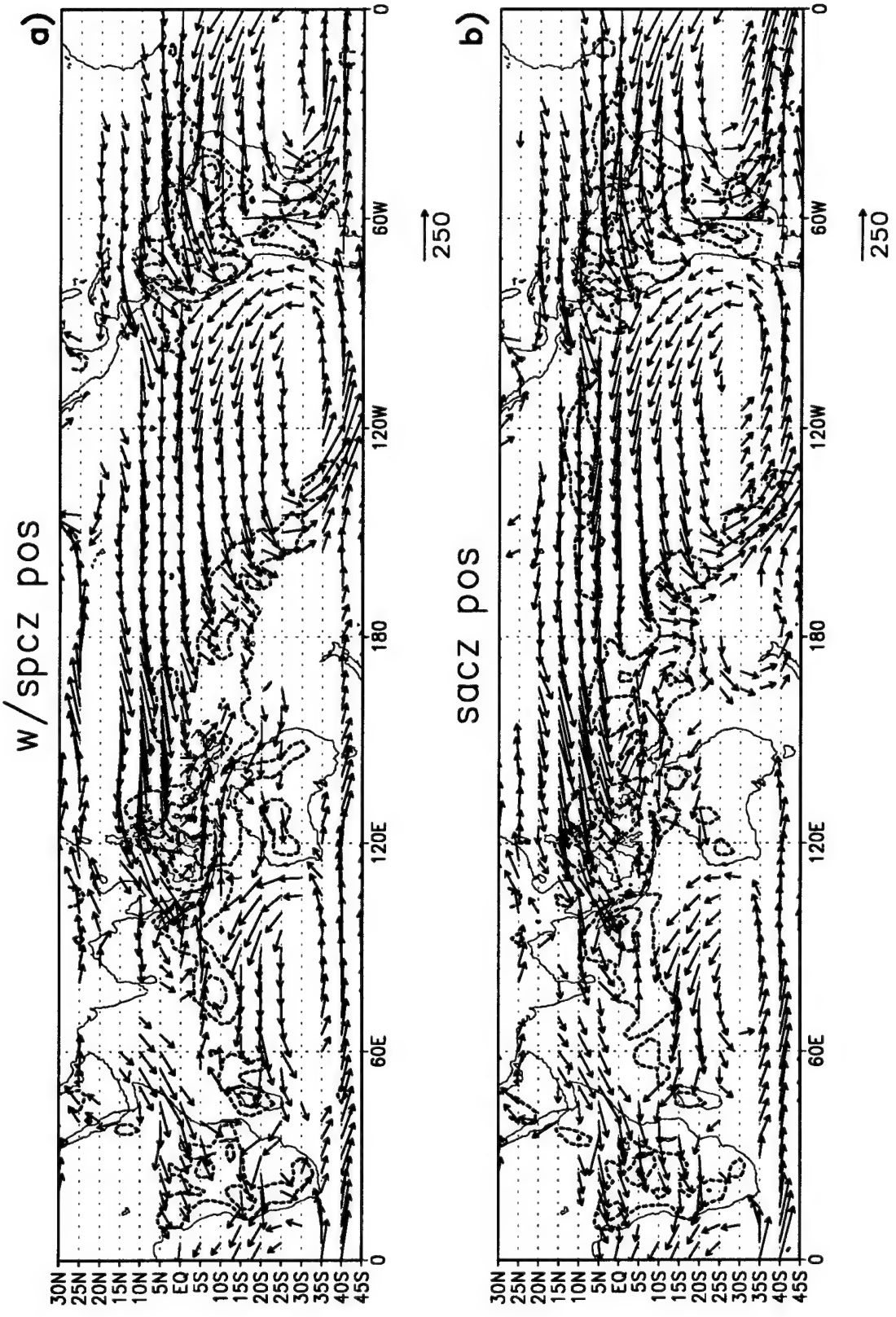
a)
w/spcz pos
b)
sacz pos
30N
25N
20N
15N
10N
5N
EQ
5S
10S
15S
20S
25S
30S
35S
40S
45S
0
60E
120E
180
120W
60W
0
250
250

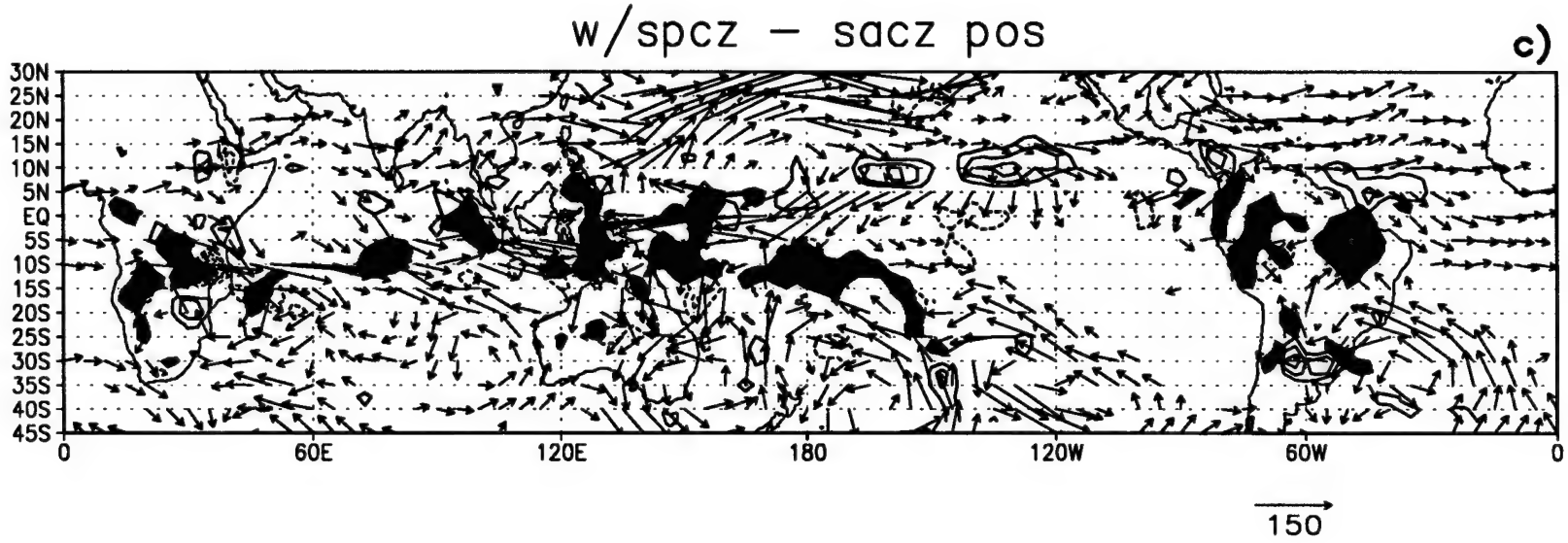

Figure 5.12 Continued

Shaded values show the convergence of moisture flux for "with SPCZ" cases for use as a reference. The flux of Atlantic air into the continent is most pronounced for the "with SPCZ" composite. Over midlatitudes, the baroclinic structure is evident in the wave-like orientation of the vectors. Other general features include the stronger convergence of moisture flux over the Central Pacific at both 10°N and 22°N for "SACZ only" cases (where precipitation shifts northward, similar to the negative cases). Along 5°N to 10°N, the meridional component of moisture flux clearly sustains the convection in the form of stronger southerlies. Also, flux convergence over the subtropical plains of South America into the Atlantic is stronger for the "SACZ only" composite. This agrees with the heavier precipitation found over this region for these type of events. In addition, the flux of warm, moist air from tropical latitudes is stronger over the South America for "SACZ only" cases (as shown by the positive vector in the differences). This is also consistent with the warm anomalies located to the north of the precipitation anomaly band (Fig. 5.10). The results found with the moisture flux show that the origin of moisture for the precipitation anomalies, as concluded for the negative composites, is in the flux of moisture. The next section compares assimilated OLR and precipitation to observational (ISCCP) data for the cases of suppressed SACZ.

5.5 ISCCP Comparisons

The composites of positive cases used for comparison to the ISCCP and observed OLR dataset (Liebmann and Smith 1996) are for the years 1985 to 1991. This provides a reasonable way to validate some of the conclusions made with the ECMWF dataset. Composites of OLR and precipitation are compared to observations of OLR and high, middle and low clouds produced by ISCCP. A limitation in this comparison is ISCCP data is missing from certain critical areas, such as over the Pacific Ocean from about 150°W to 130°W.

Precipitation tends to correspond well with the OLR over tropical and subtropical latitudes in Fig. 5.13. The precipitation and OLR show general features of "with SPCZ"

Figure 5.13 Average composite fields of "with SPCZ" positive events for the years 1985-1991, showing (a) ECMWF precipitation (contoured every 3 mm/day), (b) ECMWF OLR (contoured every 20 W m^{-2}), and (c) ECMWF OLR minus satellite-derived OLR observations (Liebmann and Smith 1996) (contoured every 20 W m^{-2}).

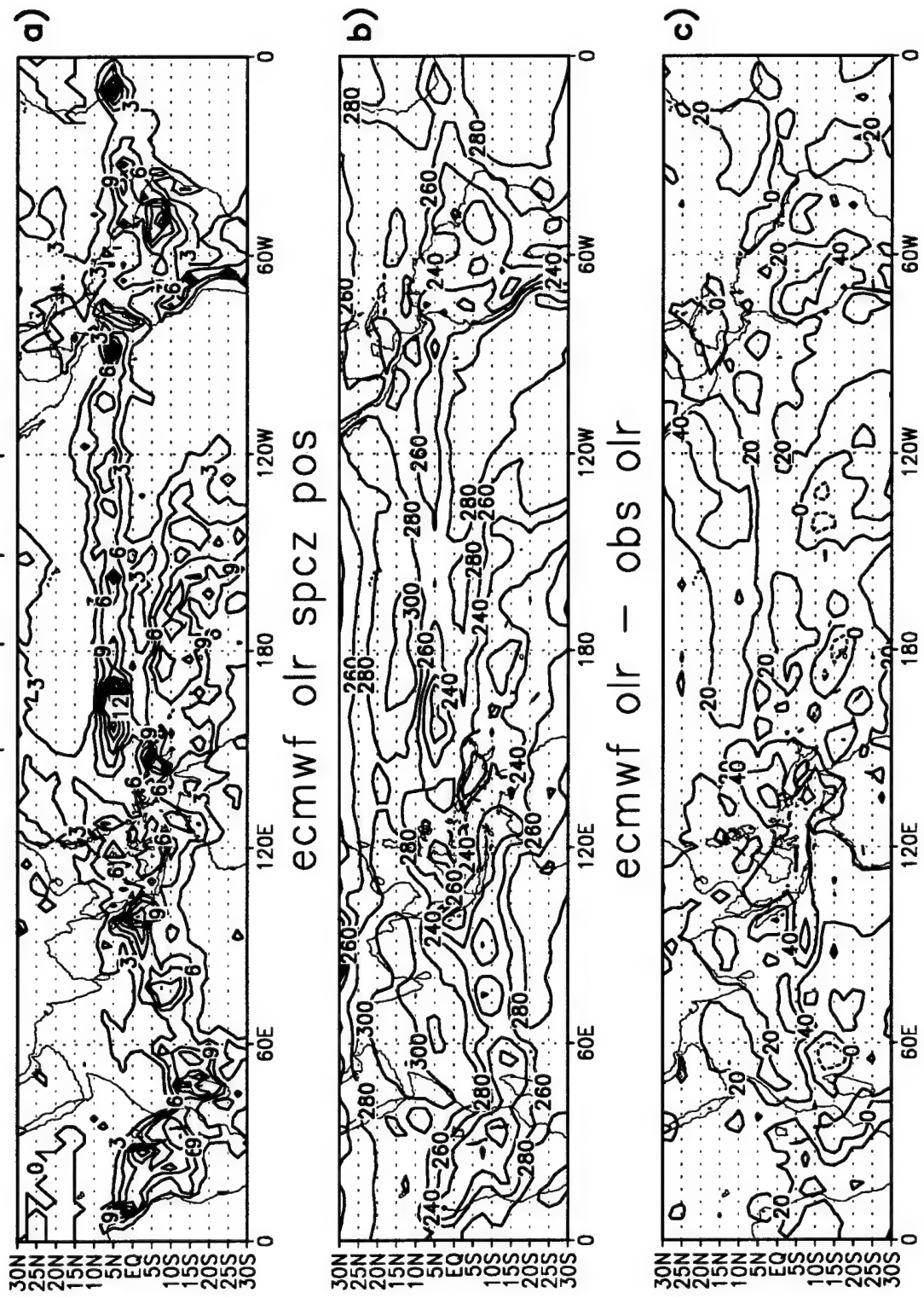
a)
ecmwf precip. spcz pos
b)
ecmwf olr spcz pos
c)
ecmwf olr – obs olr
30N
25N
20N
15N
10N
5N
EQ
5S
10S
15S
20S
25S
30S
0
60E
120E
180
120W
60W
0

events, such as suppressed convection over the SACZ and precipitation signals over the SPCZ and the ITCZs in both the Pacific and Atlantic. Deviations from observed OLR (Fig. 5.13 c) suggest the ECMWF produces too few clouds (up to 40 W/m^2 difference) over South America and over the Pacific compared to observations.

Differences in OLR and precipitation between the two types of cases are taken in Fig. 5.14. The precipitation and OLR fields correlate well and show positive and negative precipitation anomalies discussed in previous sections. In Fig. 5.14 c, the differences in the observed OLR are taken. Comparison of Fig. 5.14 b with c shows that assimlated differences generally match observations. For example, over the Central Pacific in the Northern Hemisphere, OLR values are lower for "SACZ only" cases in both analyses. This is also the case over the SPCZ, where convection is more intense for "SACZ only" events, though differences are higher for the observed fields.

The assimilated precipitation and OLR match well with the middle and high cloudiness in the ISCCP dataset (Fig. 5.15). This good correlation can be attributed to the prognostic equation for cloud water used in the ECMWF reanalysis. ISCCP differences are shown in Fig. 5.16. Mid- and upper-level cloudiness over the Pacific tend to agree with assimilated results, though much of the area over the Pacific is void of data. Over South America from 5°S to 10°S, "with SPCZ" cases produce more precipitation in the assimilated reanalysis (Fig. 5.14 a), and this agrees with the higher amounts of mid- and upper-level cloudiness shown in the ISCCP differences (Fig. 5.16 a and b).

Stratus decks over the Southeastern Pacific are significant features shown for these events in the ISCCP low cloud analyses. One explanation of the magnitude and extent of the clouds may be a relationship to the temperature field. At low levels, differences in stratus over the cool waters of the Southeastern Pacific (Fig. 5.16 c) are similar to the results found for the negative cases, as "with SPCZ" cases have more stratus off the coast of South America. The amount of low cloudiness, however, is lower for “with SPCZ” positive cases, as shown in the differences in Fig. 5.17. Negative events have 5-10%

Figure 5.14 Average composite differences between "with SPCZ" and "SACZ only" positive events for the years 1985-1991, showing (a) ECMWF precipitation (contoured every 3 mm/day), (b) ECMWF OLR (contoured every 10 W m^{-2}), and (c) satellite-derived OLR observation differences (Liebmann and Smith 1996) (contoured every 10 W m^{-2}).

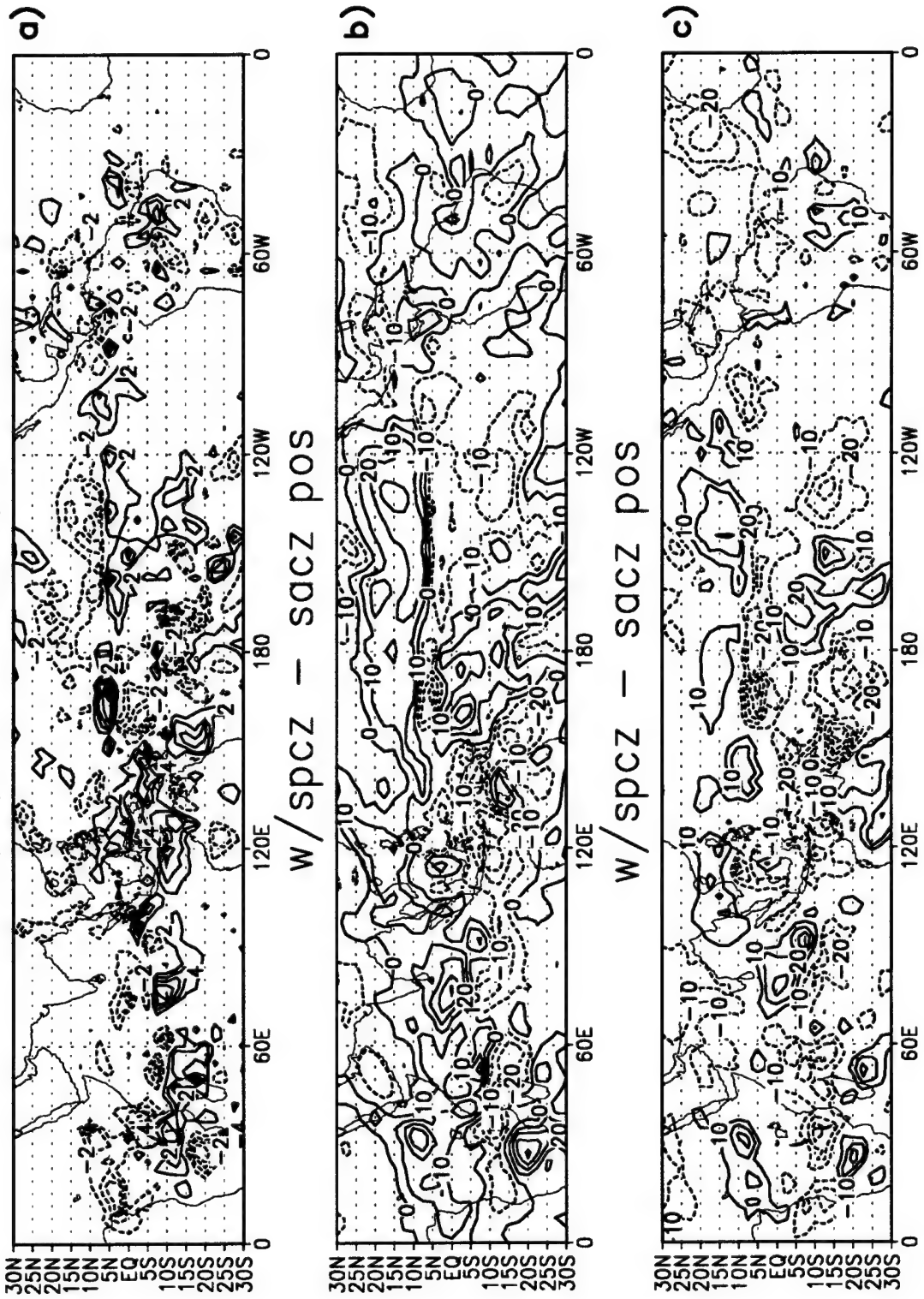
a)
W/spcz – sacz pos
b)
W/spcz – sacz pos
c)
W/spcz – sacz pos
30N
25N
20N
15N
10N
5N
EQ
5S
10S
15S
20S
25S
30S
0
60E
120E
180
120W
60W
0

Figure 5.15 Composite ISCCP data for "with SPCZ" positive events (1985-1991) for (a) high, (b) medium, and (c) low cloud percentages. Contours are every 10%.

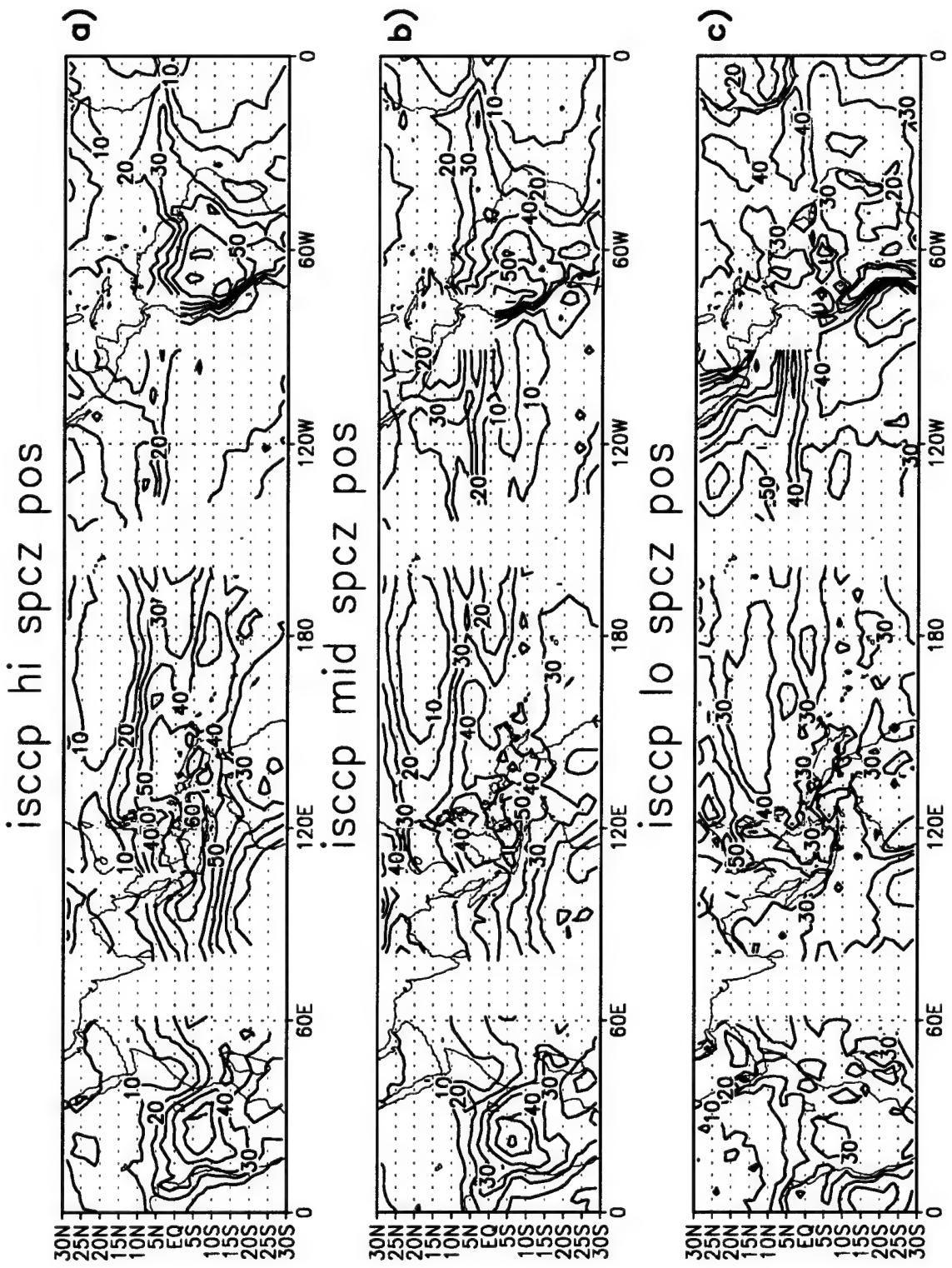
a)
isccp hi spcz pos
b)
isccp mid spcz pos
c)
isccp lo spcz pos
30N
25N
20N
15N
10N
5N
EQ
5S
10S
15S
20S
25S
30S
0
60E
120E
180
120W
60W
0

Figure 5.16 Composite ISCCP cloud differences for "with SPCZ" and "SACZ only" positive events (1985-1991) for (a) high, (b) medium, and (c) low cloud percentages. Contours are every 5%.

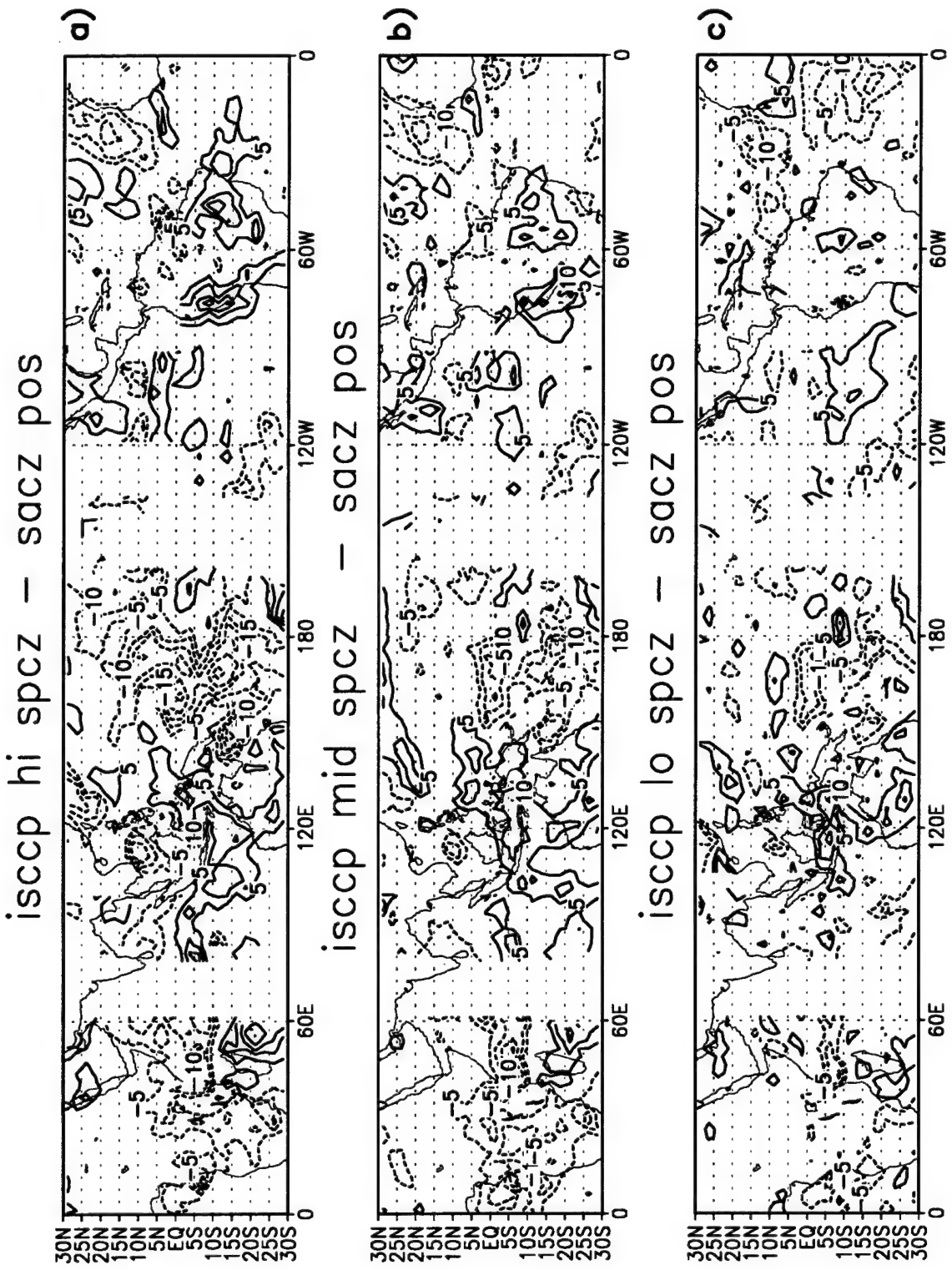
a)
isccp hi spcz – sacz pos
b)
isccp mid spcz – sacz pos
c)
isccp lo spcz – sacz pos
30N
25N
20N
15N
10N
5N
EQ
5S
10S
15S
20S
25S
30S
0
60E
120E
180
120W
60W
0

Figure 5.17 Composite ISCCP low cloud percentage differences between positive and negative events (1985-1991) for (a) "with SPCZ," and (b) "SACZ only." Contours are every 5%. Composite temperature differences between positive and negative events are shown in (c) for "with SPCZ," and (d) for "SACZ only." Temperature contours are every 0.5 K.

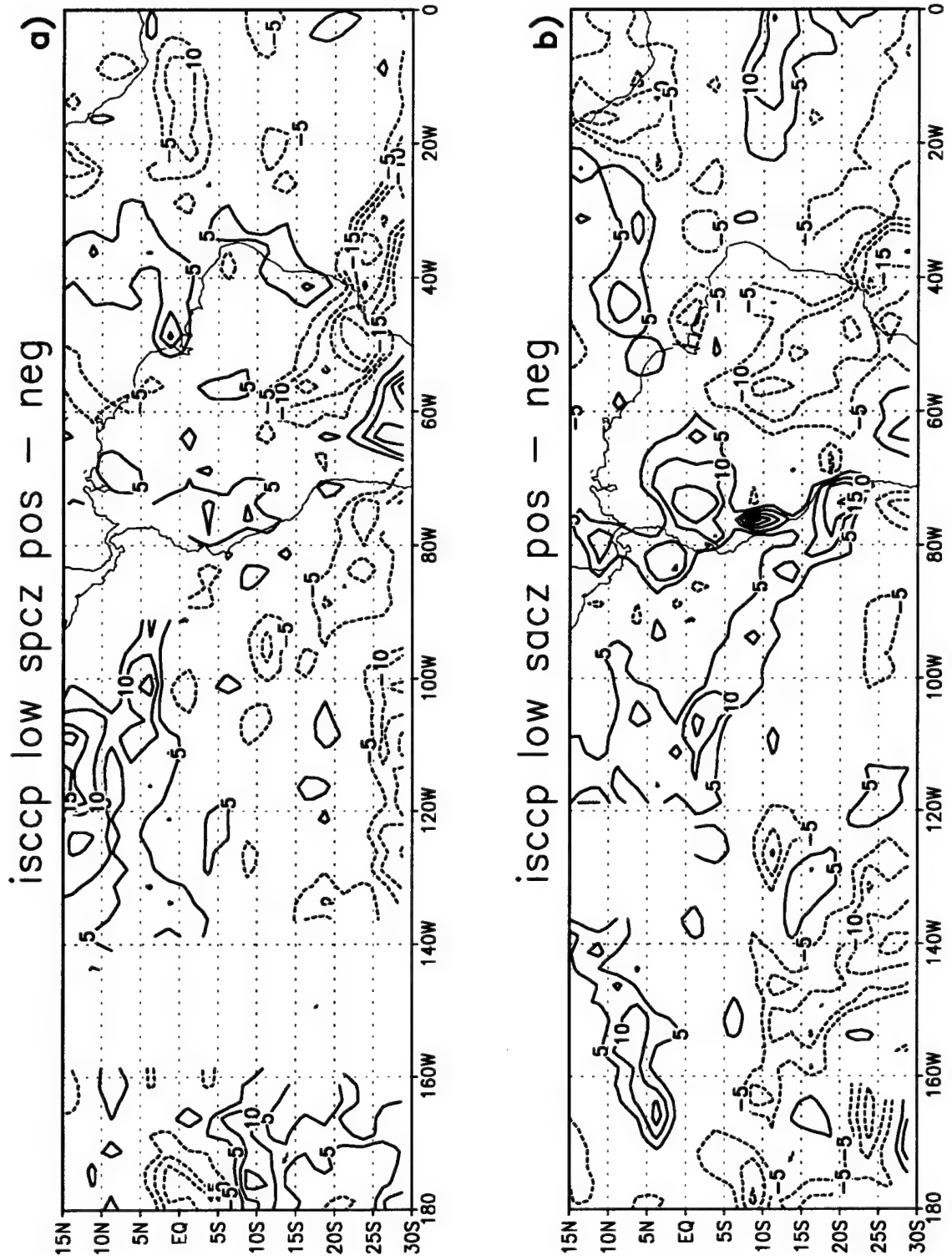
a)
isccp low spcz pos – neg
b)
isccp low sacz pos – neg
15N
10N
5N
EQ
5S
10S
15S
20S
25S
30S
180
160W
140W
120W
100W
80W
60W
40W
20W
0

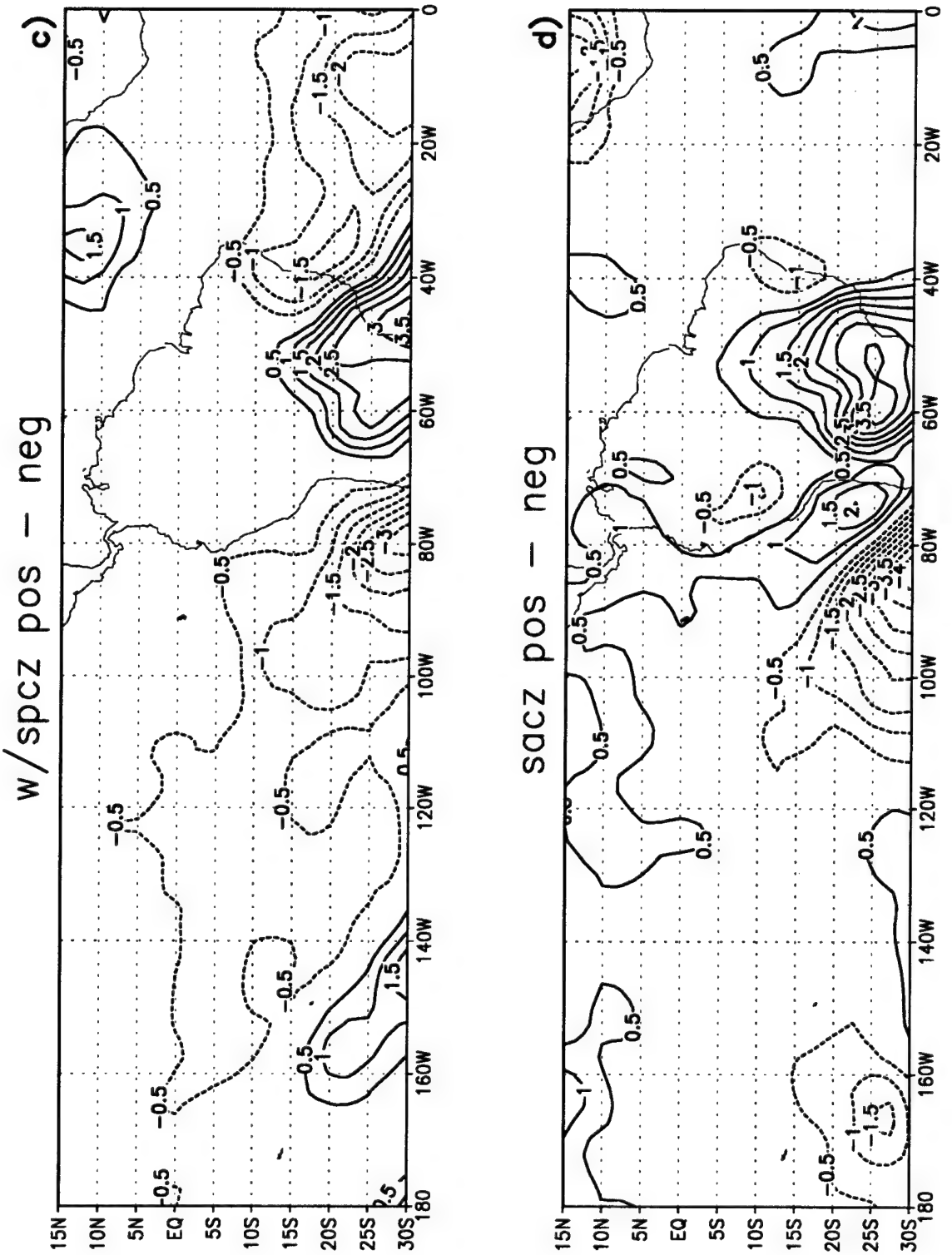

Figure 5.17 Continued

more cloudiness over the Southeastern Pacific. Warmer temperatures in this region for negative "with SPCZ" cases may account for the higher stratus amounts, as evident with 850 mb ECMWF temperature differences (Fig. 5.17 c). Low cloudiness differences for "SACZ only" events (Fig. 5.17 b) show higher amounts of stratus for positive events. This corresponds to warmer temperatures off the coast of South America (Fig. 5.17 d). Overall, comparisons of observed OLR and cloudiness to ECMWF OLR, precipitation and temperature fields suggest a reasonable depiction of observations.

Two types of suppressed SACZ, identified by REOF analyses, have been described using diagnostics of ECMWF OLR and precipitation, upper- and low-level variables, transients and moisture sources. "With SPCZ" events represent the opposite phase of the "seesaw" in precipitation over South America. Precipitation anomalies over the Southern Hemisphere are not as pronounced for positive "with SPCZ" events as they are for negative "with SPCZ" events. For the 2-week time scale considered, "SACZ only" events amplify slowly and more strongly without apparent ties to activity in the Pacific. For both types of suppressed SACZ over South America, a low-level jet transports moisture from the Atlantic and the Amazon basin southward into the subtropical plains. Atlantic air is advected into the continent by a displaced Atlantic subtropical high. Convergence of vertically integrated moisture flux sustains the precipitation over the subtropical plains.

CHAPTER 6

DISCUSSION AND SUMMARY

The South American continent exhibits a unique blend of steep mountains, tropical forests, desert areas and fertile subtropical plains. The Bolivian altiplano provides an elevated source of sensible heat during summer (e.g., Rao and Ergodan 1989). It influences large-scale vertical motion patterns and results in atmospheric overturnings and associated rainfall and convective heating. A high pressure system is found during summer at upper levels over this 3000 m-high plateau. Nevertheless, the summer circulation over South America has been qualitatively reproduced as the response to transient tropical convection (Silva-Dias et al. 1983) using a linear model similar to that of Gill (1980). Resulting features in this model include the Bolivian high, suggesting it may be more a result of tropical convection than the elevated heat source. A prominent feature of the summer convection over South America is the South Atlantic Convergence Zone (SACZ), a convective band which extends, at times, from the Amazon basin into the Atlantic Ocean. The present study focuses on the intraseasonal variability of the SACZ and describes its horizontal structure.

The 30- to 60- day oscillation (e.g., Madden and Julian 1971) is a strong modulator of tropical convection on the intraseasonal time scale. It was originally identified as a pulse of organized convection that propagates eastward along the equator from the Indian Ocean to the Central Pacific. It has been shown to propagate all the way around the equator and to be strongest during austral summer. Strengthening of the SPCZ and the subsequent enhancement of the SACZ have been documented by NPM97, who also show the existence of a meridional seesaw of dry and wet conditions over tropical and subtropical

South America. The present study further examines the intraseasonal variation of precipitation regimes over South America. It seeks to identify the importance of the upstream intraseasonal modulation of the SPCZ on the SACZ and related meridional propagation patterns.

This is accomplished using rotated empirical orthogonal function analyses of filtered OLR anomalies confined to two regions: one includes the SPCZ from the dateline eastward to 20°E; and the other extends from 100°W to 0°W, including South America and the SACZ. Four convective patterns are identified in this fashion: those with an enhanced/suppressed SACZ with a well-defined SPCZ (referred to as "with SPCZ"), and those with an enhanced/suppressed SACZ without a clear signature in the SPCZ ("SACZ only"). The investigation describes midlatitude patterns, synoptic transients, and moisture sources for all four of these events. The main results are:

1) An enhanced SACZ is associated with a suppressed SPCZ (as in NPM97) and is preceded about 8 days prior by a pronounced SPCZ. These are features of the intraseasonal oscillation. The seesaw pattern between the SACZ and precipitation over the South American plains is also apparent in these analyses. Both an enhanced and a suppressed SACZ with a well-defined SPCZ are more frequent during warm ENSO events. This result is consistent with stronger convection in the Eastern Pacific, a typical signature of ENSO events.

2) Four well-defined, northwest-to-southeast-oriented precipitation bands located over surface low pressure are found for negative "with SPCZ" cases. These are located from the SACZ eastward, east of Africa, over Australia, and in the Central Pacific, with extensions from the tropics into midlatitudes. These bands acquire a more zonally-oriented tilt as they merge into the westerly flow. Approximately 5 waves are found in the 200 mb height anomaly pattern between 40°S and 50°S, suggesting a possible link between precipitation and height fields. This is not the case for the "SACZ only" negative events. They show strong precipitation anomalies over South America and the dateline in the

Southern Hemisphere subtropics. A dominant wave number 2 pattern in midlatitudes may be related to these two subtropical convective anomalies.

3) The wave number 5 pattern in the height field composite, referred to above, is found in conjunction with high synoptic variability at midlatitudes over the Southern Hemisphere. This high wave number pattern is consistent with increased synoptic wave activity and possibly increased frequency of frontal passages over South America and the neighbouring Atlantic Ocean. "SACZ only" cases appear less variant with steady in-situ amplification and no apparent meridional link between the tropics and the subtropics. Both types of negative events consist of a similar number of cases (14 "with SPCZ" and 16 "SACZ only"), suggesting an equal role for both types in the overall climatology of the SACZ.

4) "With SPCZ" positive cases (suppressed SACZ) correspond to the opposite phase of the "seesaw" in precipitation over South America with ties to intraseasonal oscillations in the Pacific. They are associated with a wave 3 pattern in the Southern Hemisphere and more wave activity over the South Pacific compared to "SACZ only" positive cases.

5) The larger precipitation amounts over tropical South America for "SACZ only" cases, compared to "with SPCZ" events, are sustained by a stronger convergence of moisture flux. Atlantic air is advected into the continent by the northerly branch of the subtropical high. This is the largest contributor to moisture flux for the SACZ. Minor contributions are due to the northwesterly flow channeled by the Bolivian altiplano, which is relatively stronger for "with SPCZ" cases. These analyses show no contributions to the SACZ from southerlies.

6) A number of similarities exist between cases of enhanced and suppressed SACZ (negative and positive cases, respectively). First, evolution of OLR anomaly composites is similar both in positive and negative "with SPCZ" events in that the seesaw pattern is apparent. No convective precursors are apparent for the "SACZ only" composites, where higher precipitation values are more evident over South America. Second, "with SPCZ"

cases exhibit more synoptic activity over the South Pacific Ocean. Third, they are more frequently found during ENSO warm events. Fourth, they are associated with a larger number of waves in Southern Hemisphere midlatitudes. Therefore, the chosen stratification (with and without a well-defined SPCZ) has successfully identified two different patterns of intraseasonal variations of summer rains over South America.

7) Positives events also coincide with an enhanced SPCZ and ITCZ. The ITCZ is displaced about 5 to 10°N. The SPCZ and ITCZ patterns are reminiscent of those associated with the mid-summer climatology.

8) ENSO-like patterns are apparent for "with SPCZ" cases. However, intraseasonal scales dominate these events.

9) Large differences are apparent in the moisture flux between the positive and negative cases. A low-level northerly jet for positive cases is responsible for transporting moisture from the Amazon Basin. The westward-flowing branch of the Atlantic subtropical high is thus deflected southward. The flux of Atlantic air into the continent is most pronounced for "with SPCZ" composites.

Comparisons of ECMWF reanalysis products with ISCCP cloud coverage indicates that the analyses do a credible job in linking regions of convective precipitation with mid- and high-level clouds. This is expected from the ECMWF physical parameterizations, as they carry prognostic equations for the cloud/ice content. OLR fields from the analyses are found to overestimate those derived from satellite observations, with differences peaking at 40 w/m^2 over tropical convection. The analyzed evaporation anomalies appear negatively correlated with cloud cover, indicating no local feedback between surface procesess and precipitation anomalies.

The ECMWF analyses resolve well-known features of the seasonally averaged climatology, including patterns of precipitation and evaporation. They also correctly resolve the convergence zones of the Southern Hemisphere; and over South America, they resolve the seasonal evolution of the Bolivian high.

REFERENCES

Buchmann, J., L.E. Buja, J. Nogués-Paegle and J. Paegle, 1995: The dynamical basis of regional vertical motion fields surrounding localized tropical heating. *J. Climate*, **8**, 1217-1234.

Dorman, C. E., and R. H. Bourke, 1978: Precipitation over the Pacific Ocean, 30S to 60N. *Mon. Wea. Rev.*, **107**, 896-910.

Eltahir, E., and R. Bras, 1994: Precipitation recycling in the Amazon basin. *Quart. J. Roy. Meteor. Soc.*, **120**, 861-880.

Figueroa, S.N., P. Satyamurty, and P.L. Silva Dias, 1995: Simulations of the summer circulation over the South American region with an Eta coordinate model. *J. Atmos. Sci.*, **52**, 1573-1584.

Gandu, A.W., and J.E. Geisler, 1991: A primitive equations model study of the effect of topography on the summer circulation over tropical South America. *J. Atmos. Sci.*, **48**, 1822-1836.

Garreaud, R.D., and J.M. Wallace, 1998: Summertime incursions of mid-latitude air into subtropical and tropical South America. *Mon. Wea. Rev.*, in press.

Gibson, J.K., P. Kållberg, S. Uppala, A. Nomura, A. Hernandez, and E. Serrano, 1997: ERA Description. ECMWF Re-Analysis Project Report Series, 1.

Gill, A.E., 1980: Some simple solutions for heat induced tropical circulation. *Quart. J. Roy. Meteor. Soc.*, **106**, 447-462.

Grimm, A.M., and P.L. Silva Dias, 1995: Analysis of tropical-extratropical interactions with influence functions of a barotropic model. *J. Atmos. Sci.*, **52**, 3538-3555.

Horel, J.D., A.N. Hahmann, and J.E. Geisler, 1989: An investigation of the annual cycle of convective activity over the tropical Americas. *J. Climate*, **2**, 1388-1403.

Hoskins, B.J., and D.J. Karoly, 1981: The steady linear response of a spherical atmosphere to thermal and orographic forcing. *J. Atmos. Sci.*, **38**, 1179-1196.

Huffman, G.J., R.F. Adler, B. Rudolph, U. Schneider, and P.R. Keehn, 1995: Global precipitation estimates based on a technique for combining satellite-based estimates, rain gauge analysis and NWP Model Precipitation Estimates. *J. Climate*, **8**, 1284-1295.

Jaeger, L., 1976: Monatskarten des Niederschlags fur die ganze Erde, Berichte ses Deutscher Wetterdienstes, Nr. 139 (Band 18). Offenbach, A. M., 33pp.

Janowiak, J.E., P.A. Arkin, P. Xie, M.L. Morrissey, and D.R. Legates, 1995: An examination of the East Pacific ITCZ rainfall distribution. *J. Climate* , **8**, 2810-2821.

Johnson, M.W., 1996: The role of radiative processes in the tropical intraseasonal oscillation. Doctoral dissertation, University of Utah, 118pp.

Kalnay, E., K.C. Mo, and J. Paegle, 1986: Large amplitude, short-scale stationary Rossby waves in the Southern Hemisphere: observations and mechanistic experiments to determine their origin. *J. Atmos. Sci.*, **43**, 252-275.

Kleeman, R., 1989: A modeling study of the effect of the Andes on the summertime circulation over tropical South America. *J. Atmos. Sci.*, **46**, 3344-3362.

Kousky, V.E., and D.P. Casarin, 1986: Rainfall anomalies in southern Brazil and related atmospheric circulation features. *Extended Abstract, Second Int. Conf. on Southern Hemisphere Meteorology*, Wellington, New Zealand, Amer. Meteor. Soc., 435-438.

Legates, D.R., and C.J. Willmott, 1990: Mean seasonal and spatial variability in gauge-corrected, global precipitation. *Int. J. Climatology*, **10**, 111-127.

Lenters, J.D., and K.H. Cook, 1995: Simulation and diagnosis of the regional summertime precipitation climatology of South America. *J. Climate*, **8**, 2988-3005.

Liebmann, B., and C.A. Smith, 1996: Description of a complete (interpolated) outgoing longwave radiation dataset. *Bull. Amer. Meteor. Soc.*, **77**, 1275-1277.

Madden, R.A., and P.R. Julian, 1971: Detection of a 40-50 day oscillation in the zonal wind in the tropical Pacific. *J. Atmos. Sci.*, **28**, 702-708.

Nogués-Paegle, J., and K.C. Mo, 1997: Alternating wet and dry conditions over South America during summer. *Mon. Wea. Rev.*, **125**, 279-291.

___, K.C. Mo, and J. Paegle, 1998: Predictability of the NCEP/NCAR reanalysis model during austral summer. *Mon. Wea. Rev.*, in press.

Rao, G.V., and S. Ergodan, 1989: The atmospheric heat source over the Bolivian Plateau for a mean January. *Bound.-Layer Meteor.*, **46**, 13-33.

Ropelewski, C.F., and M.S. Halpert, 1996: Quantifying Southern-Oscillation precipitation relationships. *J. Climate*, **9**, 1043-1059.

Rossow, W.B., and R.A. Schiffer, 1991: ISCCP cloud data products. *Bul. Amer. Meteor. Soc.*, **72**, 2-20.

Schemm, J., S. Schubert, J. Terry, and S. Bloom, 1992: Estimates of monthly mean soil moisture for 1979-1989. NASA Tech. Mem. 104571, October 1992, Goddard Space Flight Center, Greenbelt, MD 20771.

Silva Dias, P.L., W.H. Schubert, and M. DeMaria, 1983: Large-scale response of the tropical atmosphere to transient convection. *J. Atmos. Sci.*, **40**, 2689-2707.

___, J.P. Bonatti, and V.E. Kousky, 1987: Diurnally forced tropical tropospheric circulation over South America. *Mon. Wea. Rev.*, **115**, 1465-1478.

Spangler, W.M., and R.L. Jenne, 1990: World monthly surface station climatology. National Center for Atmospheric Research, Boulder, CO 80303.

Spencer, R.W., 1993: Global oceanic precipitation from the MSU during 1979-1991 and comparisons to other climatologies. *J. Climate*, **6**, 1301-1326.

Tiedtke, M., 1993: Representation of clouds in large-scale models. *Mon.Wea. Rev.*, **121**, 3040-3061.

Vincent, D.G., 1994: The South Pacific convergence Zone (SPCZ): A review. *Mon. Wea. Rev.*, **122**, 1949-1970.

Wallace, J.M., and P.V. Hobbs, 1977: *Atmospheric Science: An Introductory Survey*. Academic Press, 467pp.

Xie, P., and P.A. Arkin, 1996: Analyses of global monthly precipitation using gauge observations, satellite estimates and numerical model predictions. *J. Climate*, **9**, 840-850.